# A Study on the Effect of Temperature and Pressure on the Removal of Cyclohexane from Non-Aqueous Extraction Gangue

By

Richard Renaud

A thesis submitted in partial fulfillment of the requirements for the degree of

Master of Science

in

Chemical Engineering

Department of Chemical and Materials Engineering

University of Alberta

## Abstract

Solvent based extraction has the potential to supplant the current hot water based extraction process as the industry standard method for recovering bitumen from mined oil sand. It has the potential for higher bitumen recovery that is less sensitive to the grade of oil sand ore being processed. More importantly, it can prevent the further accumulation of tailings ponds because it does not produce aqueous tailings. Instead, a mixture of sand with residual solvent and bitumen, referred to as extraction gangue, is produced. When solvent is recovered from extraction gangue, the remaining mixture is suitable for backfilling a mined out area. While solvent based recovery processes have been thoroughly studied, gaps remain in the literature regarding the recovery of solvent from extraction gangue, which is critical for the process to be economically viable.

Experiments were performed on extraction gangue from high and low grade oil sand ores that had bitumen extracted using cyclohexane. The effects of temperature and pressure on the removal of cyclohexane from extraction gangue were tested. An apparatus was designed that could accurately measure and control both temperature and pressure and separately measure the evaporation of both cyclohexane and water. Tests were performed drying high and low grade extraction gangue between 25 and 95 °C with increments of 10 °C combined with pressures of 300, 500, 700 mbar, as well as a simulation atmospheric pressure condition above 900 mbar. Tests were conducted in duplicate with 2 additional runs at 105 °C and the atmospheric pressure simulation for a total of 66 tests per grade of gangue.

In comparing the gangue produced by the different grades of oil sand ore, mass flux was higher in all stages of the cyclohexane removal process for high grade gangue. This was attributed partly to the higher water content in low grade gangue with a mean initial concentration of 12.5% ± 1.9% (n=66) by mass compared to just 2.1% ± 1.1% (n=66) for high grade gangue. Higher mass flux in high grade gangue in the final drying stages may have been attributed to a lower fines content prior to extraction of 11.2% ± 0.7% (n=3) by mass compared to 19.4% ± 0.9% (n=2) in low grade ore. The amount of cyclohexane remaining at the transition point between high and low mass flux cyclohexane removal was also higher for low grade gangue, so more cyclohexane needed to be recovered at a lower mass flux. All in all, total completion time was an average of 3.2 ± 0.9 (n=33) times longer in low grade gangue than in high grade gangue for experiments conducted at the same temperature and pressure.

It was found that increasing temperature and decreasing pressure both had the effect of increasing mass flux of evaporating cyclohexane. Total time required to reach a goal residual cyclohexane concentration of 250 ppm was found to decay following a power law relationship with both increasing temperature and decreasing pressure, and the benefits of adding more energy through use of vacuum or heating were found to lose significance at higher temperatures. Energy analysis of these batch experiments found that while minimum energy input would occur at atmospheric pressure and 25 °C temperature, operating at higher temperatures and applying vacuum would drastically reduce the time required to recover cyclohexane without dramatically increasing the required energy input.

## Acknowledgements

I would like to thank Dr. Murray Gray for accepting me as a student and for his wise guidance throughout the completion of my degree, especially the insights provided during the editing of my thesis.

I would like to thank Krupal Pal for her assistance running experiments, her advice throughout the completion of my work, and her help editing my thesis.

I would like to thank Tobias Weiss for working diligently to obtain experimental results that were incorporated into the thesis.

I would like to thank Xiaoli Tan for his help calibrating the DSMS and maintaining it in operating condition.

Finally, I would like to thank Imperial Oil for their assistance in funding the project as well as their feedback.

# Table of Contents

ABSTRACT .......... II

ACKNOWLEDGEMENTS .......... V

TABLE OF CONTENTS .......... VI

INTRODUCTION .......... 1

CURRENT COMMERCIAL EXTRACTION PROCESSES .......... 1
DISADVANTAGES OF CURRENT COMMERCIAL PROCESS .......... 2
NON AQUEOUS EXTRACTION PROCESSES .......... 3
PERMISSIBLE SOLVENT LOSSES .......... 6
DRYING MECHANISM .......... 6

OBJECTIVES .......... 12

METHODOLOGY .......... 12

CONVERTING INSTRUMENT READINGS TO EVAPORATION RATES .......... 15
SAMPLES TESTED .......... 20
TEMPERATURE AND PRESSURE COMBINATIONS TESTED .......... 21
BITUMEN MIGRATION ANALYSIS .......... 23
BATCH ENERGY CALCULATIONS .......... 23

RESULTS AND DISCUSSION .......... 26

COMPOSITION OF SAMPLES TESTED .......... 26
HIGH GRADE GANGUE .......... 26
LOW GRADE GANGUE .......... 28
REPRESENTATIVE RESULTS .......... 31
HIGH GRADE GANGUE .......... 31
LOW GRADE GANGUE .......... 36
STEADY STATE MASS FLUX .......... 39
SUBCOOLING .......... 47
TOTAL TIME TO REMOVE CYCLOHEXANE .......... 51
HIGH GRADE GANGUE .......... 51

LOW GRADE GANGUE........................................ 53
**RESIDUAL SOLVENT AT THE END OF THE HIGH MASS FLUX PERIOD ........................................ 56**
**CYCLOHEXANE REMOVAL STAGES ........................................ 58**
**MASS FLUX IN FINAL DRYING STAGES ........................................ 61**
HIGH GRADE GANGUE........................................ 61
LOW GRADE GANGUE........................................ 64
**UNRECOVERED SOLVENTS ........................................ 66**
**BITUMEN MIGRATION ANALYSIS........................................ 67**
**BATCH ENERGY CALCULATIONS ........................................ 72**
HIGH GRADE GANGUE........................................ 72
LOW GRADE GANGUE........................................ 77

**CONCLUSIONS........................................ 82**

**RECOMMENDATIONS ........................................ 84**

**REFERENCES ........................................ 86**

**APPENDIX A – DESIGN CALCULATIONS........................................ 90**

**APPENDIX A1 – VACUUM OVEN ........................................ 90**
DESCRIPTION OF DESIGN ........................................ 90
TIME TO ACHIEVE SET PRESSURE ........................................ 93
CARRIER GAS FLOW RATE SELECTION........................................ 96
CHOICE OF THERMOCOUPLES........................................ 98
SEALING THERMOCOUPLES INTO THE OVEN ........................................ 98
RESIDENCE TIME ........................................ 99
**APPENDIX A2 – BRASS VESSEL ........................................101**
RESIDENCE TIME ........................................103
O-RING DESIGN CALCULATIONS........................................103
PREHEATING THE CARRIER GAS........................................106

**APPENDIX B – CALIBRATION AND VALIDATION OF DSMS........................................110**

**APPENDIX B1 – CALIBRATION OF DSMS ........................................110**
**APPENDIX B2 - VALIDATING THE CALIBRATION ........................................113**

APPENDIX C – MATLAB SCRIPTS ......117

APPENDIX C1 – PUMP DOWN CALCULATION ......117

APPENDIX C2 – CALCULATING LENGTH OF TUBING NECESSARY TO PREHEAT CARRIER GAS ......119

APPENDIX C3 – MAIN SCRIPT USED TO PROCESS THESIS RESULTS ......122

APPENDIX D – ENGINEERING DRAWINGS ......139

APPENDIX D1 – THERMOCOUPLE SEALING ADAPTER ......139

APPENDIX D2 – BRASS DRYING VESSEL ......141

## List of Tables

Table 1 - Composition of Oil Sand Ores Prior to Bitumen Extraction ...... 21

Table 2 – Liquid Content of High and Low Grade Gangue Prior to Drying on Wet Basis ...... 31

Table 3 - Summary of Parameters for Representative Results of High Grade Gangue ...... 36

Table 4 - Summary of Parameters for Representative Results of Low Grade Gangue ...... 39

Table 5 - Coefficients For Antoine Equation Giving Cyclohexane Vapour Pressure in mm Hg ...... 40

Table 6 - Summary of Coefficients for Fitting Mass Flux to Equation 25 ...... 43

Table 7 - Summary of Coefficients for Fitting Subcooling to Equation 26 ...... 49

Table 8 - Summary of Coefficients for Fitting Completion Time to Equation 27 ...... 55

Table 9 - Pump Down Times for Potential Pumps ...... 96

Table 10 –Calculated Values for O-Ring Design ......105

Table 11 - Values Used to Calculate Length of Required Tubing to Preheat Carrier Gas ......108

Table 12 - Linear Calibration Data for Cyclohexane and Water ......113

## List of Figures

Figure 1 - Possible Drying Mechanisms with and without Liquid Films ......7

Figure 2 - Capillary Pressure Causes Liquid in Cylindrical Capillary to Rise ......9

Figure 3 - Formation of Corner Films in a Square Capillary ........ 10
Figure 4 - Schematic of Experimental Apparatus ........ 13
Figure 5 - Computer Generated View of Brass Drying Vessel ........ 13
Figure 6 - Control Volume Used in Derivation of Main Equation........ 16
Figure 7 – Temperature and Pressure Combinations Tested in Data Sets ........ 22
Figure 8 - Energy Inputs to Batch Evaporation Experiments........ 24
Figure 9 - Cyclohexane Content Prior to Drying for High Grade Gangue ........ 27
Figure 10 – Water Content Prior to Drying for High Grade Gangue ........ 27
Figure 11 - Cyclohexane Content Prior to Drying for Low Grade Gangue ........ 29
Figure 12 - Water Content prior to drying for Low Grade Gangue ........ 30
Figure 13 - Mass Flux and Temperature Curves for High Grade Gangue Dried at 25 °C and 300 mbar........ 32
Figure 14- Mass Flux and Temperature Curves for High Grade Gangue Dried At 500 mbar and 95 °C........ 33
Figure 15 - Mass Flux and Temperature Curves for High Grade Gangue Dried At 950 mbar and 45 °C........ 35
Figure 16 - Mass Flux and Temperature Curves for Low Grade Gangue Dried at 300 mbar and 25 °C........ 36
Figure 17 - Mass Flux and Temperature Curves for Low Grade Gangue Dried at 500 mbar and 95 °C........ 38
Figure 18 - Maximum Cyclohexane Mass Flux for High Grade Gangue Plotted with Vapour Pressure on a Different Axis........ 41
Figure 19 - Maximum Cyclohexane Mass Flux with Fitted Model for High Grade Gangue ........ 42
Figure 20 - Maximum Cyclohexane Mass Flux with Fitted Model for Low Grade Gangue ........ 42
Figure 21 - Effect of Initial Cyclohexane Content on Maximum Mass Flux for Low Grade Gangue........ 44
Figure 22 - Ratio of Cyclohexane to Water Mass Flux at the Point of Maximum Cyclohexane Mass Flux for High Grade Gangue........ 46

Figure 23 - Ratio of Cyclohexane to Water Mass Flux at the Point of Maximum Cyclohexane Mass Flux for Low Grade Gangue ... 47
Figure 24 - Degree of Subcooling at Maximum Mass Flux vs. Temperature and Pressure for High Grade Gangue with Fitted Curve ... 48
Figure 25 - Comparison of Sample Temperature and Boiling Point for High Grade Gangue ... 49
Figure 26 - Comparison of Sample Temperature and Boiling Point for Low Grade Gangue ... 51
Figure 27 – Completion Time on a Linear Scale for High Grade Gangue ... 52
Figure 28 – Completion Time on a Logarithmic Scale for High Grade Gangue Including Curve Fit ... 53
Figure 29 - Completion Time on a Logarithmic Scale for High Grade Gangue Including Curve Fit ... 54
Figure 30 – Ratio of Completion Time Between Low and High Grade Gangue ... 56
Figure 31 - Residual Concentration at End of High Mass Flux Evaporation Stage for High Grade Gangue ... 57
Figure 32 - Residual Concentration at End of High Mass Flux Evaporation Stage for Low Grade Gangue ... 58
Figure 33 - Drying Time Broken into Stages for High Grade Gangue at 700 mbar ... 59
Figure 34 - Drying Time Broken into Stages for Low Grade Gangue at 700 mbar ... 60
Figure 35 - Cyclohexane Mass Flux in High Grade Gangue When Residual Concentration was 5000 ppm ... 61
Figure 36 - Cyclohexane Mass Flux in High Grade Gangue When Residual Concentration was 250 ppm ... 62
Figure 37 - Relationship Between Mass Flux and Temperature at Decreasing Concentrations of Cyclohexane for High Grade Gangue ... 63
Figure 38 - Cyclohexane Mass Flux in Low Grade Gangue When Residual Concentration was 250 ppm ... 64
Figure 39 – Relationship Between Mass Flux and Temperature at Decreasing Concentrations of Cyclohexane for Low Grade Gangue ... 65

Figure 40 - Further Mass Loss After Samples Left in Vacuum Oven Over Night for High Grade Gangue ..... 66
Figure 41 - Further Mass Loss After Samples Left in Vacuum Oven Over Night for Low Grade Gangue ..... 67
Figure 42 – High Grade (left) and Low Grade (right) Extraction Gangue after Drying ..... 68
Figure 43 - Assumed Composition of Remaining Gangue ..... 70
Figure 44 - Enrichment Ratio as a Function of Temperature and Pressure in High Grade Gangue ..... 71
Figure 45 - Breakdown of Net Energy Input for Tests Conducted at 300 mbar on High Grade Gangue ..... 73
Figure 46 - Breakdown of Net Energy Input for Tests Conducted at 500 mbar on High Grade Gangue ..... 74
Figure 47 - Breakdown of Net Energy Input for Tests Conducted at 700 mbar on High Grade Gangue ..... 74
Figure 48 - Breakdown of Net Energy Input for Tests Conducted at 950 mbar on High Grade Gangue ..... 75
Figure 49 – Net Energy Input to High Grade Gangue as a Function of Temperature and Pressure ..... 76
Figure 50 - Breakdown of Net Energy Input for Tests Conducted at 300 mbar on Low Grade Gangue ..... 77
Figure 51 - Breakdown of Net Energy Input for Tests Conducted at 500 mbar on Low Grade Gangue ..... 78
Figure 52 - Breakdown of Net Energy Input for Tests Conducted at 700 mbar on Low Grade Gangue ..... 78
Figure 53 - Breakdown of Net Energy Input for Tests Conducted at 915 mbar on Low Grade Gangue ..... 79
Figure 54 - Net Energy Input to Low Grade Gangue as a Function of Temperature and Pressure ..... 80
Figure 55 - Schematic for Original Experimental Apparatus ..... 91
Figure 56 - Original Experimental Apparatus ..... 92

Figure 57 - Apparatus to Embed Thermocouples in Sample ........ 93
Figure 58 - Pump Curve for Vacuubrand MD 4 NT Vario ........ 94
Figure 59 - Predicted Pump Down Curve for MD 4 NT Vario ........ 95
Figure 60 - Adapter to Seal Thermocouples into Vacuum Oven ........ 99
Figure 61 - Schematic for New Apparatus ........ 101
Figure 62 - Computer Generated Sectional View of Brass Drying Vessel........ 102
Figure 63 - Calculated Air Temperature vs. Tube Length for Preheated Carrier Gas ........ 109
Figure 64: Calibration Setup Schematic ........ 110
Figure 65 - DSMS Calibration Data for Cyclohexane........ 112
Figure 66 - DSMS Calibration Data for Water ........ 112
Figure 67 - Results from Validation Runs ........ 114
Figure 68 - Renormalized Results from Validation Runs ........ 116

# Introduction

The oil sands deposit located in Alberta, Canada represents a vast source of wealth and energy. With proven reserves of 167.9 billion bbl, the deposit is the third largest crude oil reserve in the world after Venezuela and Saudi Arabia[1]. It is estimated that 20% of the reserves may be recovered by mining operations, while the remaining 80% must be recovered through in-situ techniques[1, 2]. The deposit underlies an area of 142,200 square kilometers, of which 4,800 square kilometers is close enough to the surface to be mined [2].

## Current Commercial Extraction Processes

Oil sand that is located more than 75 m below ground must be recovered in place by drilling wells, known as in-situ recovery. Steam assisted gravity drainage (SAGD) is the current industrial standard technique for in-situ recovery. In this process, two parallel horizontal wells are drilled into lower part of the oil sands formation. Steam is injected into the upper well in order to heat the bitumen and reduce its viscosity. The bitumen then drains with the condensed steam to the lower well, where it is collected and pumped to the surface[3]. A recent study has found that well to wheel carbon emissions per barrel of oil extracted through SAGD and upgraded to synthetic crude oil prior to shipping were 19% higher than the U.S. average, while the emissions from oil produced from mining operations and shipped to refineries as diluted bitumen were only 1% higher[4]. This thesis will be focused on the treatment of bitumen recovered by oil sands mining operations.

In an oil sands mining operation, oil sand ore is stripped from the mine by large excavators and brought to an extraction facility in large trucks. The ore is blended with hot water, and the slurry is piped downstream to separation vessels. The bitumen is extracted through a flotation process where bitumen is separated from the sand and floats to the top of the vessel with the help of added air. The froth is collected from the top and treated to remove fine particles and water leaving clean bitumen product.

## Disadvantages of Current Commercial Process

Bitumen has been successfully extracted using this process at an industrial scale since the first operation started in 1967, producing 45,000 bbl of crude oil per day[5]. Since then, the operation has expanded significantly. Daily production from the oil sands is now estimated at 1.9 million bbl per day [1, 2], and is forecasted to increase further to 3.8 million bbl per day by 2020[1]. The process has proven to be economical; however it has a limitation of producing tailing ponds that cause significant environmental problems.

The current industrial standard hot water extraction process produces wet tailings that make land reclamation extremely difficult. The tailings consist of process affected water mixed with sand, clay, residual bitumen, and chemical aids used in the process. In order to recycle the water in the process, tailings must be stored in large settling basins, or tailings ponds. The heaviest sand particles settle to the bottom of these ponds, and the water floats to the top where it can be recycled. The fine clay particles, however, form a sludge layer in the middle known as fluid fine tailings (FFT). Over a period of 3 to 5 years, fluid fine tailings settle until they stabilize at a solids concentration of 30-40 wt%, at which point they are known as mature fine tailings (MFT), which will not settle further without expensive treatment[6]. Syncrude is spending $1.9 billion on a centrifuge facility to treat FFT that will open in 2015[7].

The difficulty in treating the tailings ponds has led to accumulation over time, and ponds now contain 720 million $m^3$ of process affected area and cover an area greater than 170 $km^2$[8]. A recent study has confirmed the long standing suspicion that tailings ponds leach chemicals like naphthenic acids into the ground water, which is likely to feed into the Athabasca river[9]. It has also been found that polycyclic aromatic hydrocarbons, which are carcinogenic pollutants, are also being released into the air from tailings ponds [8, 10]. Furthermore, tailings ponds present a risk to wildlife such as migratory birds that have been known to land in the ponds despite attempts to keep them away[11]. These problems are small compared to the massive risk associated with a tailings pond breach that could release catastrophic amounts of poisonous chemicals into the Athabasca river. This concern was highlighted when a tailings pond of an upstream coal mine was breached in 2013[8].

Another problem with hot water extraction is that the current water based extraction process is ineffective for “poor processing ores” [12-18]. Oil sand ores that do not process well with the current method often have too large an amount of fine particles that attach to bitumen droplets during the extraction process. This is problematic because it prevents air bubbles from attaching to bitumen droplets, thereby decreasing the efficiency of bitumen rising to the froth. The quality of froth is also reduced, increasing the treatment required for fine solid separation. [12]. The hot water extraction process also requires that oil sand ores be dominated by hydrophilic particles and contain a thin film of water acting as a barrier between the particles and the bitumen. As the bitumen is not in direct contact with the particles, it is easily liberated from them by hot water. Without this property, it would be infeasible to extract bitumen from oil sands with a water based extraction process[12]. Even high grade oil sand ores contain some hydrophobic particles, and thus 100% recovery of bitumen is not feasible using the hot water extraction method.

## Non aqueous extraction processes

As a result of the problems associated with the hot water extraction method, oil sands companies are looking for alternatives. One promising method that has been gaining traction is non-aqueous extraction, also known as solvent based extraction. In this process, water, which is immiscible with bitumen, is replaced by a hydrocarbon solvent that readily dissolves bitumen. Thus, the mechanism of bitumen recovery shifts from a flotation process, that only works on high grade oil sands, to a washing type process. As a result, the sensitivity of bitumen recovery to the grade of oil sand is significantly reduced and good bitumen recovery can be achieved even with low grade ores[13-19].

Non-aqueous extraction takes many different forms. The use of ionic liquids in conjunction with hydrocarbon solvents has received some attention lately [13, 20, 21]. Ionic liquids, which are salts in a liquid state, work by engaging in electrostatic reactions with the surfaces of solids that decrease the adhesive forces between bitumen and silica[21]. Bitumen recovery higher than 90% with minimal fine solids in the product was reported[13, 20, 21]. However, ionic liquids need to be separated from water after recovery by distillation, which will be energy intensive due to the high heat capacity and enthalpy of vaporization of water. The organic solvent will also need to be recovered from the bitumen product by distillation.

Solvent extraction using a switchable hydrophilicity solvent, where the wettability of the solvent can be altered by the presence or lack of carbon dioxide, has also been investigated[17]. The study found promising results both in terms of bitumen recovery and product quality, but the long residence times required on the lab scale may be problematic when scaling up to an industrial scale. In both of the above extraction methods, water is used to recover solvent from the waste stream.

Some work has also been done researching water assisted solvent extraction, where water is used with a hydrocarbon solvent in order to reduce fines content in the extracted bitumen[18, 22]. Yang et al. found that introducing a water layer made it easier to separate the bitumen product from the solids, and reduced fines content in the product by more than half when treating Chinese oil sands[18]. Nikakhtari et al. studied the effect of adding water to a solvent extraction process with Athabasca oil sands. They found that while connate water already in the oil sand played a very important role in preventing fines from migrating to the product, additional water did not reduce fines migration[22].

One common concern for all three of the above treatments is that because water is used in the process, wet tailings will still be produced. Non-aqueous extraction using only a volatile hydrocarbon solvent on the other hand, can produce dry extraction gangue suitable for backfilling a mine[23]. Many research studies have been carried out to investigate solvent extraction using hydrocarbon solvents[14-16, 19, 22-33]. In each of these studies, solvent was assumed to be recovered through evaporation so that it can be recovered and recycled.

Kenchington and Phillips performed an economic sensitivity analysis of operating costs in a solvent extraction process [34]. The model was based on an extraction system with a multi-stage counter current washing process that, like all solvent based extraction processes, produced a waste stream of coarse and fine solids mixed with residual solvent and water. This waste stream will hereafter be referred to as gangue. Solvent was to be recovered from the gangue using steam stripping, and from the product using steam distillation. Due to the heating costs associated with the solvent recovery processes, they found that minimizing the ratio of solvent to oil sand was critical to achieving profitability. As a result, they recommended a multi-stage process to minimize the amount of solvent used in the process. It was also reported that choice of solvent played a big role in cost effectiveness, more volatile solvents were preferable to less volatile ones. They also found that solvent recovery from the gangue was the most significant economic parameter. The cost sensitivity per percentage point recovery of solvent was over 20 times as significant as that for recovery of bitumen, which was the next most sensitive parameter Furthermore, the difficulty in achieving efficient solvent recovery from extraction gangue is a major limitation for non-aqueous extraction to work on a commercial scale [19].

Some interesting work has been done regarding solvent recovery from non-aqueous extraction gangue. Three separate studies showed drying curves to illustrate the recovery of solvent from residual solids at ambient temperatures[14, 23, 24]. Funk et al. observed that drying rates significantly decreased after the unbound solvent had been extracted, and only 1 to 3% of the original solvent remained. Tests performed on gangue from a pentane extraction showed that a drying temperature 65 °C higher than the boiling point of pentane was required to fully vaporize the solvent in the gangue. To compensate for this, they recommended a two stage drying process with separate fluidized beds for each stage. The first stage is completed using superheated solvent as a carrier gas to simplify the recycling of solvent, and the final 1-3% is recovered in a second stage using nitrogen as a carrier gas[31]. Yu et al. found that the amount of residual solvent found in the gangue prior to drying increased by 42% when median particle diameter in the oil sand decreased from 1335 μm to 125 μm[14], and Hooshiar et al. suggested that clay minerals are responsible for poor recovery of solvent from extraction gangue[19]. It is possible that the effect is a result of capillary condensation where solvent remains in a liquid phase because it is trapped in small pores.

## Permissible Solvent Losses

The Alberta Energy Regulator sets a limit for solvent losses in the current water based extraction process of 4 volumes of solvent lost per 1000 volumes of bitumen produced, and companies have managed to sustain losses as low as 3 $m^3$/1000 $m^3$. Nikakhtari et al. found that a residual solvent concentration of 260 ppm by dry mass would exceed current industry performance for an average grade ore with 10 wt% bitumen[24]. A goal residual cyclohexane concentration of 250 ppm was set for this work to ensure that environmental regulations can be met.

## Drying Mechanism

In order to build a model of the solvent removal process, a strong understanding of the underlying mechanism of solvent removal from the extraction gangue is critically important. The process being investigated here is two phase drying of porous media wetted by light hydrocarbon solvents, water, and residual bitumen. Drying of porous media under these circumstances is underrepresented in the literature, but drying of porous media wetted by water has been thoroughly studied and that literature can give useful insights on the mechanism of drying under these circumstances.

Drying of Porous media can be thought of as a drainage process where air penetrates the pores and replaces the evaporating liquid [35]. There are two basic drying mechanisms that must be considered. The most intuitive drying mechanism features liquid evaporating inside the pores of the drying material and diffusing to the surface in the vapour phase. It is also possible, however, that hydraulic connectivity is maintained between the saturated pores below the drying front and the surface via a liquid film that is maintained as a result of capillary pressure[35-38]. In this scenario, liquid moves towards the free surface and evaporates there. Figure 1 shows these first two scenarios, as well as a third scenario where liquid films still act as a transport mechanism to move liquid towards the free surface, but evaporation still occurs in the substrate.

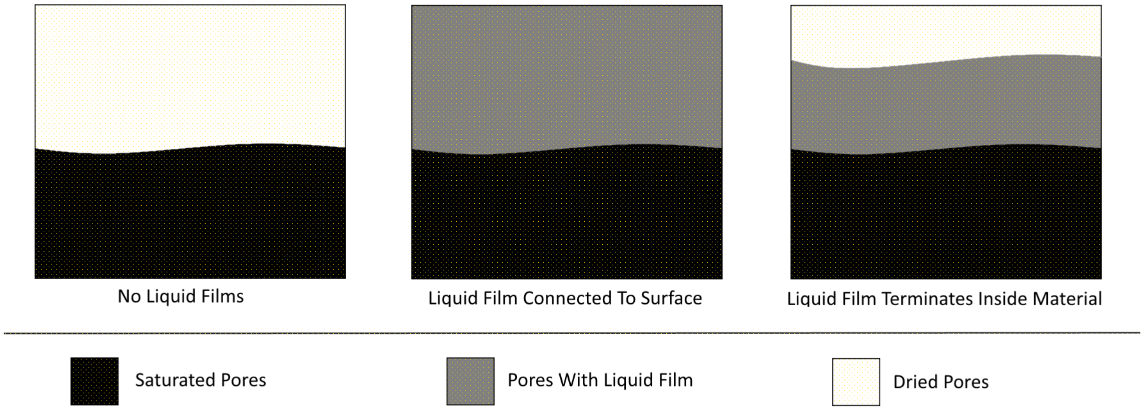

Figure 1 - Possible Drying Mechanisms with and without Liquid Films

It has been observed that when liquid films are present, the drying rate drastically increases [35, 36, 38, 39] especially when the liquid film maintains connectivity with the free surface [36]. These films form as a result of capillary forces within the pores of the material. To better understand how capillary forces influence liquid movement, an example of a cylindrical capillary is used. Capillary pressure, which is the difference in pressure between the liquid and gas phase, is easy to derive for a cylindrical capillary. It is derived from the well known Young-Laplace equation to calculate the pressure difference between two substances or phases.

$$\Delta P = \gamma \left( \frac{1}{R_1} + \frac{1}{R_2} \right) \tag{1}$$

The pressure difference is proportional to the interfacial tension, $\gamma$, and inversely proportional to the two principal radii of curvature of the interface. In the specific case of a cylindrical capillary, the meniscus forms a spherical interface with a radius equal to $r/\cos\theta$, where $r$ is the radius of the capillary and $\theta$ is the contact angle between the wetting liquid and solid capillary. The resulting equation for capillary pressure is as follows:

$$P_c = P_{gas} - P_{liquid} = \frac{2\gamma\cos\theta}{r} \tag{2}$$

When the contact angle is between 0 and 90°, meaning the liquid wets the capillary wall, the formation of the meniscus will result in a suction pressure within the liquid that will cause the liquid to rise in the capillary as is illustrated in Figure 2. Electrostatic forces between the solid capillary wall and the liquid molecules as well as between liquid molecules cause the meniscus to form and create suction pressure that causes the liquid to rise.

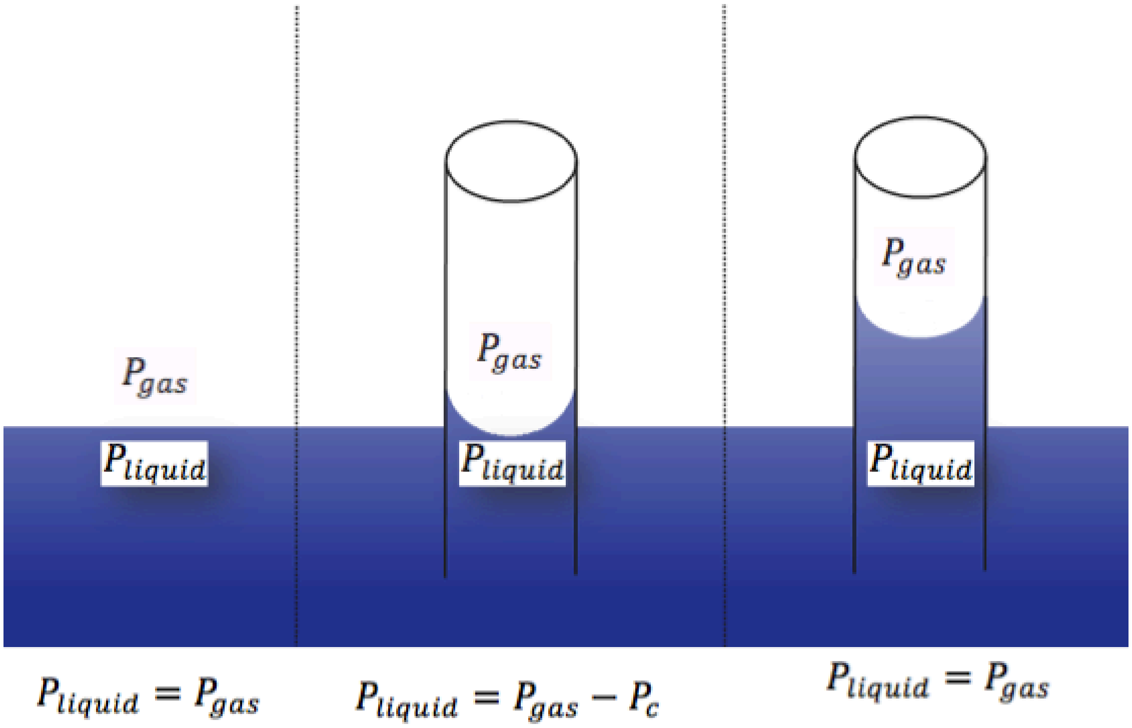

Figure 2 - Capillary Pressure Causes Liquid in Cylindrical Capillary to Rise

In real extraction gangue, solids will form uneven pores, and a cylindrical capillary is inadequate to represent the real geometry. A slightly more complex geometry that has been used to help understand the real geometry is a capillary with a square cross section [35, 36] as is shown in Figure 3.

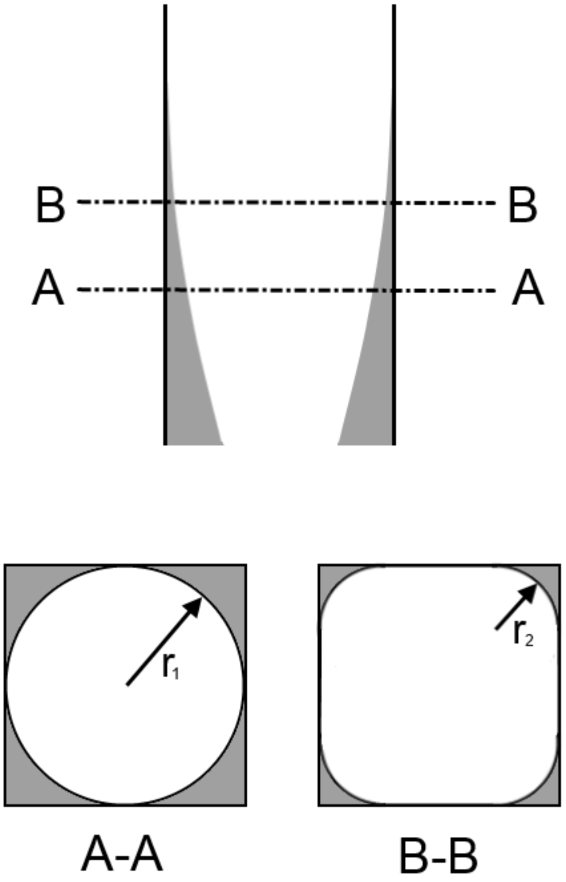

Figure 3 - Formation of Corner Films in a Square Capillary

A liquid film is formed in the corners of the square capillary. Capillary pressure inside this liquid film is inversely proportional to the radius of curvature of the film. As is shown in Figure 3, the thickness of the corner film and its radius of curvature decreases as the liquid moves farther from its source, and the suction pressure drawing the liquid up increases as a result. This is balanced by evaporation, which occurs mainly at the film tips as the gas phase becomes quickly saturated with evaporated vapour closer to the liquid source[35]. It has been demonstrated that these corner films drastically increase the overall rate of evaporation in capillaries [36], and that the presence of thick liquid films such as those formed in the corners of real pores will also increase the rate of evaporation [35, 36]. It is emphasized that the increased rate of evaporation is the result of liquid transport decreasing the need for vapour diffusion within the porous media, since evaporation is practically restricted to the film tips [35].

It has been observed in the literature that liquid films will only form when the solids are wetted by the evaporating liquid [37]. More specifically, Shokri et al. found that when hydrophilic particles were placed beside hydrophobic particles, evaporating water migrated to the hydrophilic side and the majority of the evaporation occurred on that side due to capillary forces drawing water to hydrophilic materials and then pushing it towards the surface. Dye dissolved in the water was deposited only on the surface of the hydrophilic side because capillary forces on that side pushed liquid water to the surface, and the dye was left behind when water evaporated[37]. In the case of extraction gangue where cyclohexane is evaporating, liquid films will only form where the solids are hydrophobic. This becomes relevant when considering that extraction gangue will contain some particles that are hydrophobic and some that are hydrophilic, indicating that preferential pathways will form allowing liquid cyclohexane to migrate upwards near hydrophobic solids.

It was also noted in preliminary experiments that bitumen migrated upwards during the drying process and left a film of bitumen on the surface of the dried gangue. A similar trend has been observed in the literature when salts are dissolved in evaporating water[38]. When water migrates to an evaporating surface in the liquid phase and evaporates there, it leaves behind dissolved salt on the surface forming what is known as an efflorescence. Efflorescence formation was drastically increased when hydrophilic particles were used compared to hydrophobic particles, indicating that liquid films played a major role in the migration of salt [38]. Measuring the extent of bitumen migration will help to determine how much of a role liquid films play in the drying process, which will ultimately help to build a model of the solvent removal process.

## Objectives

Given how critical solvent recovery is to the commercial viability of solvent based extraction, it is surprising that so little work has been done studying the recovery of solvent from extraction gangue. There is a gap in the literature on this subject, and this thesis will take steps towards filling this gap, laying the foundation for future work. The objective of this work is to give further understanding of the solvent recovery process.

The variables that are considered to be the most important are the amount of time and energy input that are necessary to achieve complete recovery of cyclohexane. This work will measure these variables and how they respond to changing process temperature between 25 and 105 °C, and pressure from 300 to 950 mbar. An experimental apparatus was designed to accurately control and measure process temperature and pressure during solvent removal. Accurate thermocouples will measure temperature of the oven, and inside the sample, while a calibrated DSMS will be used to separately measure mass flux of both cyclohexane and water. Measurements will help understand the effect of temperature and pressure on mass flux both in the steady state period and the decaying rate period when the last of the cyclohexane is removed. Inferences into the mechanism of solvent removal, and how it changes with changing process temperature and pressure will be drawn from measurements if they are consistent with known mechanisms.

## Methodology

In order to measure the evaporation rate of both cyclohexane and water under increased temperature and decreased pressure, an apparatus was designed. The detailed design of the apparatus is outlined in Appendix A – Design Calculations. The apparatus is pictured schematically in Figure 4 below.

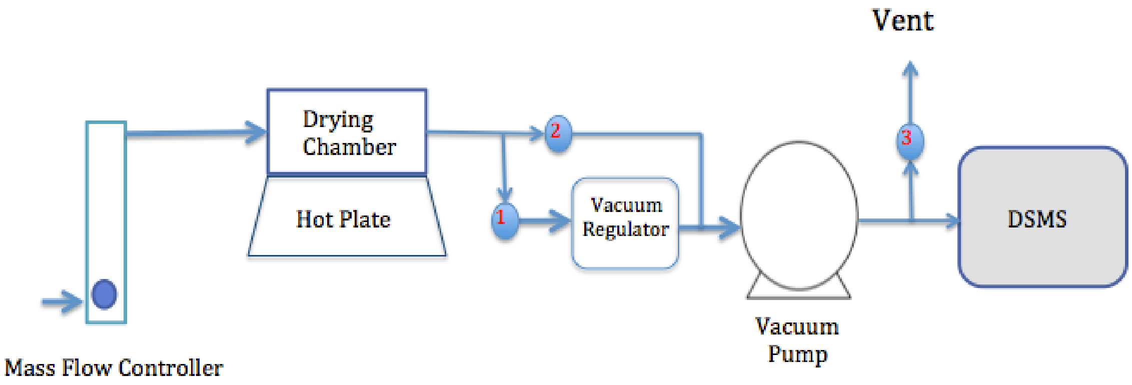

Figure 4 - Schematic of Experimental Apparatus

The apparatus featured an electronic mass flow controller (Omega FMA-7407) to maintain constant flow rate of nitrogen carrier gas through the experiment. A vacuum regulator (Equilibar EVR-2) was used in conjunction with a vacuum pump (Vacuubrand MD 4 NT Vario) to maintain constant pressure. Temperature was controlled by placing a specially designed brass drying vessel, shown in Figure 5, on a hot plate with electronic temperature control. A Dynamic Sampling Mass Spectrometer (DSMS) from Hiden Analytical was used to detect how much water and cyclohexane were evaporating from a sample in the drying chamber at any given time.

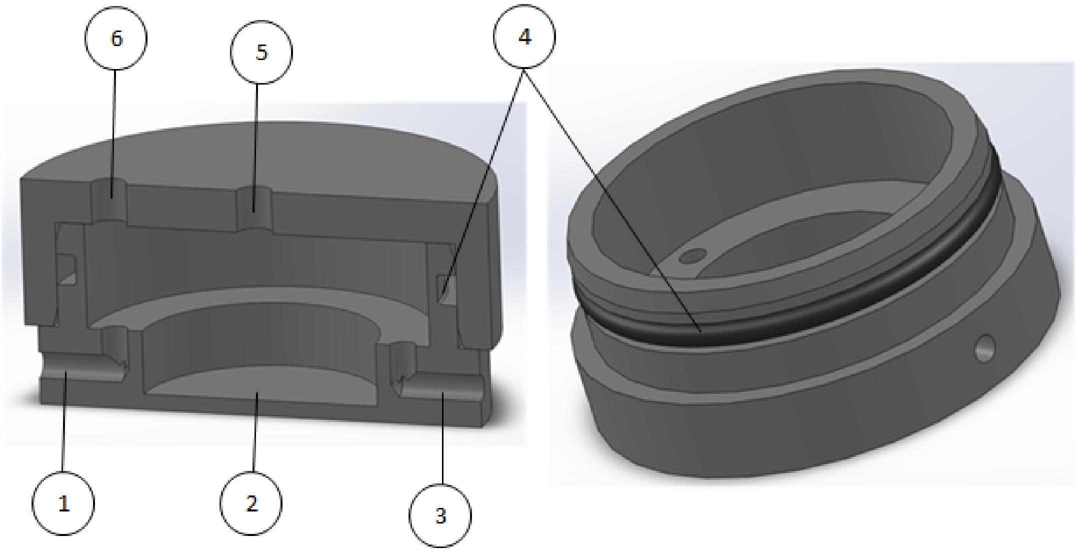

Figure 5 - Computer Generated View of Brass Drying Vessel

Figure 5 shows a computer generated sectional view of the drying vessel on the left, and a full view of the base of the vessel on the right. The vessel consisted of a base and a lid that were sealed with an O-ring (4). Nitrogen carrier gas flowed in through the inlet (1), picked up vapours that had evaporated from the sample in the recess (2), and exited the vessel through the outlet (3). Type T thermocouples were sealed in through a port in the lid (5) to measure temperature during the experiment. Two thermocouples were placed inside the sample at heights of 2 and 4 mm to measure temperature within the sample during the experiment, and a third was placed in the middle of the chamber to measure air temperature in the vessel. At the end of the experiment, the temperature readings of all 3 thermocouples were identical. A pressure transducer was sealed in through a port in the lid of the drying vessel (6) to measure pressure in the vessel throughout the experiment. Another pressure transducer and thermocouple were placed after the vacuum pump to measure pressure and temperature at the point from which the DSMS sampled

Prior to the start of each experiment, the hot plate was turned on and nitrogen gas was passed through the system for at least an hour to establish a stable starting point for all equipment in the system. At the start of each experiment, a previously prepared jar of non-aqueous extraction gangue was taken from a freezer held at -13 °C and left sealed for some time to thaw. The thaw time was kept constant at 10 minutes for high grade gangue and 20 minutes for low grade gangue. Next, a 15 g sample of the wet gangue was weighed into a tin dish. The sample was placed in the recess at the bottom of the drying chamber, and the chamber was sealed fixing the thermocouples in place. Nitrogen carrier gas was passed over the sample at a rate of 1 SLPM to carry the solvent from the sample, through the vacuum regulator and pump, and to the DSMS for detection. The point of detection was held at the atmospheric pressure of the lab by a vent connected to a fume hood. The DSMS only sampled a very small portion of the outlet gas, but its signal was directly proportional to concentration of solvent vapour at the outlet, so it was acceptable to vent the majority of gas to the fume hood.

After each experiment was completed, the sample was weighed after drying to determine the total mass loss so that it could be compared to the total mass loss measured by the DSMS. It was then placed in a vacuum oven overnight at a temperature of 70 °C and a pressure below 150 mbar. It was weighed again after removal to determine the residual volatile content. The data from all sensors as well as the DSMS was processed after the experiment and the results can be found in the results and discussion section of this thesis.

### Converting Instrument Readings to Evaporation Rates

The DSMS was calibrated to measure the concentration of cyclohexane and water in g/ml, using the method described in Appendix B1. As the calibration was performed at atmospheric pressure, the DSMS was connected to the outlet of the vacuum pump, rather than directly to the drying chamber held under vacuum. After evaporating from the sample, the solvent vapour was swept out by the carrier gas, and travelled through the vacuum pump to the DSMS. There was also a constant leak of atmospheric air into the system that was necessary to maintain a set point pressure in the drying chamber. This leak diluted the DSMS signal at the point of sampling. As a result of these factors, a direct integration of the DSMS signal with respect to time would be insufficient to obtain a mass balance for the solvent removed from the sample. To compensate, a differential equation was derived to give the rate of solvent removal at any given time in the experiment.

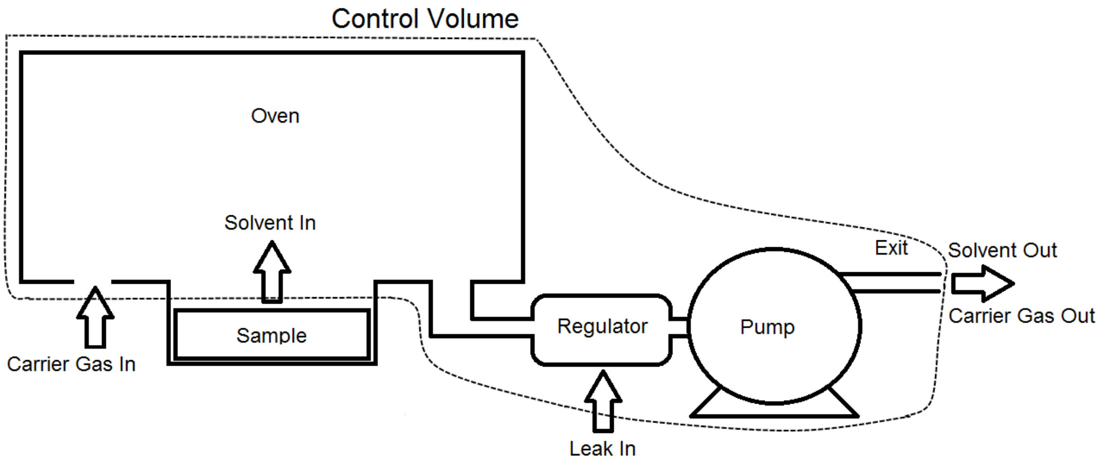

Figure 6 - Control Volume Used in Derivation of Main Equation

Figure 6 shows the control volume (CV) that was used in this derivation. The CV encapsulates the drying chamber, or oven, as well as the pump, vacuum regulator, and all the tubing in between. The sample is not considered as a part of the CV, so that solvent first enters when it evaporates from the sample. Nitrogen carrier gas enters the CV on the left, and exits together with evaporated solvents and leaked in air on the right, where they were detected by the DSMS.

The exit of the CV is at atmospheric pressure, but the oven is at a lower pressure. As a result, the derivation must be conducted with concentration in terms of mole fraction, which is independent of pressure, instead of concentration by volume.
Since all fluid is moving in these experiments, mole fraction is defined in terms of molar flow rates:

$$y = \frac{\dot{n}_{solvent}}{\dot{n}_{total}} \tag{3}$$

The mole fraction just before the pump will be equal to the mole fraction just after the pump. However, the mole fraction will be diluted at the point of measurement by the leaked in air. The ratio of mole fractions is calculated using the molar flow rates of the leak, the carrier gas, and the solvents.

$$f = \frac{y_{oven}}{y_e} = \frac{\dot{n}_{solvent} + \dot{n}_{carrier}}{\dot{n}_{solvent} + \dot{n}_{carrier} + \dot{n}_{leak}} \tag{4}$$

Molar flow rate of the carrier gas can be easily calculated using the ideal gas law, as the mass flow controller was calibrated to give volume flow rate at standard temperature and pressure. The molar flow rate of the leak at the vacuum regulator was calculated by measuring the partial pressure of oxygen at the pump exit. Since the carrier gas is pure nitrogen, the only way for oxygen to get into the system was for atmospheric air to leak in. An oxygen reference signal, $S_{O2,ref}$, was taken by the DSMS with the probe exposed to atmospheric air, which was assumed to be 21% oxygen, and the calibration for partial pressure was assumed to be linear with a zero intercept. Thus, the partial pressure of oxygen at the exit can be calculated using the DSMS reading for oxygen, $S_{O2}$.

$$P_{O2} = 0.21 P_{atm} \frac{S_{O2}}{S_{O2,ref}} \tag{5}$$

Neglecting the partial pressure contribution of the solvents, the ratio of partial pressure attributed to the leak to that of the carrier gas is equal to the ratio of molar flow rates.

$$\frac{P_{leak}}{P_{carrier}} = \frac{\dot{n}_{leak}}{\dot{n}_{carrier}} \tag{6}$$

Since the partial pressure at the exit from the leak is only 21% oxygen, the partial pressure attributed to the leak was calculated by dividing oxygen partial pressure by 0.21. The leak rate was assumed to be constant throughout the experiment. Using these assumptions in conjunction with the above equation, an equation for average leak rate was derived.

$$\dot{n}_{leak} = \dot{n}_{carrier} \frac{P_{O2}}{0.21P_{atm} - P_{O2}} \tag{7}$$

While the leak rate can be assumed constant, cyclohexane and water have an expanding effect on the total flow rate at the output that varies with time. The partial pressure of cyclohexane and water at the exit was measured directly using the calibrated DSMS signals. The ratio of solvent molar flow rate to total molar flow rate is used to derive an equation for both water and cyclohexane.

$$\frac{\dot{n}_{solvent}}{\dot{n}_{total}} = \frac{P_{solvent}}{P_{total}} \tag{8}$$

Expanding the total molar flow rate and pressure and grouping like terms gives:

$$\dot{n}_{cyclo} = \frac{P_{cyclo}(\dot{n}_{carrier} + \dot{n}_{leak} + \dot{n}_{water})}{P_{atm} - P_{cyclo}} \tag{9}$$

$$\dot{n}_{water} = \frac{P_{cyclo}\left(\dot{n}_{carrier} + \dot{n}_{leak} + \dot{n}_{cyclo}\right)}{P_{atm} - P_{water}} \tag{10}$$

The above equations are not independent, but can be substituted into each other to give molar flow rates of each solvent based on measurable properties.

$$\dot{n}_{cyclo} = \frac{P_{cyclo}(\dot{n}_{carrier} + \dot{n}_{leak})}{P_{atm} - P_{cyclo} - P_{water}} \tag{11}$$

$$\dot{n}_{water} = \frac{P_{water}(\dot{n}_{carrier} + \dot{n}_{leak})}{P_{atm} - P_{cyclo} - P_{water}} \tag{12}$$

The molar flow rate of each species as well as the total molar flow rate was calculated. Using the ideal gas law with previously derived equations, an expression for the total volume flow rate at the pump exit was obtained.

$$Q_e = \frac{\left(\dot{n}_{carrier} + \dot{n}_{leak} + \dot{n}_{cyclo} + \dot{n}_{water}\right) R T_e}{P_{atm}} \tag{13}$$

Finally, the molar concentration of each solvent at the exit was calculated using the ideal gas law. Multiplying by molar mass gives concentration in g/ml, which can be directly measured using the calibrated DSMS.

$$C_e = \frac{\dot{n}_{solvent}}{Q_e} M_{solvent} = y_e \frac{P_e}{RT_e} M_{solvent} \tag{14}$$

All properties in the equation above are known or can be measured except for the mole fraction. Re-arranging the above equation yields an equation to find the mole fraction at the exit using known parameters.

$$y_e = \frac{C_e R T_e}{M_{solvent} P_e} \tag{15}$$

Returning to the control volume in Figure 6, the main equation can now be derived by taking a mass balance on the solvent inside the control volume. In other words, the molar flow rate of solvent in minus the molar flow rate of solvent leaving must equal the rate of change of solvent in the CV. The only source for solvent to enter the control volume is by evaporating from the sample. To calculate the rate of change of solvent in the CV, it is assumed that the gas inside the CV behaves as an ideal gas. Neglecting the volume of tubing between the vessel and the DSMS as well as the volume of the vacuum pump gives the following formula:

$$\frac{\dot{m}_{evap,solvent}}{M_{solvent}} - \frac{C_e Q_e}{M_{solvent}} = \frac{V_{oven} P_{oven}}{R T_{oven}} \frac{d y_{oven}}{dt} \tag{16}$$

Substituting in the equation for mole fraction and the previously defined ratio of mole fractions, f, the above equation can be re-arranged to solve for evaporation rate of the solvent using only known parameters. After a chain rule expansion, the time derivative of the ratio of mole fractions, f, as well as the pressure and temperature inside the oven were found to be negligible and were removed. The resulting equation converting outlet concentration as measured by the DSMS to evaporation rate is given below.

$$\dot{m}_{evap,solvent} = C_e Q_e + f \frac{V_{oven} P_{oven} T_e}{P_e T_{oven}} \frac{dC_e}{dt} \tag{17}$$

The above equation was solved numerically using the Matlab code found in Appendix C3. Validation work shown in Appendix B2 found that a final step was necessary to improve accuracy. A linear correction factor was applied to the DSMS signals for cyclohexane, water, and oxygen to force parity on the total mass measured by the DSMS and the total mass lost in the experiment as measured by an accurate balance.

$$Correction\ Factor = \frac{m_{loss,balance}}{m_{measured,cyclo} + m_{measured,water}} \tag{18}$$

### Samples Tested

In order to produce results that would translate directly towards non-aqueous extraction on an industrial scale, all drying experiments were performed on non-aqueous extraction gangue. The gangue was produced from Athabasca oil sand extracted according to the procedure used by Nikakhtari et al[24]. Using extraction gangue has inherent disadvantages in that the ratios of cyclohexane, water, bitumen, sand, and clay cannot be directly controlled. However, non-aqueous extraction gangue from experiments was considered to be more representative of the gangue that would be produced on an industrial scale than a reconstituted sample. Extraction gangue is produced from oil sand that has developed underground over thousands of years, contains connate water that directly coats sand and clay, and has bitumen spread out between its pores. Cyclohexane was used to extract the bitumen in a way that is similar to what would be practical on an industrial scale. It would be difficult to produce reconstituted gangue with water coating the sand and clay, and to replicate other properties of extraction gangue that could affect drying but are as yet unknown. Therefore, experiments were performed on extraction gangue.

Tests were performed on extraction gangue produced from both low and high grade oil sand ore. The water and bitumen contents of both grades of oil sand ore were measured by exhaustive dean stark extraction repeated 6 times, and the fines content was measured using repeated runs on a particle size analyzer. Table 1 below gives the shows the measured water, bitumen, and fine solids contents for both grades of ore prior to bitumen extraction. Values are reported in mean wt% ± standard deviation with the number of tests conducted. The remainder of the mass was made up of coarse solids.

**Table 1 - Composition of Oil Sand Ores Prior to Bitumen Extraction**

| | Mass Fraction in Low Grade Gangue (wt%) | Mass Fraction in High Grade Gangue (wt%) |
|---|---|---|
| Water | 10.7 ± 0.2 (n=6) | 3 ± 0.9 (n=6) |
| Bitumen | 3.4 ± 0.4 (n=6) | 13.5 ± 1.1 (n=6) |
| Fine Solids (<45 um) | 19.4 ± 0.9 (n=2) | 11.2 ± 0.7 (n=3) |

Prior to extraction, low grade ore contained significantly more water and fine solids than high grade ore, and the differences are expected to have a significant impact on the gangue produced. Both ores were processed through bitumen extraction in an identical manner and the gangue that was produced, which are referred to as low and high grade gangue, was stored in a freezer at -13 °C for later processing.

## Temperature and Pressure Combinations Tested

In order to determine the effects of pressure and temperature on the time and energy required to remove solvent from gangue, oven temperature and pressure were varied between tests. Experiments were conducted on high grade gangue between 25 and 95 °C with an increment of 10 °C and at absolute pressures of 300, 500, 700 mbar, and the atmospheric pressure in the lab of 950 mbar. Each combination was tested twice, and 2 additional runs were conducted at 105 °C and 950 mbar for a total of 66 experiments. An identical set of conditions was tested for low grade gangue, with the exception that the atmospheric simulation pressure was changed after it was discovered that atmospheric pressure in the lab varied from 920 to 960 mbar. An pressure of 915 mbar was used instead of 950 mbar to give a higher level of consistency between runs. Figure 7 below outlines the pressure and temperature combinations tested in a graphical form.

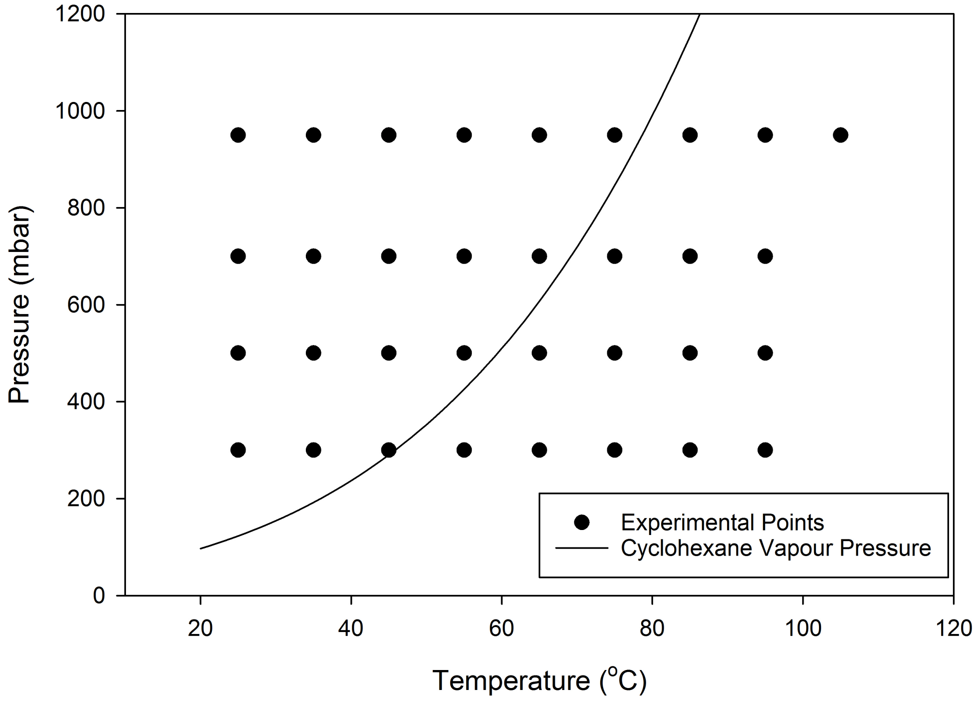

Figure 7 – Temperature and Pressure Combinations Tested in Data Sets

Each extraction that was performed on oil sand ore produced 4 jars of gangue weighing approximately 150 g each. All jars were stored in a freezer immediately after extraction and in between all drying experiments to prevent evaporative losses. To compensate for any discrepancies between jars, each repeated run on the same temperature and pressure was performed using a different jar than the previous run. More specifically, 2 jars were chosen for use at a constant temperature, with one test per jar for each pressure tested. This was done so that any large deviations from a curve could be explained by the discrepancies between jars, and runs could be repeated to verify.

The 66 experiments described above constitute one data set. One data set was obtained using low grade gangue, and a separate data set was obtained using high grade gangue.

## Bitumen Migration Analysis

Over the course of the drying experiments, bitumen migrated upwards and the gangue formed 2 or 3 distinct layers with varying bitumen content. The layers were carefully, separated, weighed, and collected in vials for carbon content analysis using an elemental analyzer (Elementar Vario Micro Cube). The analyzer makes use of combustion analysis techniques whereby the samples are burned in excess oxygen at 1200 °C, and the gas combustion products are measured. The machine measures the elemental breakdown of each sample, giving the percentage by mass of Carbon, Hydrogen, Nitrogen, and Sulfur. Prior to analysis, the gangue in each vial was thoroughly mixed so that the carbon percentage measured from any small sample taken would be representative of the average carbon percentage of the entire layer. 15 mg samples were analyzed with the elemental analyzer, and analysis was carried out in triplicates.

## Batch Energy Calculations

In order to better understand the energy requirements to recover cyclohexane from gangue, the energy use in these batch experiments was calculated. Net Energy input was defined as the additional energy that needed to be added to the sample to achieve evaporation compared to a base case of evaporation in open air at 25 °C. In open air, all cyclohexane and water will evaporate with energy supplied by the surroundings. The extent of water removal at the point when cyclohexane has been completely removed from the system was expected to vary with temperature and pressure, but measured water content in both high and low grade data sets was too variable to be able to draw conclusions on this. For these reasons, the energy to evaporate cyclohexane and water was not included in these calculations.

Energy requirements were broken down into 5 categories: energy to heat the sand, carrier gas, cyclohexane, and water, along with energy to maintain vacuum throughout the experiment. Figure 8 gives a summary of energy inputs to the experiment. The amount of energy needed to evaporate liquids is included in Figure 8 because they will make a contribution to energy requirements on an industrial scale, but they were not included in this analysis.

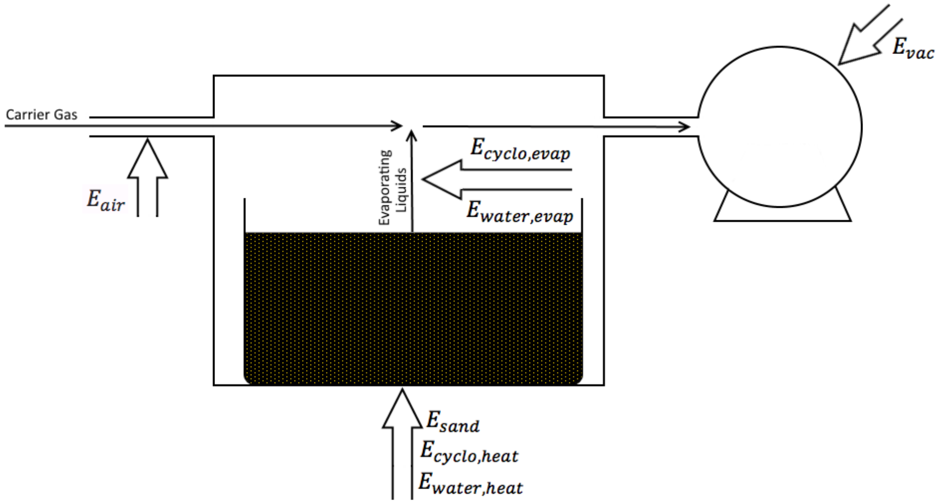

Figure 8 - Energy Inputs to Batch Evaporation Experiments

The energy to maintain vacuum was calculated using the flow rate of 1 SLPM, an assumed atmospheric pressure of 1 bar, and an assumed pump efficiency of 90%. The total time that the vacuum needed to be maintained was taken as the time to reach 250 ppm drying time, also referred to as the completion time. Completion time for the energy model was calculated using a curve fit to reduce the impact of unaccounted for variables and varying liquid contents. The fit was a power law function for both temperature and pressure and will be presented in the results and discussion section.

$$E_{vac} = \frac{Q\left(P_{atm} - P_{exp}\right)}{0.9} t_{250ppm} \tag{19}$$

The energy requirement to heat each component was calculated using its specific heat capacity, $C_p$. It was assumed that sand must be heated from a lab temperature of 25 °C to the oven temperature.

$$E_{sand} = m_{sand} Cp_{sand} (T_{oven} - T_{lab}) \tag{20}$$

The energy requirement to heat the carrier gas was found by multiplying the mass flow rate of the carrier gas by total time needed to achieve 250ppm residual cyclohexane concentration.

$$E_{air} = Q \rho_{air} Cp_{air} (T_{oven} - T_{lab}) t_{250ppm} \tag{21}$$

In order to calculate the energy requirement to heat cyclohexane and water, it was assumed that the majority of both liquids evaporated during the steady state evaporation period, and therefore only needed to be heated to the steady state evaporation temperature. The steady state evaporation temperature was calculated using a 2 dimensional function of temperature and pressure that was fitted to the level of subcooling, defined as the difference between oven temperature and steady state temperature measured by the top probe thermocouple.

$$E_{cyclo,heat} = m_{cyclo} Cp_{cyclo} \left(T_{steady\ state} - T_{lab}\right) \tag{22}$$

$$E_{water,heat} = m_{water} Cp_{water} \left(T_{steady\ state} - T_{lab}\right) \tag{23}$$

Results will show the average energy breakdown for each temperature and pressure combination tested.

# Results and Discussion

Results were processed according to the equations outlined in the methodology section of this thesis. Data from the DSMS and all other sensors were combined to build curves for mass flux, sample temperature, and evaporated mass vs. time. These curves were then processed further to determine the total drying time to reach a residual concentration of 250 ppm, as well as other intermediate concentrations. Data was processed using a Matlab script that can be found in Appendix C3.

## Composition of Samples Tested

### High Grade Gangue

Experiments were conducted on extraction gangue obtained from a developed laboratory extraction protocol, as it was thought to be more comparable to gangue on an industrial scale than a reconstituted sample would be. The disadvantage of this approach is that the ratios of sand, bitumen, water, and cyclohexane were all variable. To examine this variability, the sample contents of cyclohexane and water on wet mass basis in the gangue are plotted in Figure 9 and Figure 10 respectively. Solvent content was found using the integrated DSMS signals including the renormalization using equation 18, so the sum of cyclohexane and water content reported in this section is equal to the total mass loss measured by an accurate balance in each experiment.

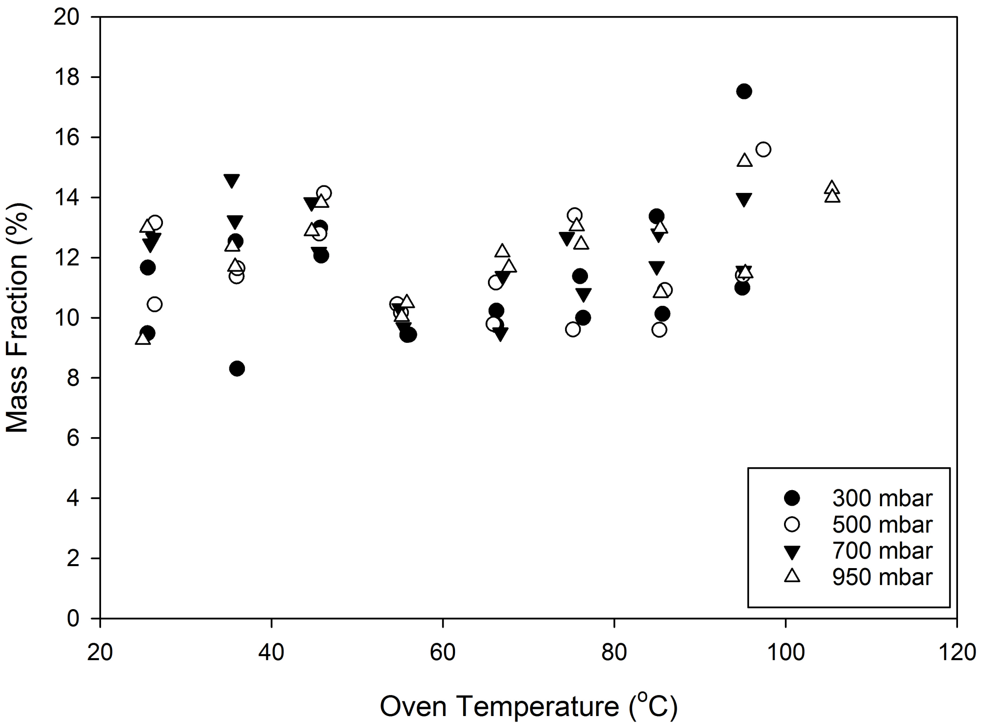

Figure 9 - Cyclohexane Content Prior to Drying for High Grade Gangue

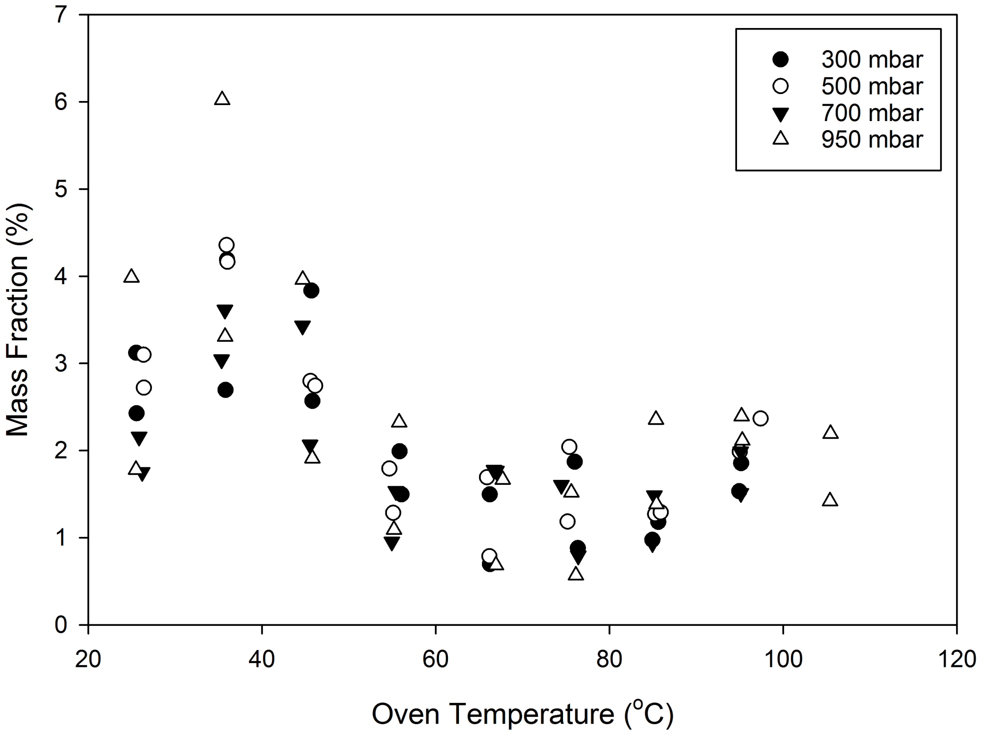

Figure 10 – Water Content Prior to Drying for High Grade Gangue

The cyclohexane content varied from 8 to 18%, with a mean concentration of 11.8% and a standard deviation of 2.1%. The water concentration was higher for some of the earlier tests conducted at lower temperatures suggesting that there was some variability between jars of extraction gangue. Mean water concentration was found to be 2.1% with a standard deviation of 1.1%. Cyclohexane content is considered to be consistent enough to give good results, but the standard deviation of water concentration is more than half of the mean water concentration. This was unexpected, as water would not be expected to move during bitumen extraction, and water content was expected to be uniform. The variability in water content may suggest that there was a scaling error with the DSMS. An attempt to renormalize the data set by forcing the mass of water contained in each sample to its mean value changed the calculated cyclohexane content by up to 30%; however, this renormalization added more variability to calculated parameters such as cyclohexane mass flux and total completion time, and every curve fit attempted under the renormalization was worsened. Therefore, it was concluded that water content was as variable as was measured, and all data processed without the further renormalization.

### Low Grade Gangue

In order to determine how the grade of oil sand ore affects the solvent removal process, experiments were also conducted on extraction gangue from low grade ore as well. The low grade ore contained a high amount of fine solids and water, and the majority of both remained in the gangue after the bitumen extraction. Cyclohexane filled the remaining pore space in the gangue, and its concentration was highly variable between tests as is shown in Figure 11.

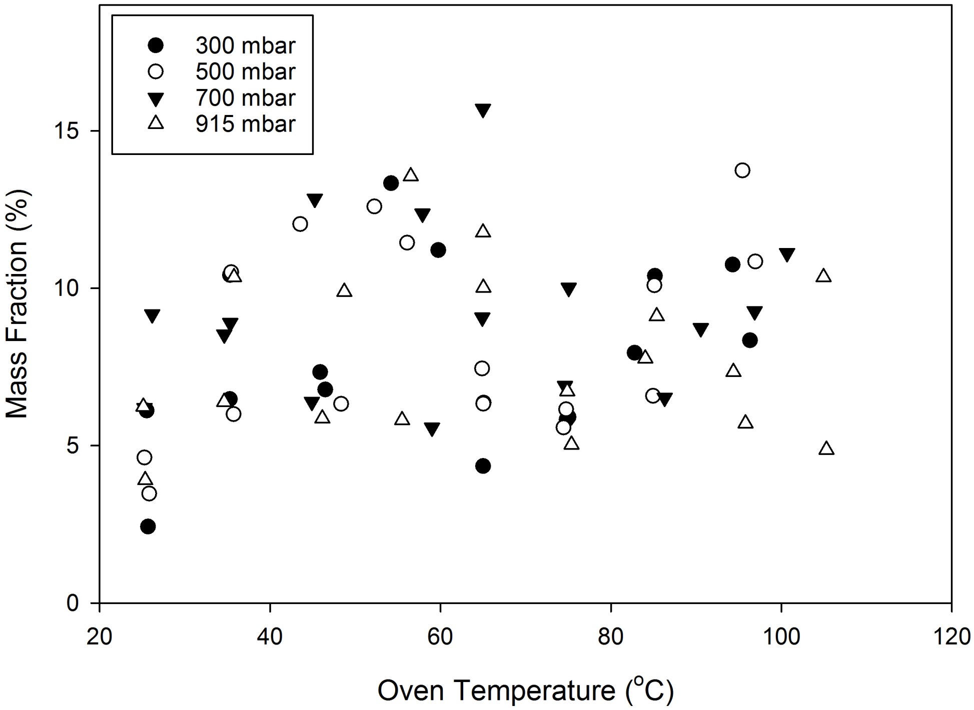

Figure 11 - Cyclohexane Content Prior to Drying for Low Grade Gangue

Figure 11 shows that measured cyclohexane content as a fraction of mass on a wet basis was as low as 2.4% and as high as 15.7%, showing a very high range. The results suggest that if the process is scaled up to an industrial scale, solvent removal equipment will need to be designed to accommodate a range of initial solvent contents. The high degree of variability in cyclohexane content will lead to difficulty in interpreting cyclohexane removal data, especially when comparing tests done at different temperatures and pressures. Figure 12 shows the water content for each test, which is much less variable.

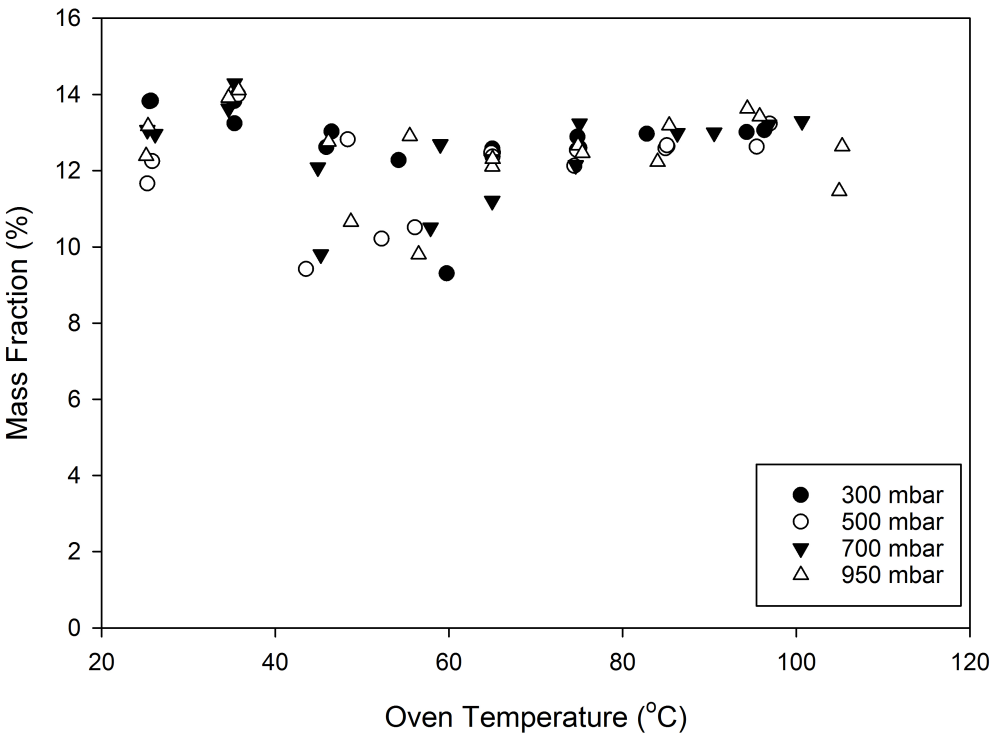

Figure 12 - Water Content prior to drying for Low Grade Gangue

The low degree of variability in water content is likely due to the fact that almost no water went to the bitumen product during extraction, and thus all the water remained in the gangue. The water content was much higher than it was for high grade gangue, and this will likely lead to significant differences in the solvent removal process. For instance, the lumping behaviour of low grade gangue shown in Figure 42 was likely the result of water holding the lumps together rather than allowing them to separate and form a more homogeneous substrate like high grade gangue. This may affect the development of liquid films, and slow the drying process. The water may also act as a physical barrier that cyclohexane must diffuse through prior to being removed from the gangue.

Table 2 shows the liquid content of both grades of gangue prior to drying for direct comparison. Values are reported in weight% on wet mass basis ± standard deviation with number of tests. High grade gangue contains more cyclohexane, and the cyclohexane content is less variable than for low grade gangue. Low grade gangue contains significantly more water, and more moisture overall than high grade gangue.

Table 2 – Liquid Content of High and Low Grade Gangue Prior to Drying on Wet Basis

| | High Grade Gangue (wt%) | Low Grade Gangue (wt%) |
|---|---|---|
| Cyclohexane | 11.8 ± 1.8 (n=66) | 8.1 ± 2.7 (n=66) |
| Water | 2.1 ± 1.1 (n=66) | 12.5 ± 1.9 (n=66) |

## Representative Results

The processed data obtained from the sensors and DSMS were processed for each experiment conducted. Representative results for single tests will be shown in this section to illustrate typical mass flux and temperature curves, and to introduce parameters that will be studied in further sections. Summary results from all experiments will be presented in the following sections.

### High Grade Gangue

Representative results will be presented for low, high, and middle temperature conditions. Figure 13 shows a representative result for a high grade gangue sample dried at 25 °C and 300 mbar.

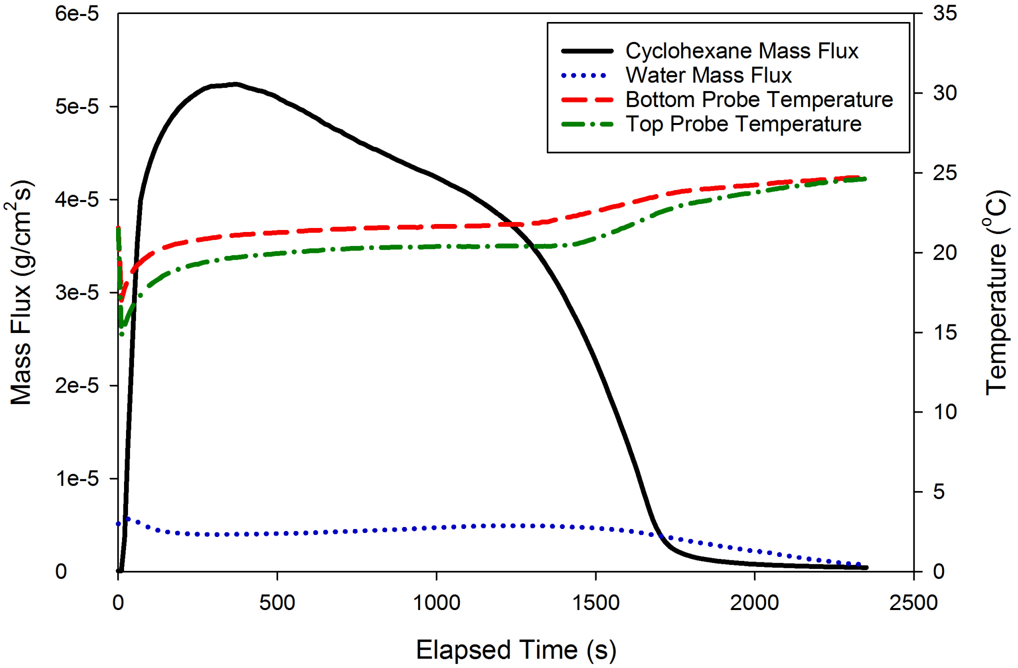

Figure 13 - Mass Flux and Temperature Curves for High Grade Gangue Dried at 25 °C and 300 mbar

Shown in the figure are separate mass flux curves for both cyclohexane and water, showing significantly higher mass flux for cyclohexane than for water during the first 1700 seconds of drying. More than 95% of cyclohexane was removed in this time frame. The figure clearly shows that evaporation of cyclohexane and water drives subcooling within the sample such that sample temperature was held at a steady state as the solvent evaporated. After the majority of solvent had evaporated, there was no longer enough solvent evaporating to maintain a high degree of subcooling, and the temperature inside the sample rose to the oven temperature. The temperature of the bottom probe was higher than that of the top probe which may indicate that more evaporation occurred at the top of the sample than within the sample, demonstrating the presence of liquid films.

The sample shown in Figure 13 was high grade ore with an initial liquid content of 2.4 % water and 11.7 % cyclohexane on wet mass basis. Conditions appear to be just such that both solvents completed the primary stage of drying at the same time, around 1700 seconds after the experiment was started. The time in the figure is cut off at the point where total mass flux dropped below 2% of its maximum value. This cutoff point occurred after the point that cyclohexane recovery exceeded 95%, but the time to reach the goal residual cyclohexane concentration of 250 ppm was 6300 seconds for this particular experiment. The time scale shown is less than half of what was necessary to achieve full recovery, indicating that a significant portion of solvent removal must be completed at a low mass flux.

For comparison with the above low temperature experiment, Figure 14 shows results for drying completed at a higher temperature of 95 °C, and a pressure of 500 mbar.

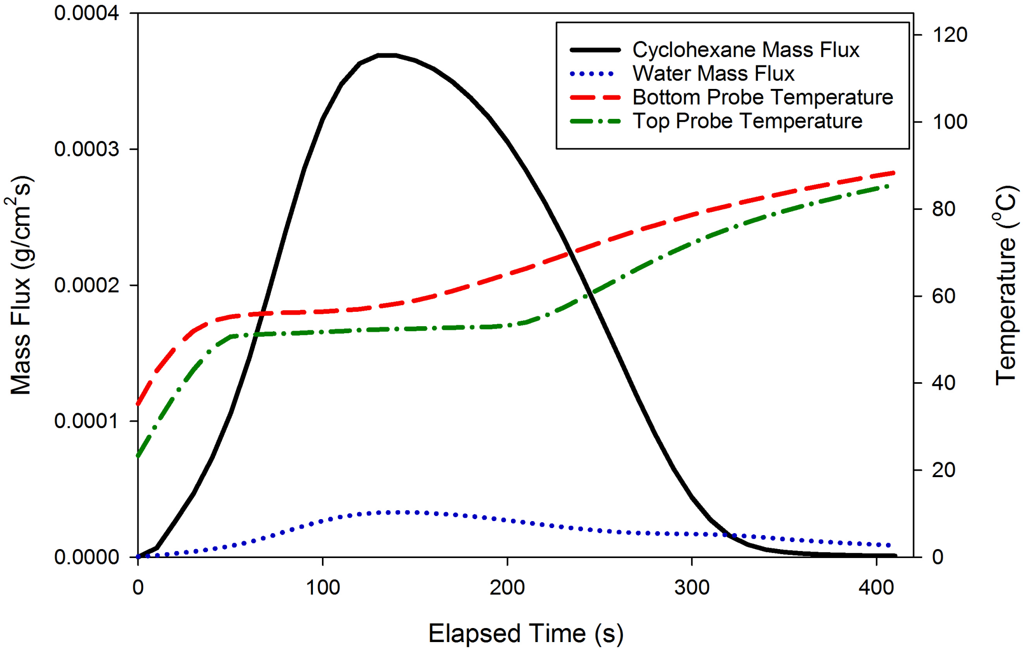

Figure 14- Mass Flux and Temperature Curves for High Grade Gangue Dried At 500 mbar and 95 °C

The stages of heating and evaporation were similar between the two experiments. The internal temperature of the sample was still held constant while the solvents evaporated, and it increased to the oven temperature after solvents were removed. The cyclohexane mass flux was still significantly higher than the water mass flux. There are also stark differences between the two cases. As expected, it took much less time to achieve drying and the mass fluxes were much higher at 95 than at 25 °C. The temperature also appears to have risen to the oven temperature before cyclohexane was finished evaporating, and the steady state temperature appears to have been reached before steady state mass flux. This may be a result of a delay in the DSMS signal response, but may also be a result of real physical phenomena.

The temperature at the bottom of the high temperature sample started rising sooner than the temperature at the top. This may indicate that liquid transport discussed in the literature review plays a role, and that the majority of evaporation occurred at the top of the sample. It may also be a result of the method of heat transfer, as the bottom of the sample was in direct contact with the brass vessel allowing for conduction through the bottom. In this particular case, cyclohexane residual concentration actually reached 250 ppm within 374 seconds, which is shown on the plot, indicating that it is possible to achieve full recovery within reasonable time frames.

Also of interest is the fact that the cyclohexane and water appear to dry up at the same time for the samples shown in Figure 13 and Figure 14. This is due mostly to having just the right ratio of cyclohexane to water in the sample, and is influenced slightly by oven pressure. To illustrate a case with higher initial water content, Figure 15 shows the results for a high grade gangue sample dried at 950 mbar and 45 °C. In this case, water content prior to drying was 4% on wet mass basis, compared to 2.4 and 2% for the results outlined in Figure 13 and Figure 14 respectively.

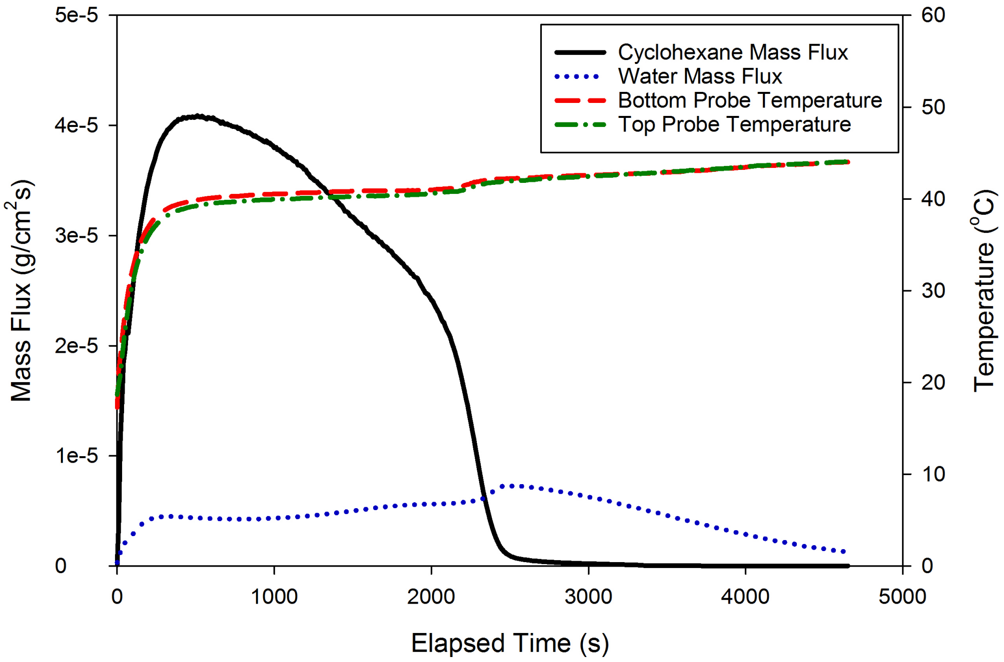

Figure 15 - Mass Flux and Temperature Curves for High Grade Gangue Dried At 950 mbar and 45 °C

In this case, the water finished drying long after the cyclohexane, which can be attributed to the increased water content in the sample. Of interest is the fact that the mass flux of water increased after most of the cyclohexane evaporated. This is understood after examining the temperature curve in conjunction with the mass flux curve. When both cyclohexane and water evaporate simultaneously, a large amount of heat is removed from the sample, driving significant subcooling. When effectively all cyclohexane has been removed, only the evaporation of water remains to drive subcooling, and the temperature of the sample increases as a result. This increase in the temperature of the sample will allow the evaporation rate of water to increase until the energy removal by water evaporation balances it out. This illustrates the coupling of sample temperature with mass transfer. For reference, the parameters for each of the representative results shown above are outlined in Table 3.

Table 3 - Summary of Parameters for Representative Results of High Grade Gangue

| Figure | Oven Temperature (°C) | Oven Pressure (mbar) | Initial Cyclohexane Content, Wet Mass Basis (%) | Initial Water Content, Wet Mass Basis (%) | Time to Residual Concentration of 250 ppm (s) |
|---|---|---|---|---|---|
| 13 | 25 | 300 | 11.7 | 2.4 | 6300 |
| 14 | 95 | 500 | 11.4 | 2.0 | 370 |
| 15 | 45 | 950 | 12.9 | 4.0 | 2800 |

## Low Grade Gangue

For comparison, representative results are given for solvent removal from low grade gangue at the same temperature and pressure combinations as those results from high grade gangue. Figure 16 shows the representative curve for drying of a low grade gangue at 25 °C and 300 mbar.

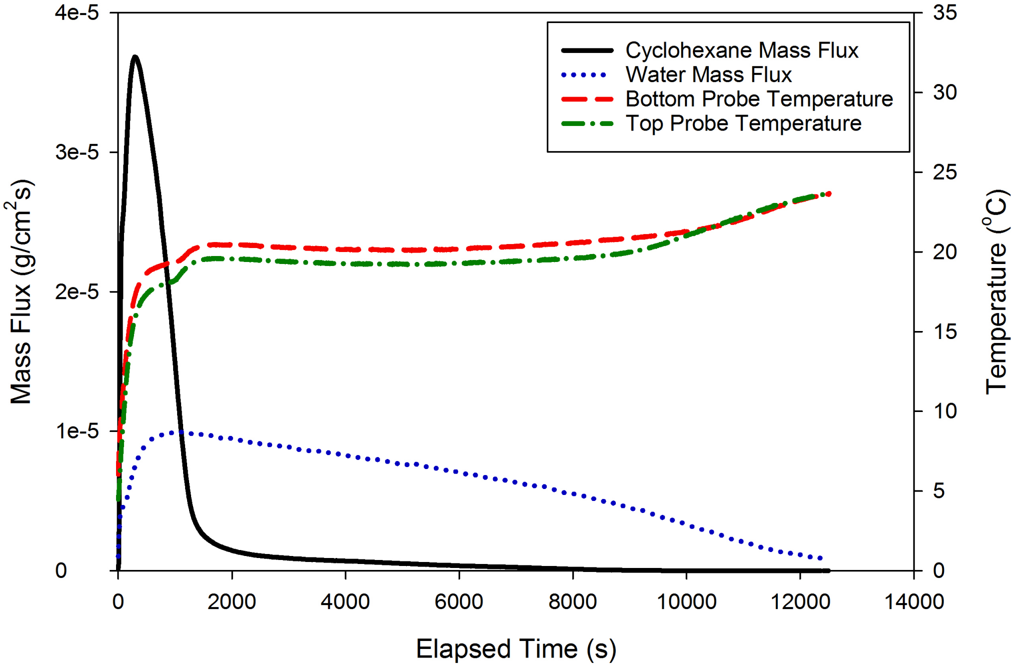

Figure 16 - Mass Flux and Temperature Curves for Low Grade Gangue Dried at 300 mbar and 25 °C

The shape of the mass flux and temperature curves observed for low grade gangue are very similar to those observed for high grade gangue. Cyclohexane still evaporates with much higher mass flux than water, and the majority of cyclohexane is still removed in the initial high mass flux period. Subcooling is also observed in both cases, where a steady state temperature lower than the oven temperature is held while evaporation occurs, and the sample temperature rises to the oven temperature when it is complete. However, there are also significant differences. The most obvious difference between the gangue samples extracted from different ores was caused by the difference in water content, which is 2.4% in Figure 13, but increases to 12.8% for Figure 16. Due to the increased water content, water continued to evaporate long after the majority of cyclohexane had been removed. As a result, there were 2 quasi-steady state temperatures held for periods of time during evaporation. The first steady state temperature was about 18 °C, held for approximately the first 1000 seconds when both cyclohexane and water evaporated simultaneously. After the majority of cyclohexane had been removed, only evaporating water was left to drive subcooling, and the temperature of the sample increased to a second steady state temperature of about 20 °C. Finally, when the evaporation of water was complete, the sample temperature raised to the oven temperature.

The initial cyclohexane content was 6.1% in this case, and the evaporation rate of cyclohexane may never have reached its maximum value as a result. The mass flux of cyclohexane reached a peak value and then decreased immediately. The maximum cyclohexane mass flux was also more than 5 times smaller than it was for the test at the same temperature and pressure for high grade gangue outlined in Figure 13. That test was performed on a sample with 11.7% cyclohexane. This result suggests that initial cyclohexane content plays a role in whether a steady state is reached for the evaporation of cyclohexane, and what the maximum mass flux in that particular experiment will be.

For further comparison, Figure 17 shows a test that was performed at 915 mbar and 95 °C.

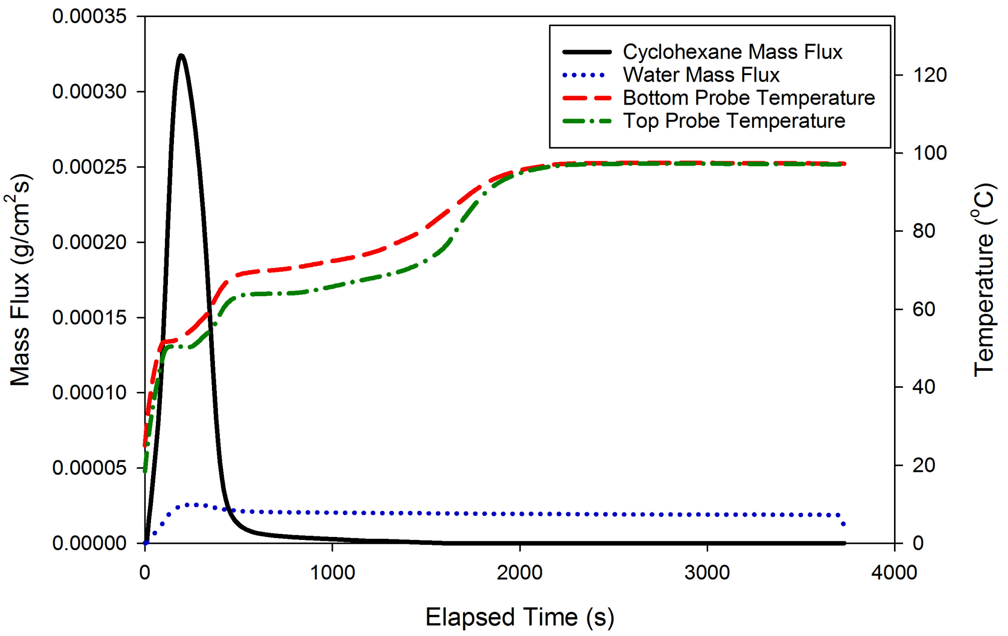

Figure 17 - Mass Flux and Temperature Curves for Low Grade Gangue Dried at 500 mbar and 95 °C

In this case, the cyclohexane content was 13.7% on wet mass basis, so the effects of decreased cyclohexane content should not appear. The maximum cyclohexane mass flux was only slightly less than the representative result for high grade gangue at the same temperature and pressure shown in Figure 15.

Here, two steady state temperatures were observed more clearly than at lower temperatures with less original cyclohexane content. The first steady state temperature of about 50 °C was held while both cyclohexane and water evaporated, and as soon as cyclohexane was finished its primary stage of evaporation, the temperature increased to a second steady state temperature of about 65 °C. After evaporation of both substances was complete, the temperature increased to that of the oven.

A problem was observed with the water mass flux curve for this test, and every other test performed on low grade ore at temperatures higher than 60 °C. The temperature in the sample increased to the oven temperature after a time of 2000 seconds, indicating that all cyclohexane and water had been removed. However, the water mass flux reading was still high beyond 2000 seconds, disagreeing with the measurement from the thermocouples. Since the total measured mass of water was consistent between tests, as is shown in Figure 12, it is likely that the water condensed somewhere between the sample and detector, and evaporated from there at a constant rate. This issue will lead to difficulties in interpreting results for water removal rates from low grade gangue, but all water that evaporated was still detected eventually, and the cyclohexane results do not appear to be affected. To summarize representative results for the low grade gangue, Table 4 shows the summary of parameters for the results tested.

Table 4 - Summary of Parameters for Representative Results of Low Grade Gangue

| Figure | Oven Temperature (°C) | Oven Pressure (mbar) | Initial Cyclohexane Content, Wet Mass Basis (%) | Initial Water Content, Wet Mass Basis (%) | Time to Residual Concentration of 250 ppm (s) |
|---|---|---|---|---|---|
| 16 | 25 | 300 | 6.1 | 13.8 | 7700 |
| 17 | 95 | 500 | 13.7 | 12.7 | 1400 |

## Steady State Mass Flux

It has been well established that increasing the temperature at which solvent based extraction is carried out will increase the efficiency of bitumen recovery at a fixed ratio of solvent to ore [14-16, 18, 26]. If the recovery of solvent is achieved by evaporation at temperatures higher than ambient, it would be logical to carry out extraction at a similar temperature to that at which solvent will be removed from the gangue. If this is done, the mass flux of cyclohexane will quickly approach a high steady state mass flux. Based on observations from these experiments, it would be expected that the majority of cyclohexane will be removed at this steady state mass flux, which will be close to the maximum mass flux measured in these experiments. Therefore, the maximum or steady state mass flux is of great interest and will be presented as a function of temperature and pressure for both high and low grade gangue. Although the effect of temperature and pressure on water mass flux was similar to that of cyclohexane, the focus of this thesis is on the removal of cyclohexane from extraction gangue, so only the results for cyclohexane will be presented.

Upon investigation, the relationship between steady state mass flux and oven temperature was very similar to the vapour pressure curve. To illustrate, Figure 18 shows steady state mass flux as a function of temperature and pressure, with vapour pressure fit to the Antoine equation, equation 24, plotted on a different axis. Coefficients for the Antoine equation summarized in Table 1 were obtained from Yaw's critical handbook [41] set to give vapour pressure in mmHg.

$$\log_{10} P_{vap} = A - \frac{B}{C + T} \tag{24}$$

**Table 5 - Coefficients For Antoine Equation Giving Cyclohexane Vapour Pressure in mm Hg**

| A ($\log_{10}$(mmHg)) | B ($\log_{10}$(mmHg)/°C) | C (°C) |
|---|---|---|
| 6.890190581 | 1200.947362 | 218.8146572 |

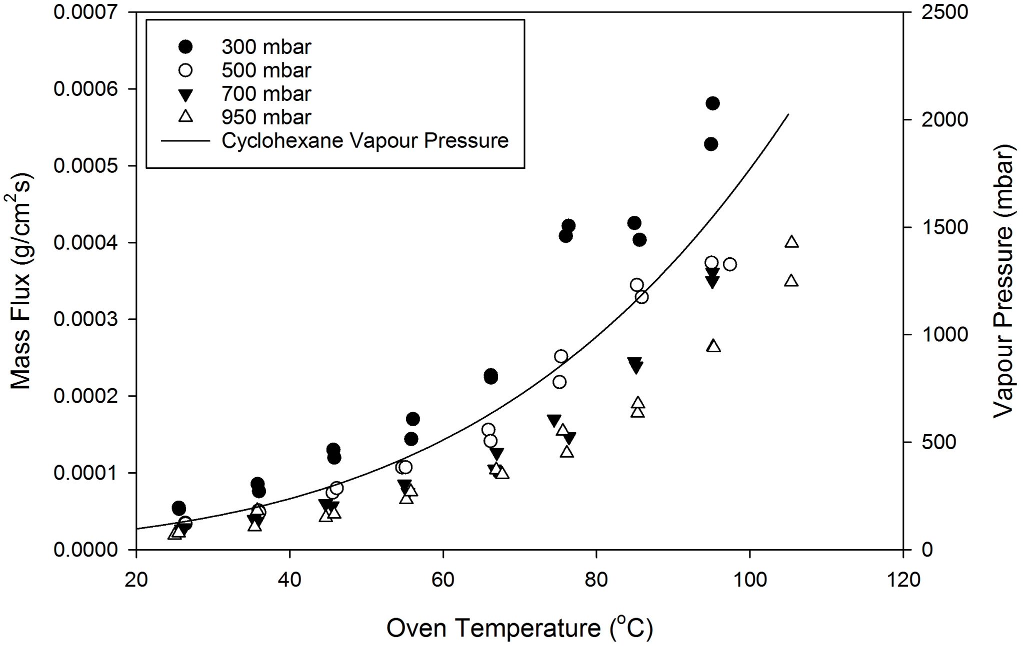

**Figure 18 - Maximum Cyclohexane Mass Flux for High Grade Gangue Plotted with Vapour Pressure on a Different Axis**

Since both mass flux and vapour pressure showed a similar relationship with oven temperature, maximum cyclohexane mass flux was fit to a function of oven pressure and cyclohexane vapour pressure shown in equation 25. Vapour pressure in equation 25 was calculated at oven temperature using the Antoine equation. Figure 19 shows the maximum cyclohexane mass flux for high grade gangue experiments plotted against temperature and pressure, and Figure 20 shows the same plot for low grade gangue.

$$Maximum\ Mass\ Flux = aP_{vap}{P_{oven}}^{b} \tag{25}$$

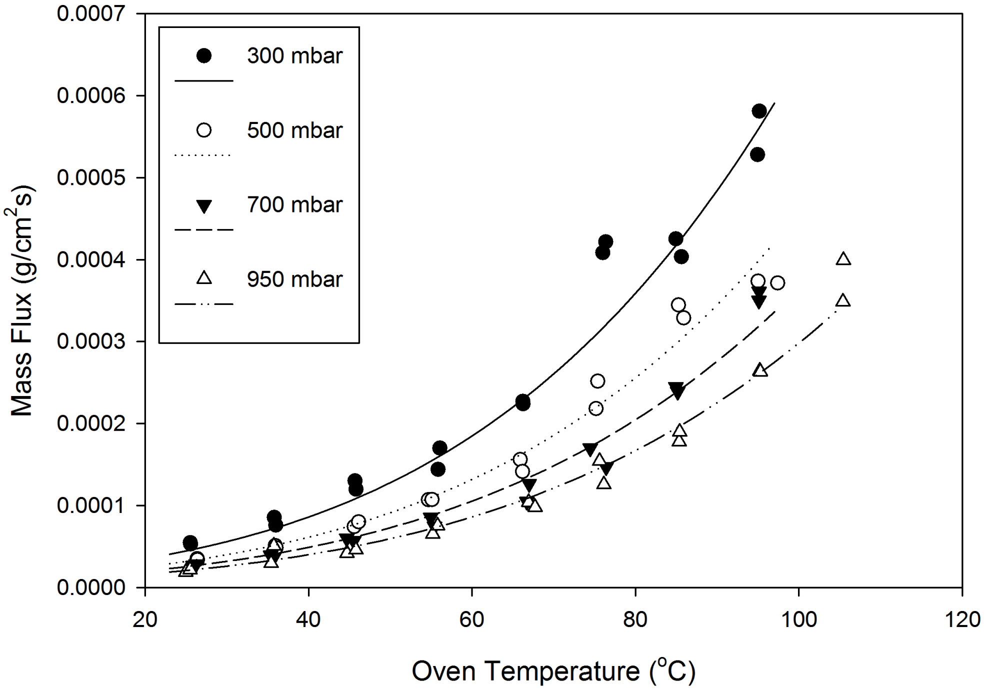

Figure 19 - Maximum Cyclohexane Mass Flux with Fitted Model for High Grade Gangue

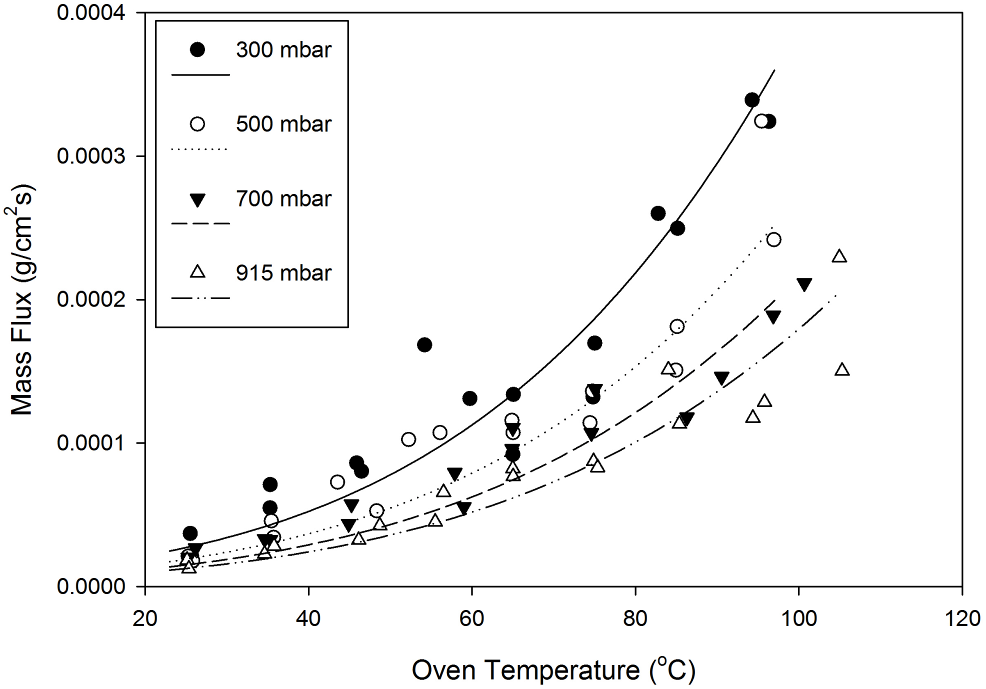

Figure 20 - Maximum Cyclohexane Mass Flux with Fitted Model for Low Grade Gangue

In both plots, there is a clear relationship where increasing temperature and decreasing absolute pressure cause an increase in steady state mass flux. Equation 25 produced a strong fit for both grades of gangue, suggesting that vapour pressure is a major driving force for cyclohexane mass flux. The fit to the curve was weaker for low grade gangue due to the higher level of variability in that data, suggesting that other variables also have a large impact. Table 6 gives the coefficients used to fit the data with upper and lower bounds for a 95% confidence interval on each coefficient.

**Table 6 - Summary of Coefficients for Fitting Mass Flux to Equation 25**

| | a ($Pa^{-1-b}$) | b | $r^2$ |
|---|---|---|---|
| High Grade Gangue | $3.42 \times 10^{-6}$<br>($1.29 \times 10^{-6}$ , $5.55 \times 10^{-6}$) | -0.66<br>(-0.72 , -0.61) | 0.97 |
| Low Grade Gangue | $2.90 \times 10^{-6}$<br>($-5.30 \times 10^{-7}$ , $6.33 \times 10^{-6}$) | -0.70<br>(-0.81 , -0.59) | 0.89 |

Maximum cyclohexane mass flux has a similar relationship with oven temperature and pressure for both grades of gangue, but there are significant differences. The maximum mass flux was an average of 1.5 ± 0.4 (n=33) times higher for high grade gangue than for low grade gangue at the same temperature and pressure. Maximum mass flux may be higher in the high grade gangue because the initial cyclohexane content was higher. As was shown in the representative results, both mass flux and temperature increased with time as the sample was heated from the ambient starting temperature to the first steady state temperature. In cases where there was not enough cyclohexane in the sample, too much cyclohexane may have been removed before the normal steady state mass flux could be reached, and thus the maximum mass flux measured would be lower. This effect could contribute to why the variability between results for low grade gangue is much higher than it is for high grade gangue, because the variability in cyclohexane content was much more significant for low grade gangue.

In order to test whether increasing cyclohexane content caused an increase in maximum mass flux, each pair of tests conducted at the same temperature, pressure, and grade of gangue were compared. The ratio of maximum cyclohexane mass flux between the two samples was calculated and plotted against the ratio of initial cyclohexane content for low grade gangue in Figure 21.

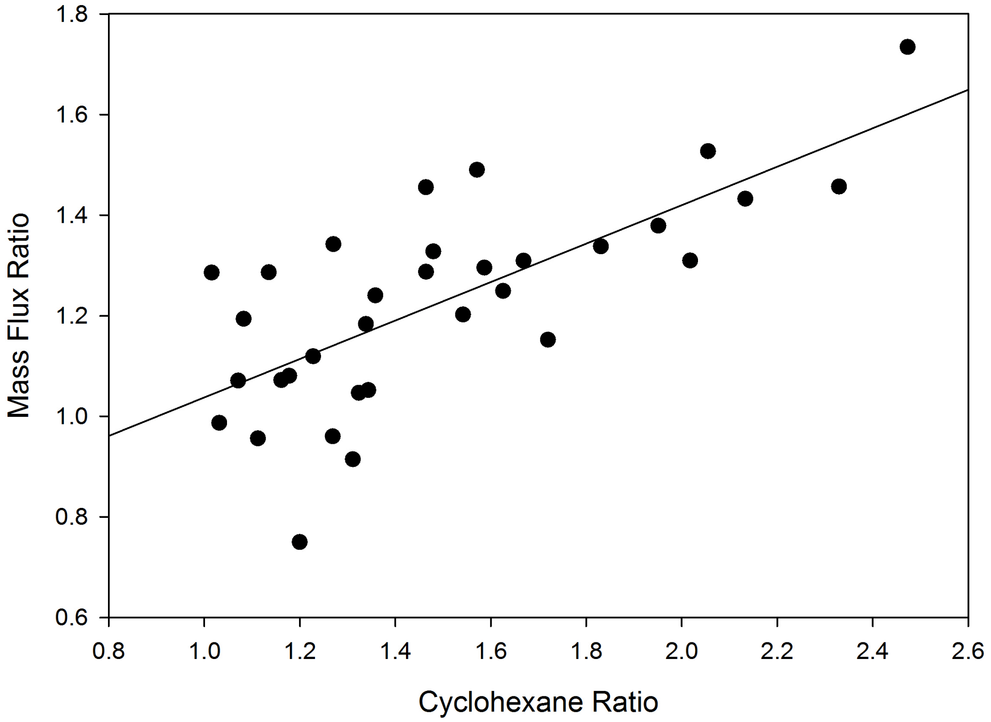

Figure 21 - Effect of Initial Cyclohexane Content on Maximum Mass Flux for Low Grade Gangue

A statistical test confirmed a positive slope with a p-value of 2 $(10)^{-6}$ . The results for low grade gangue show that increasing cyclohexane content will lead to a higher maximum mass flux, indicating that the maximum steady state cyclohexane mass flux was not reached when low grade gangue had insufficient cyclohexane content, or that the free evaporation surface was less saturated with cyclohexane when there was less cyclohexane in the sample.

Another possible reason that mass flux was measured to be lower in low grade gangue is related to the increased water content relative to cyclohexane content in low grade gangue. Low grade gangue has significantly more water and fine particles than high grade gangue. Prior to bitumen extraction, low grade ore contained 19.4% ± 0.9% (n=2) fine particles by mass compared to just 11.2% ± 0.7% (n=3) in high grade ore. In low grade gangue, these fine particles clumped together and formed lumps with water as the likely binding agent, suggesting that there are more hydrophilic particles in low grade gangue. If hydrophilic particles clump together, and the clumps were homogeneously dispersed throughout the matrix of gangue, the free surface would contain pools of water and pools of cyclohexane. The surface concentration of cyclohexane and water is likely highly variable between samples as a result of this clumping, and the effect contributes to the higher variability in steady state cyclohexane mass flux.

Since low grade gangue contains significantly more water, and is likely to contain significantly more hydrophilic particles, it is likely that more of the free surface of low grade gangue is occupied by water, and that cyclohexane is partially blocked from evaporating as a result. If water occupies more space on the free surface in low grade gangue, then water would be expected to have a higher evaporation rate. To investigate, the ratio of cyclohexane to water mass flux was calculated at the point of maximum cyclohexane mass flux for each grade of gangue. Figure 22 shows this ratio for high grade gangue.

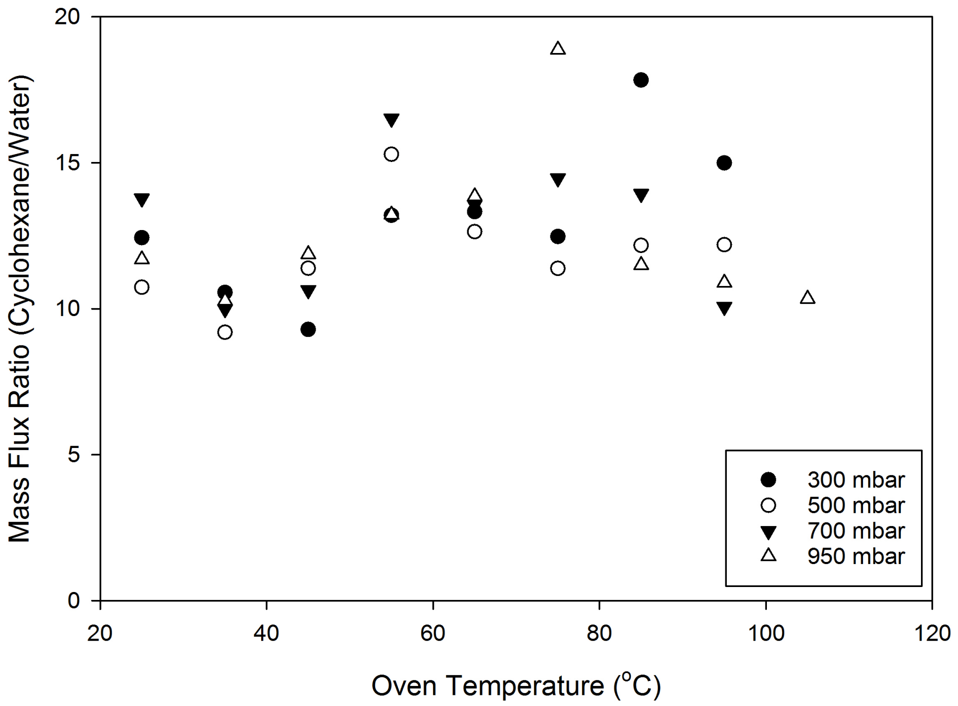

Figure 22 - Ratio of Cyclohexane to Water Mass Flux at the Point of Maximum Cyclohexane Mass Flux for High Grade Gangue

The same ratio was calculated for low grade gangue, with an added complication. Due to a condensation problem presented in Figure 17, the measured mass flux for water evaporation in any test performed on low grade gangue above 60 °C was under-predicted. In order to compensate for this error, the water mass flux at all points above 60°C was calculated by dividing the total water mass in the sample by the time it took for top probe temperature to rise close to the oven temperature. This calculation assumes that water mass flux is constant throughout the experiment, which is inaccurate, but works as an effective approximation. Figure 23 shows the same ratio of cyclohexane mass flux to water mass flux at the point of maximum cyclohexane mass flux for low grade gangue.

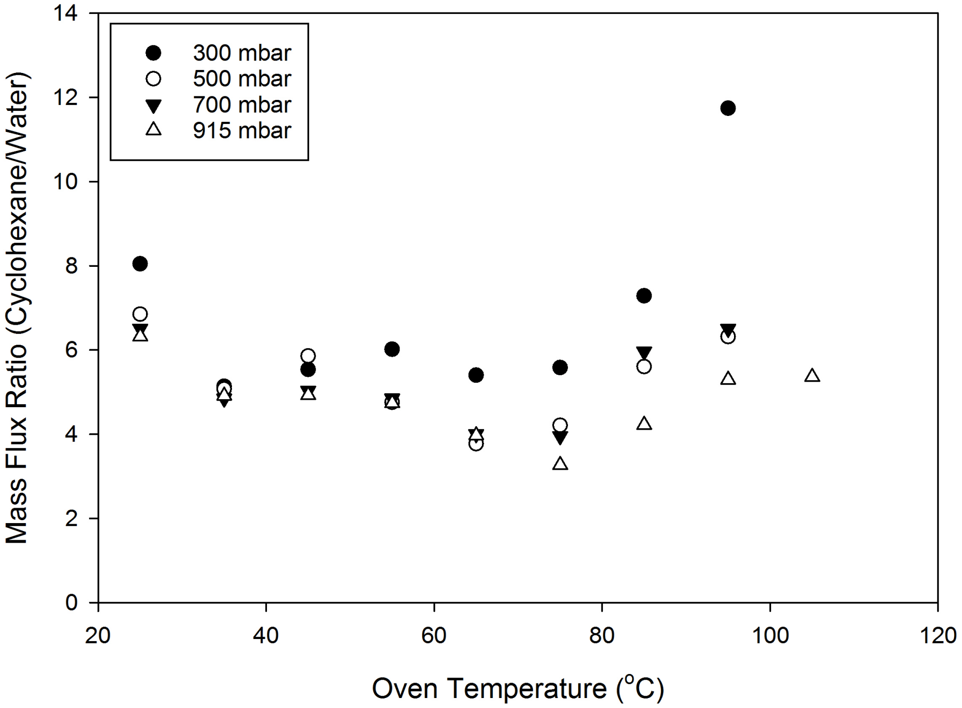

Figure 23 - Ratio of Cyclohexane to Water Mass Flux at the Point of Maximum Cyclohexane Mass Flux for Low Grade Gangue

There is no apparent trend with temperature or pressure for the ratio shown in Figure 22 or Figure 23, but the average the ratio of mass fluxes is 13 ± 2 (n=33) in high grade gangue, but only 6 ± 2 (n=33) in low grade gangue. This indicates that much more water evaporates in cyclohexane relative to the amount of cyclohexane that evaporates, and supports the conclusion that the difference in steady state cyclohexane mass flux is related to a difference in surface saturation with cyclohexane.

## Subcooling

As was shown in the representative results, temperature was held at a steady state during the period of relatively steady high mass flux. As solvent transitions from the liquid to gas phase, it absorbs energy from the sample and causes the sample temperature to drop. This phenomena will be referred to as subcooling. Since there is a direct relationship between heat and mass transfer in evaporative processes, the degree of subcooling should be strongly related to mass flux of evaporating liquids. The degree of subcooling was calculated by subtracting the temperature of the top probe from the oven temperature at the point when maximum cyclohexane mass flux was observed. The temperature of the top probe was used instead of the bottom probe because most of the evaporation was expected to occur at the top of the sample due to the presence of liquid films. Figure 24 shows the degree of subcooling as a function of temperature and pressure for high grade gangue, and also includes a curve for subcooling fitted to equation 26 below.

$$Subcooling = ae^{bT}P^c \tag{26}$$

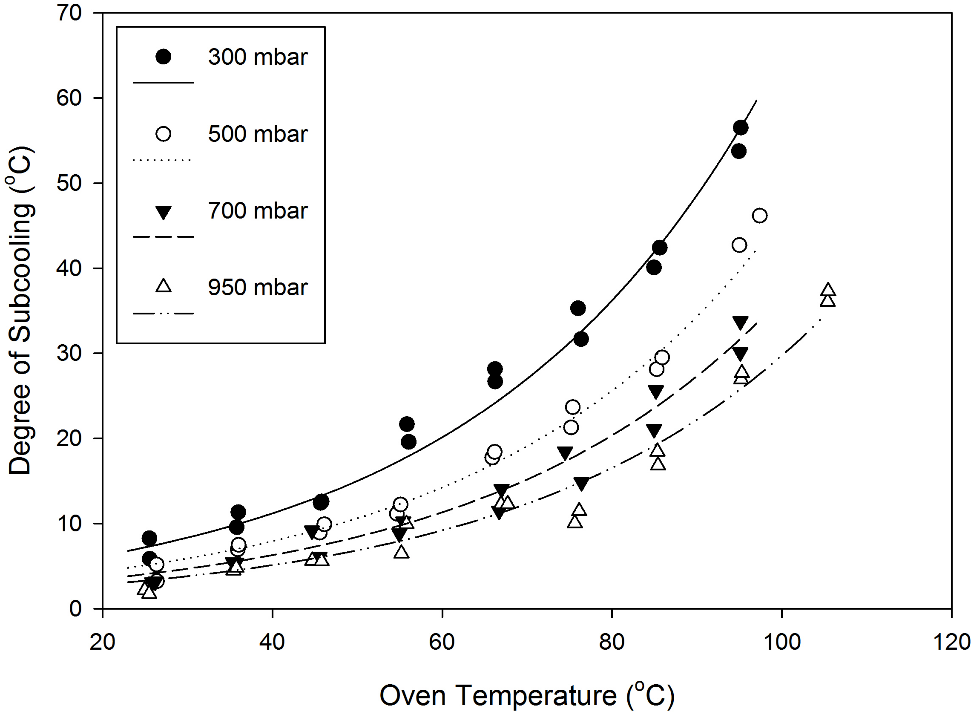

Figure 24 - Degree of Subcooling at Maximum Mass Flux vs. Temperature and Pressure for High Grade Gangue with Fitted Curve

Just as with maximum mass flux, there is a clear relationship between degree of subcooling and temperature and pressure. Cyclohexane is the main driver for subcooling in high grade gangue, but evaporation of water also contributes. As a result, attempts to fit the degree of subcooling to equation 25 did not produce a strong fit, especially with low grade gangue, and equation 26 was used instead.

Table 7 summarizes the fitted coefficients for subcooling in both grades of gangue with upper and lower bounds for a 95% confidence interval on each coefficient.

Table 7 - Summary of Coefficients for Fitting Subcooling to Equation 26

| | a<br>(°C $Pa^{-c}$) | b<br>(°$C^{-1}$) | c | $r^2$ |
|---|---|---|---|---|
| High Grade Gangue | 3841<br>(1933 , 5749) | 0.029<br>(0.028 , 0.031) | -0.68<br>(-0.73 , -0.63) | 0.98 |
| Low Grade Gangue | 1552<br>(899 , 2206) | 0.025<br>(0.024 , 0.026) | -0.55<br>(-0.59 , -0.51) | 0.98 |

Of significant interest is the extremely high level of subcooling. In the experiments conducted at 95 °C and 300 mbar, which produced the maximum mass flux, the steady state temperature of the gangue is almost 60 °C lower than the oven temperature. To help understand this phenomena, the top probe sample temperature was plotted with pressure alongside the vapour pressure curve for cyclohexane in Figure 25.

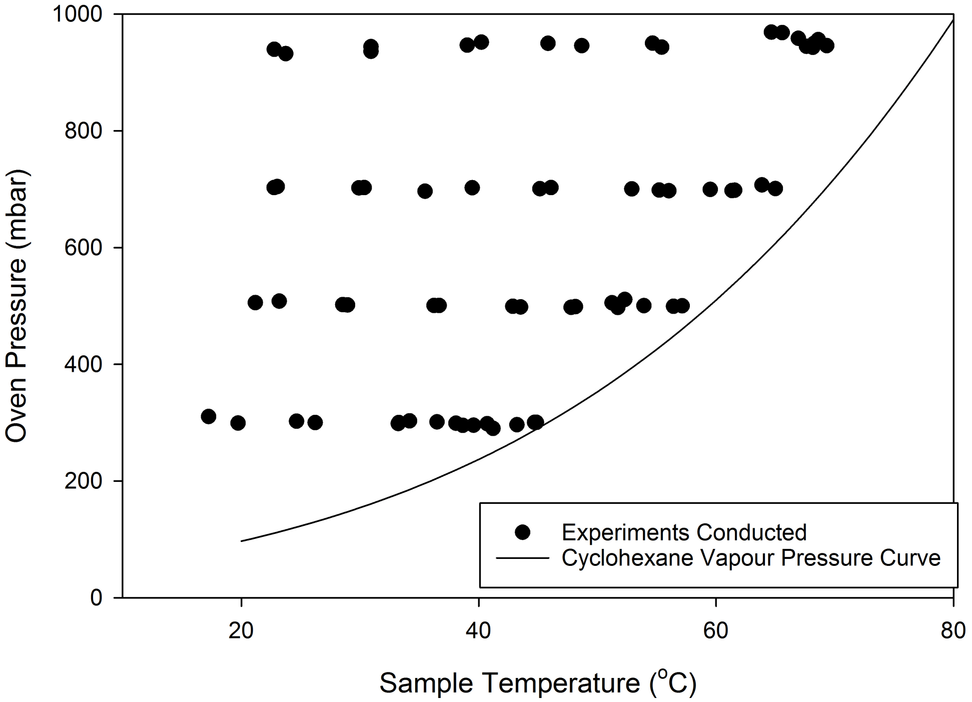

Figure 25 - Comparison of Sample Temperature and Boiling Point for High Grade Gangue

The reason for the high level of subcooling is that cyclohexane cannot exceed its boiling point at the respective pressure of testing until it has finished evaporating. When the sample temperature approaches the boiling point of cyclohexane, mass transfer is expected to be driven by heat transfer to the sample. The rate of heat transfer will increase as the difference between oven temperature and sample temperature is increased, which will be enhanced when the sample temperature cannot exceed cyclohexane's boiling point. However, although cyclohexane starts to boil after oven temperature is increased beyond 65 °C at 300 mbar, there is no sudden jump in mass flux evident in Figure 19, but rather a smooth curve. This indicates that it is not necessarily beneficial to operate at oven temperatures higher than the boiling point of cyclohexane. In fact, there may be significant energy savings that can be achieved by operating at a lower temperature, and this will be investigated in a later section.

Interestingly, there is a large gap of about 10 °C in Figure 25 between the maximum sample temperature and the boiling point at 950 mbar. This gap may be the result of a high rate of cyclohexane removal from the air above the sample preventing the establishment of a saturated boundary layer above the sample, which would increase the rate of evaporation and drive further subcooling. The gap may also be explained by the simultaneous evaporation of water, which may also drive subcooling. In order to investigate the effect of water on subcooling, the same plot is generated for low grade gangue, which has a significantly higher water content than high grade gangue. The resulting plot is shown in Figure 26.

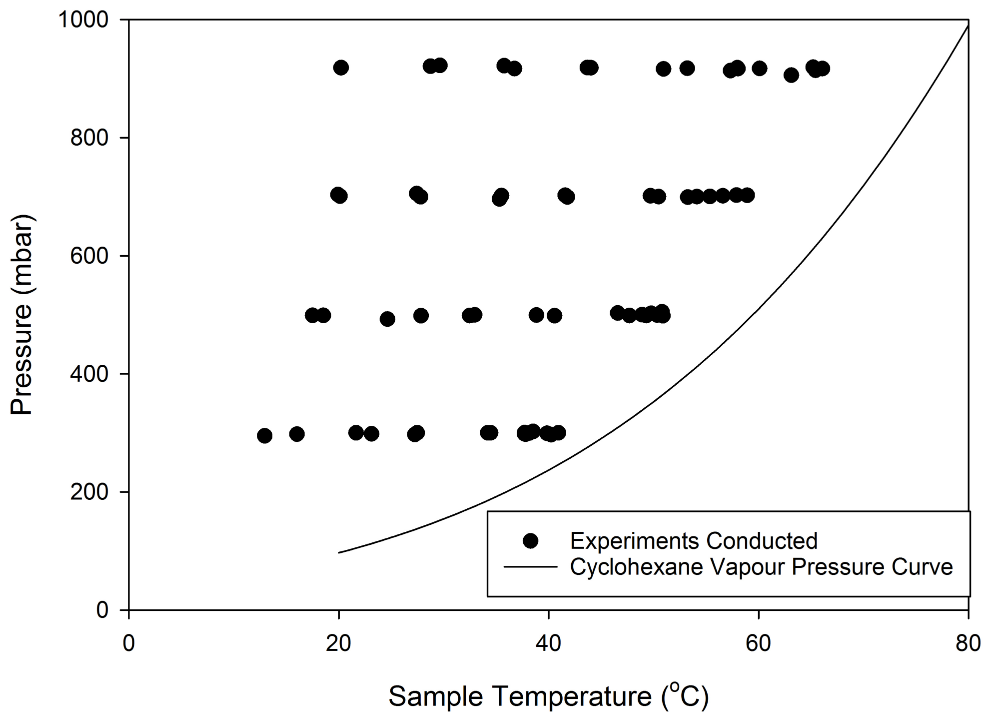

Figure 26 - Comparison of Sample Temperature and Boiling Point for Low Grade Gangue

The level of subcooling is similar between high and low grade gangue, but the low grade gangue consistently shows a slightly higher level of subcooling. The gap between the boiling point of cyclohexane at each respective pressure and the sample temperature is much more pronounced. The similarity between the curves indicates that the evaporation of cyclohexane is the main driver for subcooling, but the difference indicates that evaporation of water enhances the level of subcooling.

## Total Time to Remove Cyclohexane

### High Grade Gangue

In order to meet environmental regulations, an objective of drying is to reach a residual cyclohexane concentration of 250 ppm. In a sample where the initial cyclohexane concentration is 11.8 wt% on wet basis, a residual concentration of 250 ppm corresponds to a cyclohexane recovery of about 99.8%. Total drying time to achieve residual concentration of 250ppm will be henceforth referred to as completion time, and is plotted for high grade gangue against temperature and pressure in Figure 27.

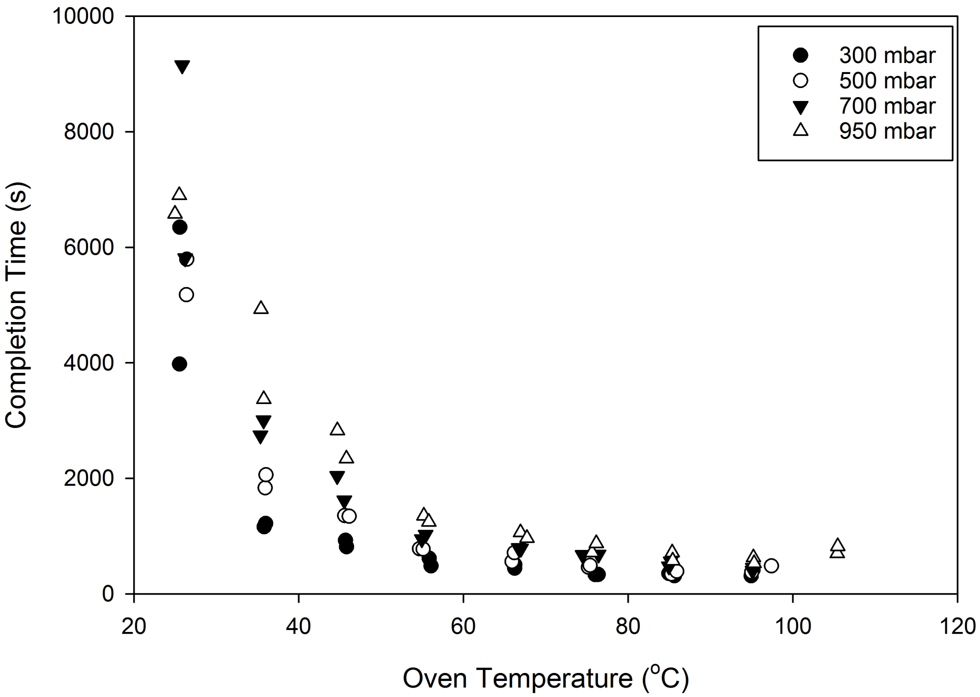

**Figure 27 – Completion Time on a Linear Scale for High Grade Gangue**

The graph shows that there appear to be significant benefits of increasing temperature up to 55 °C, but the benefits of increased temperature and pressure appear to diminish after the oven temperature is increased beyond 65 °C. To explore this further, the same data is re-plotted with drying time on a logarithmic scale in Figure 28.

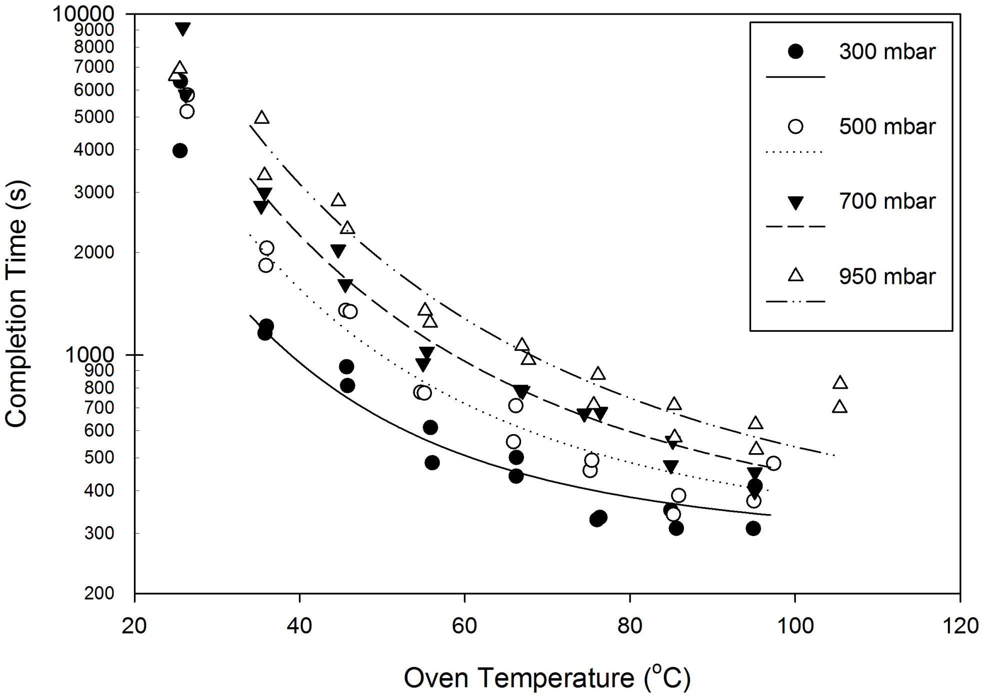

Figure 28 – Completion Time on a Logarithmic Scale for High Grade Gangue Including Curve Fit

Figure 28 shows that, while the effects are not as drastic as they are at lower temperatures, increasing temperature and decreasing pressure are still beneficial at lower temperatures from a completion time standpoint. Figure 28 also includes a curve fit to equation 27 below. Results at 25 °C had to be neglected in order to produce an acceptable fit to data. With the notable exception of the increased completion time observed at 105 °C, the data fit excellently to the curve with a coefficient of restitution of 0.959. Coefficients fit to the curve will be summarized with those found for low grade gangue in Table 8.

$$t_{250ppm} = aT^bP^c + d \tag{27}$$

## Low Grade Gangue

Low grade ore was passed through the same bitumen extraction and drying process as was high grade ore, but the structure of the gangue that was produced was significantly different between the two grades of ore. This led to significant differences in the solvent removal process. Figure 29 shows the total time that was taken to reach a residual cyclohexane concentration of 250 ppm on a logarithmic scale as a function of temperature and pressure for low grade gangue.

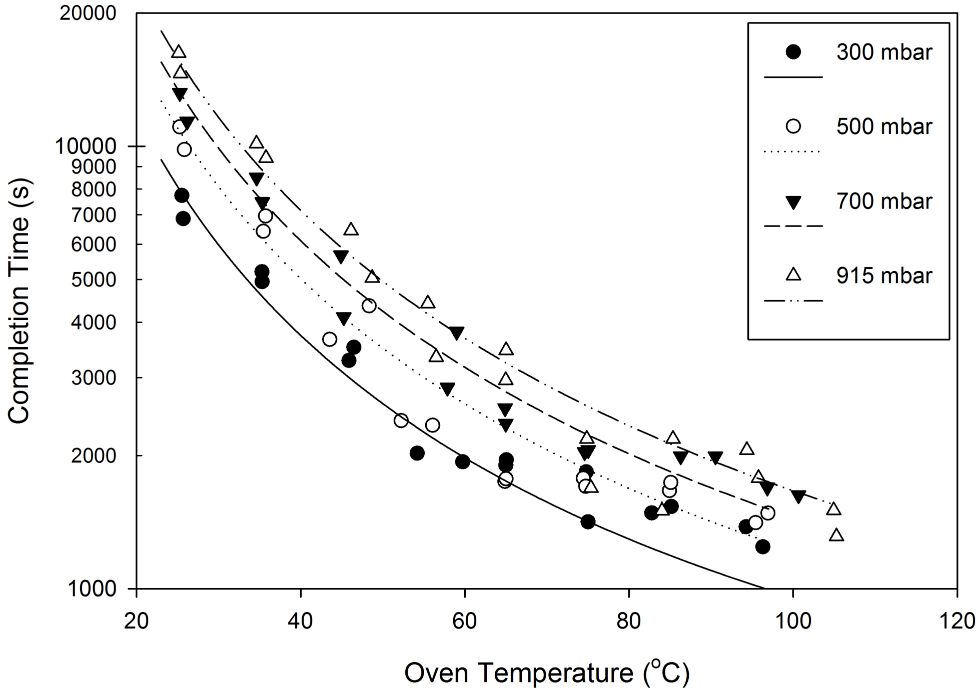

Figure 29 - Completion Time on a Logarithmic Scale for High Grade Gangue Including Curve Fit

Once again, a trend is visible where increasing temperature and decreasing pressure lead to an increased drying rate. The effect of these variables also becomes less significant at higher temperatures just as with high grade gangue. However, the completion time was significantly larger for low grade gangue than high grade gangue. The fit to data was strong with a coefficient of restitution of 0.981, but there is noticeable variability in the data set as a result of varying cyclohexane content in the samples and other uncontrolled variables. Table 8 summarizes the coefficients for fitting completion time to equation 27 for both grades of gangue. Minimum and maximum bounds are reported for each coefficient at a 95% confidence level.

Table 8 - Summary of Coefficients for Fitting Completion Time to Equation 27

| | a<br>(s °C$^{-b}$ Pa$^{-c}$) | b | c | d<br>(s) | r$^2$ |
|---|---|---|---|---|---|
| High Grade Gangue | 23.1<br>(-21.9 , 68.0) | -2.61<br>(-2.99 , -2.23) | 1.26<br>(1.06 , 1.46) | 272<br>(145 , 400) | 0.96 |
| Low Grade Gangue | 3276<br>(717 , 5834) | -1.68<br>(-1.87 , -1.50) | 0.61<br>(0.53 , 0.69) | 170<br>(-326 , 666) | 0.98 |

In order to more clearly illustrate the difference in completion time between the two different grades of gangue, the average completion time for each pair of tests conducted at the same temperature, pressure, and grade of gangue was calculated. The completion time ratio was calculated as the ratio between average completion time for low grade gangue to that of high grade gangue, more simply stated in the following formula.

$$Completion\ Time\ Ratio = \frac{\left(t_{complete,A} + t_{complete,B}\right)_{Low\ Grade\ Gangue}}{\left(t_{complete,A} + t_{complete,B}\right)_{High\ Grade\ Gangue}}$$

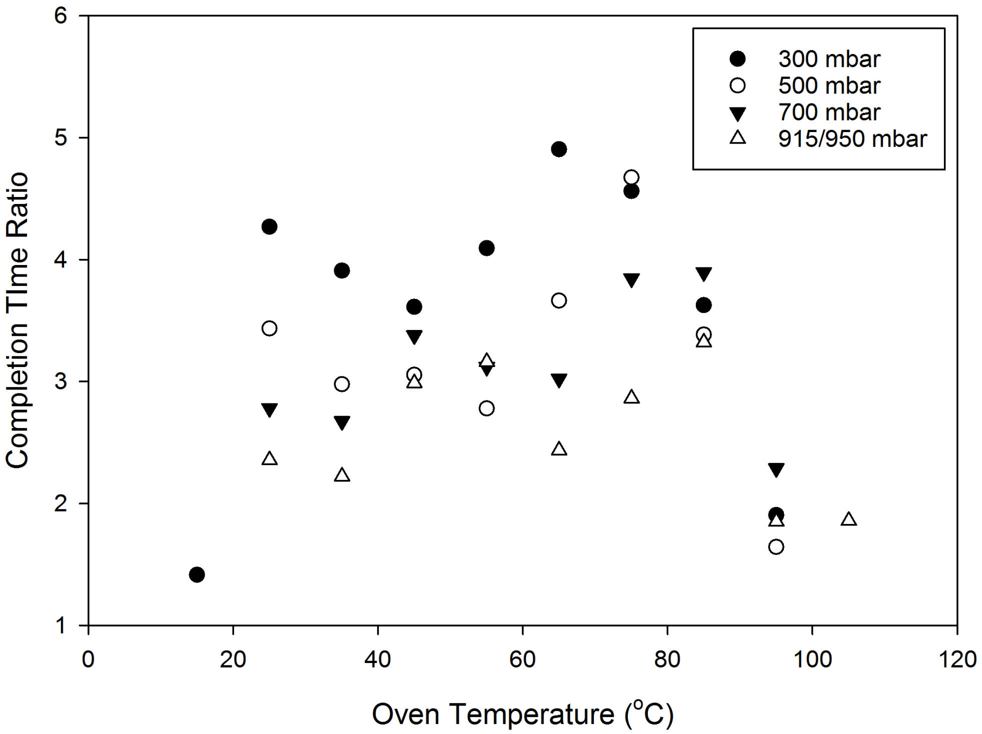

Figure 30 – Ratio of Completion Time Between Low and High Grade Gangue

Figure 30 shows the completion time ratio as a function of temperature and pressure. Despite having, on average, 50% less cyclohexane to remove, the completion time was an average of 3.3 ± 0.9 (n=33) times higher for low grade gangue than for high grade gangue for tests conducted at the same temperature and pressure. It also appears that the effect of decreasing pressure has a more significant impact on high grade gangue than it does on low grade gangue, as the completion time ratio is higher for lower pressures.

## Residual Solvent at the End of The High Mass Flux Period

As was shown in the representative results, cyclohexane mass flux first increased to a maximum value as the temperature of the sample increased to a steady state, and then decreased as cyclohexane removal progressed and the amount of remaining cyclohexane decreased. It was found that the point at which mass flux dropped below 18% of its maximum value was a good point to consistently mark the transition from high mass flux to a slowly decreasing low mass flux for high grade gangue. In order to understand when this transition occurs, the residual concentration of cyclohexane in parts per thousand (ppt) at this transition point was plotted against temperature and pressure in Figure 31 for high grade gangue and Figure 32 for low grade gangue.

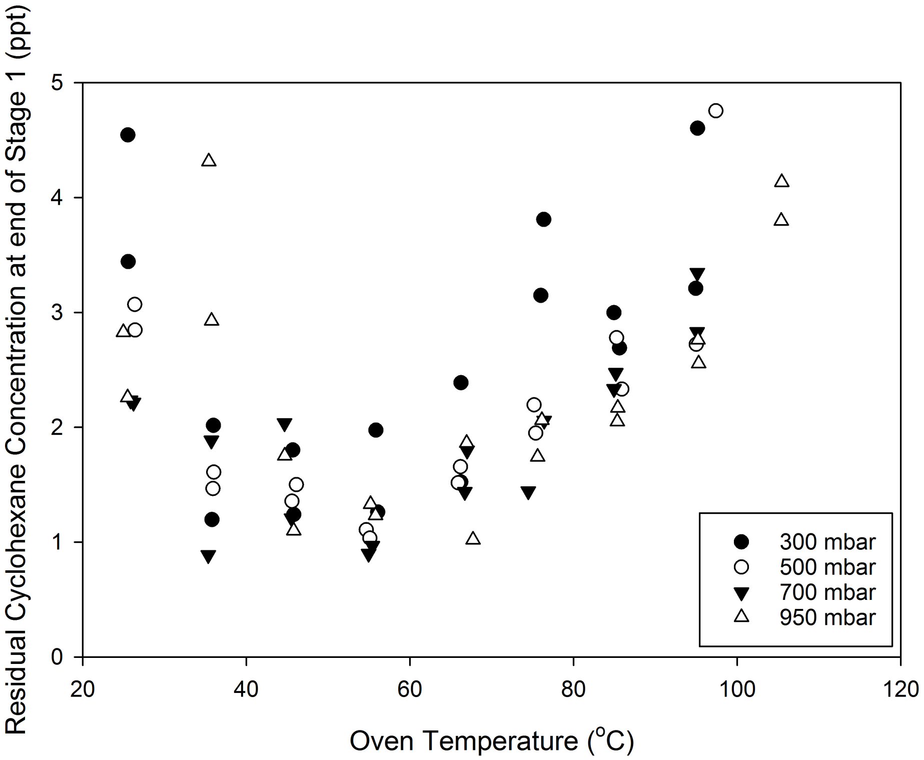

Figure 31 - Residual Concentration at End of High Mass Flux Evaporation Stage for High Grade Gangue

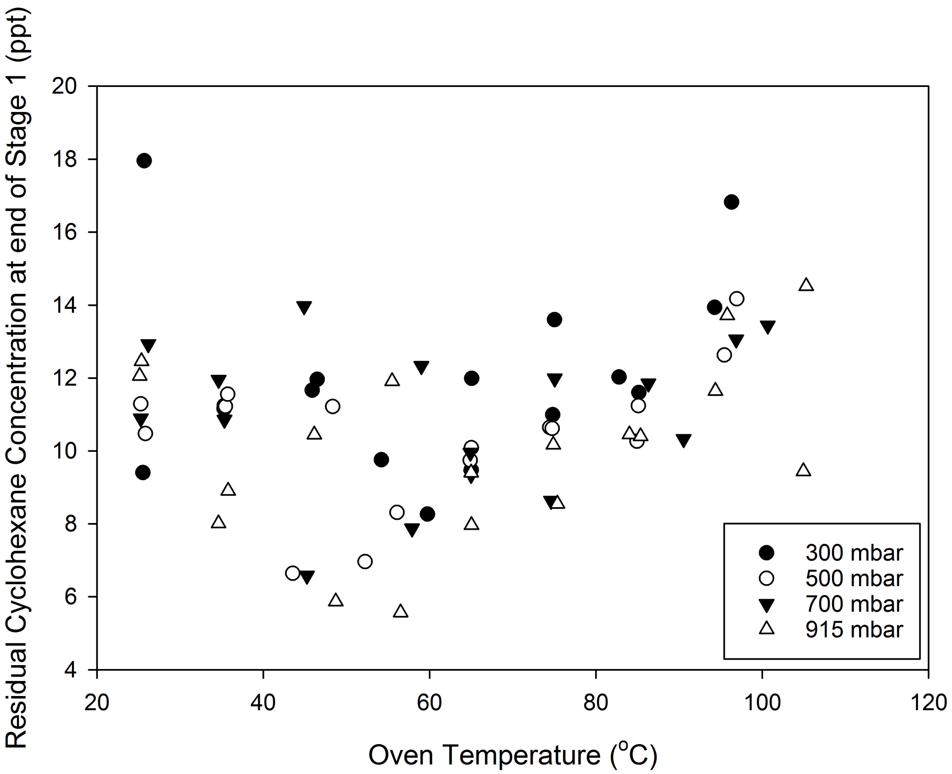

**Figure 32 - Residual Concentration at End of High Mass Flux Evaporation Stage for Low Grade Gangue**

The residual concentration of cyclohexane at the end of stage 1 was consistently higher for low grade gangue than it is for high grade gangue, with a mean value of 11 ± 2 ppt (n=66) for low grade gangue, but only 2.1 ± 0.9 ppt (n=66) for high grade gangue. This means that more cyclohexane must be recovered at a low mass flux for low grade gangue, and the overall process of cyclohexane removal will thus take longer. This phenomenon may be the result of liquid films being more dominant in high grade gangue than in low grade gangue, extending the high mass flux period by maintaining hydraulic connectivity with the free surface. It may also be caused by liquid water physically blocking cyclohexane from evaporating.

## Cyclohexane Removal Stages

Delving deeper into the cyclohexane removal process, the drying time was broken down into stages. The time to achieve residual concentrations of 20,000 ppm and 1,000 ppm by dry mass, were calculated for every test performed. A residual concentration of 20,000 ppm corresponds to about 85% and 80% cyclohexane removal for high and low grade gangue respectively. 20,000 ppm was chosen to approximate the first stage completion time as the level of residual cyclohexane was always lower than 20,000 ppm at the end of stage 1 for both ores, so the mass flux leading up to this concentration was always relatively high. A residual concentration of 1,000 ppm corresponds to about 99% cyclohexane removal for both high and low grade gangues. The drying time was broken into stages, first to reach a concentration of 20,000 ppm, then to get to 1,000 ppm, then to complete the process by reaching a residual concentration of 250 ppm. Figure 33 shows results for high grade gangue dried at a pressure of 700 mbar and varying pressure, while Figure 34 shows the results for low grade gangue dried at the same pressure. The results shown are averaged for each pair of tests completed at the same temperature.

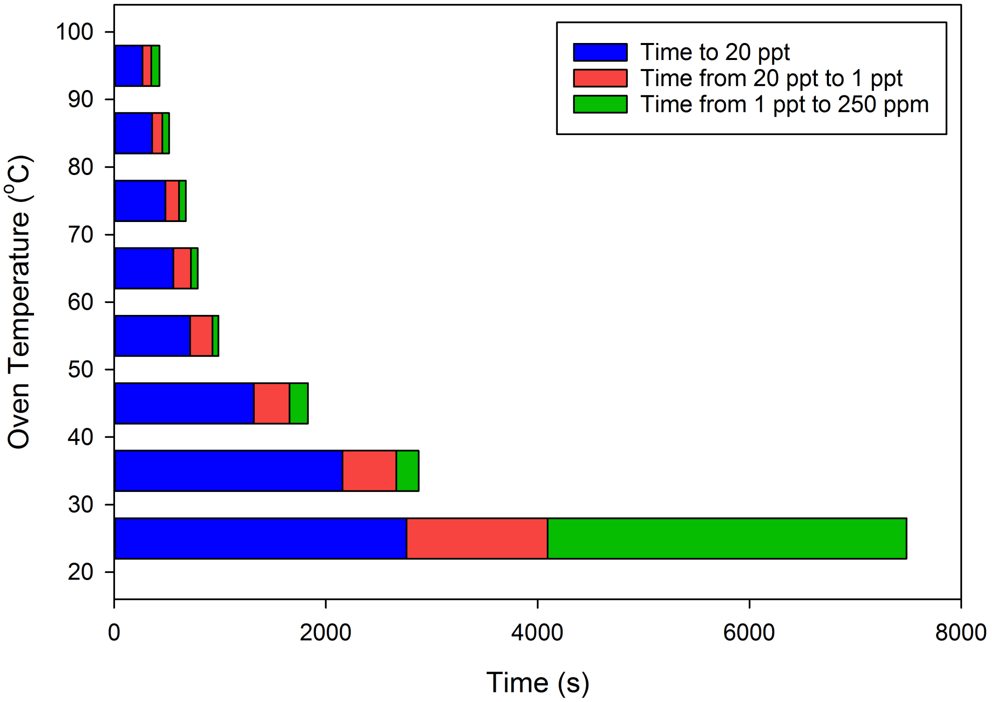

Figure 33 - Drying Time Broken into Stages for High Grade Gangue at 700 mbar

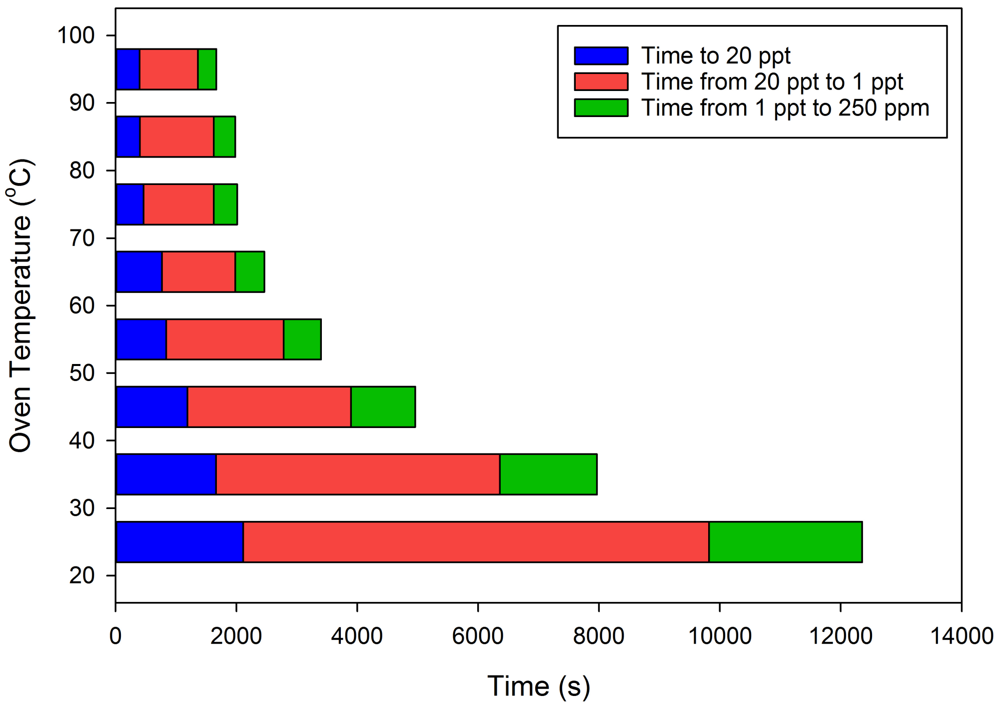

Figure 34 - Drying Time Broken into Stages for Low Grade Gangue at 700 mbar

With high grade gangue, the first stage took up the majority of the completion time, while the final stages were completed relatively quickly. Low grade gangue shows the opposite trend where the first drying stage was completed quickly, but the remaining 20,000 ppm took a very long time to remove. The slow removal of cyclohexane in the final drying stages may be caused by cyclohexane becoming trapped within pores of fine particles, as the vapour pressure within small pores will be suppressed by the Kelvin effect thereby slowing the evaporation of cyclohexane. Low grade ore contains an initial fines content of 20% by mass, while high grade ore only contains 10%. The effect of vapour pressure suppression will thus contribute more in low grade gangue, and can help explain the time difference in the final cyclohexane removal stage. Cyclohexane may also be physically blocked from evaporation in the final drying stages by films of liquid water, which exists in much higher concentrations in low grade gangue.

## Mass Flux in Final Drying Stages

### High Grade Gangue

In order to achieve full recovery, the cyclohexane mass flux at low residual concentrations must be considered. Of particular interest is how the effect of temperature and pressure on mass flux changes at lower residual concentrations. It is already clear that increasing temperature and decreasing pressure will increase the steady state mass flux. However, more information is still needed to determine if this relationship exists at low residual concentrations. To investigate, cyclohexane mass flux was plotted against temperature and pressure for many different residual concentrations. It was found that a clear relationship between mass flux and temperature and pressure still existed up to a residual cyclohexane concentration of 5000 ppm by dry mass, as is shown in Figure 35. A residual concentration of 5000 ppm corresponds to a cyclohexane recovery of about 96% for average high grade gangue.

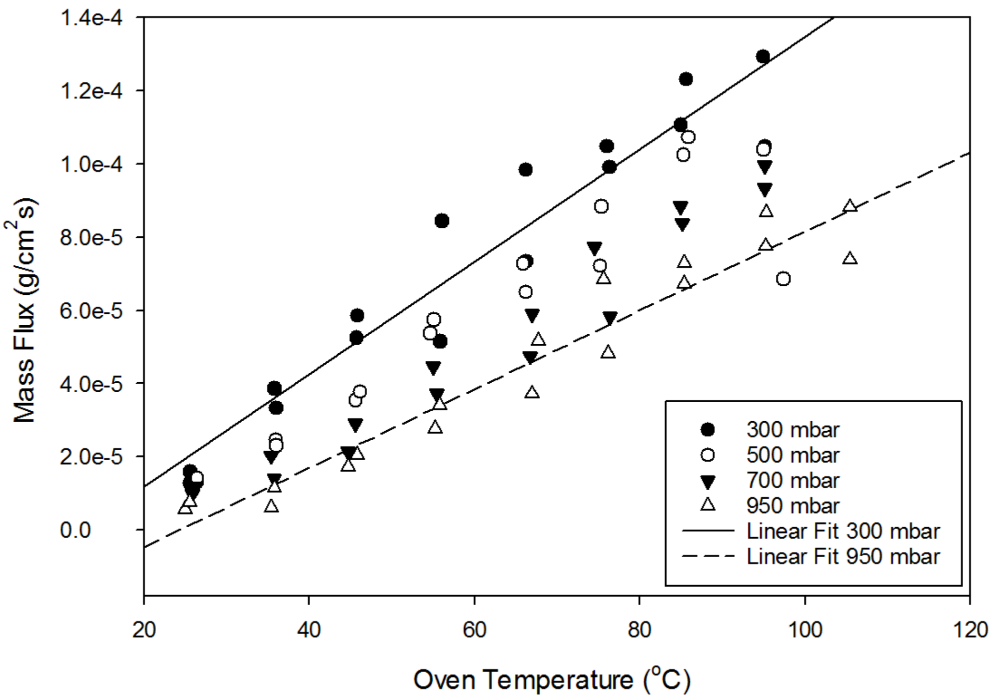

Figure 35 - Cyclohexane Mass Flux in High Grade Gangue When Residual Concentration was 5000 ppm

Clearly cyclohexane mass flux at this point still has a strong relationship with both temperature and pressure. When the concentration was reduced further, the relationship became less clear. For comparison, Figure 36 shows cyclohexane mass flux plotted against temperature and pressure when residual concentration was at 250 ppm, the point where cyclohexane removal is considered to be finished.

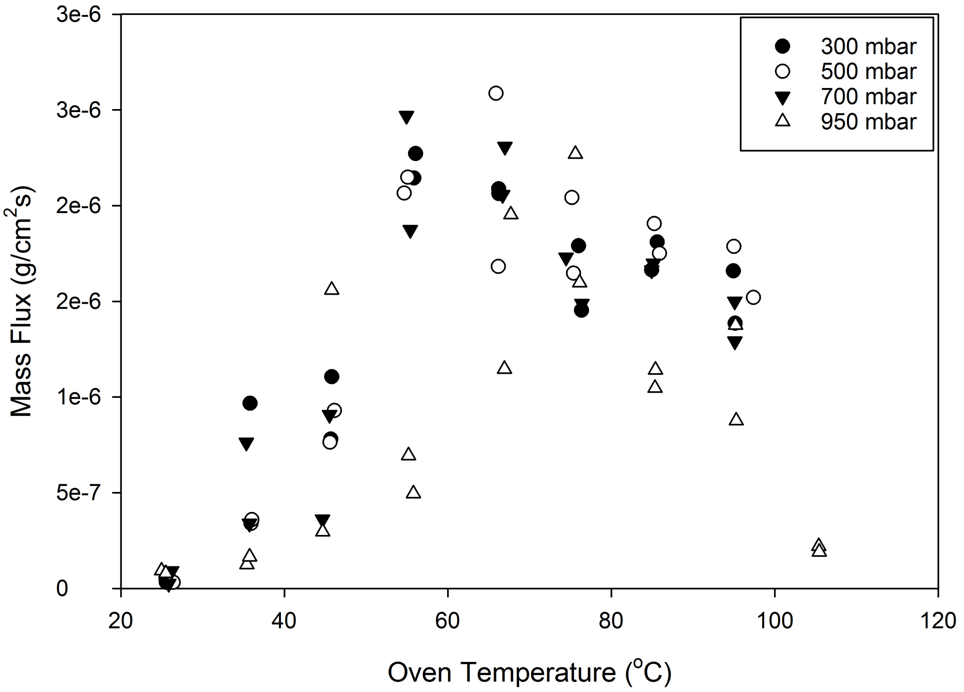

**Figure 36 - Cyclohexane Mass Flux in High Grade Gangue When Residual Concentration was 250 ppm**

In this case, mass flux does not show a clear relationship with temperature or pressure, unlike the case at 5000 ppm. Therefore, there is a point where the linear trend disappears somewhere between 5000 and 250 ppm. To further analyze where this point may be, linear relationship was assumed between mass flux and temperature to evaluate slopes for each tested pressure. The 4 slopes, along with their associated uncertainties, were obtained at residual concentrations of 10000, 5000, 2000, 1500, 1000, 500, and 250 ppm. The results for pressures of 300 and 950 mbar are plotted on a double logarithmic scale in Figure 37. Error bars shown are for a 95% confidence level on slope.

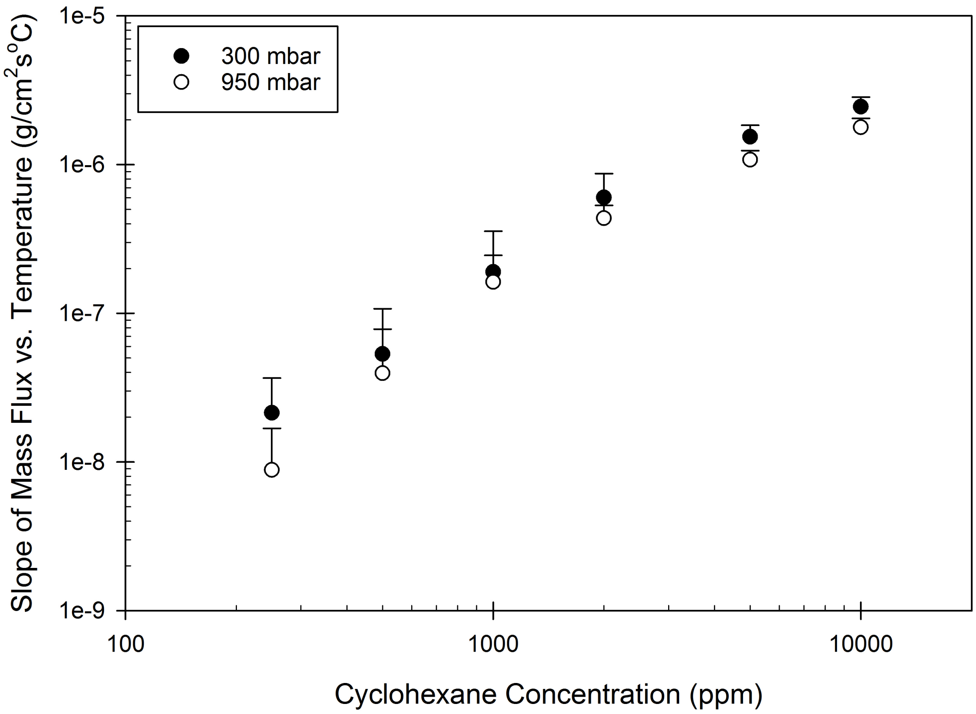

**Figure 37 - Relationship Between Mass Flux and Temperature at Decreasing Concentrations of Cyclohexane for High Grade Gangue**

Error bars represent an estimate of the uncertainty in linear slope of mass flux vs. temperature, and large error bars indicate poor linearity of the relationship. The size of the vertical space between 300 mbar and 950 mbar data points shows how the relationship between mass flux and temperature changes at different pressures. When error bars overlap, it indicates that the relationship of mass flux with temperature, pressure, or both loses significance. Error bars do not overlap at concentrations of 5000 and 10000 ppm, but do overlap at 2000 ppm and below. A student's t-test confirmed that there was a statistical difference between slopes at concentrations above 2000 ppm, but there was not enough evidence to make the same conclusion at and below 2000 ppm.

Error bars start to intersect the x-axis at and below a concentration of 500 ppm, indicating that the relationship between mass flux and temperature becomes insignificant at a residual concentration of 500 ppm. The effect of pressure also appears to diminish as concentration decreases, and may become insignificant at a concentration of 2000 ppm. It appears that the last stage of cyclohexane removal may be less dependent on temperature and pressure than it is on other uncontrolled variables. Factors that may slow the final stage of recovery include: size of pores that may trap cyclohexane, as smaller pores will slow evaporation, residual bitumen content that may block cyclohexane diffusion, geometry of the remaining gangue that could make the path of vapour diffusion to release cyclohexane more tortuous, and residual liquid water content that would slow evaporation of cyclohexane.

## Low Grade Gangue

Low grade gangue showed a different trend from high grade gangue in the final drying stages. With low grade gangue, a relationship between mass flux and temperature was still visible even at a low cyclohexane concentration of 250 ppm, as is shown in Figure 38.

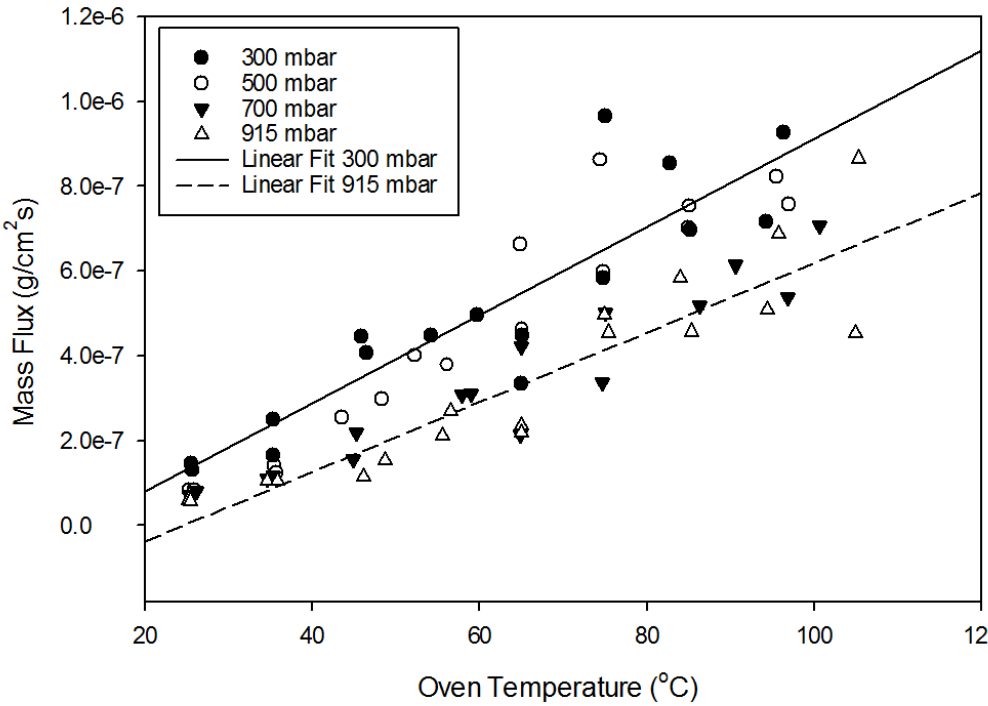

Figure 38 - Cyclohexane Mass Flux in Low Grade Gangue When Residual Concentration was 250 ppm

In order to help understand how the relationship changes as residual concentration decreases, slope of a linear fit between mass flux and temperature was plotted against residual concentration on a double logarithmic scale in Figure 39.

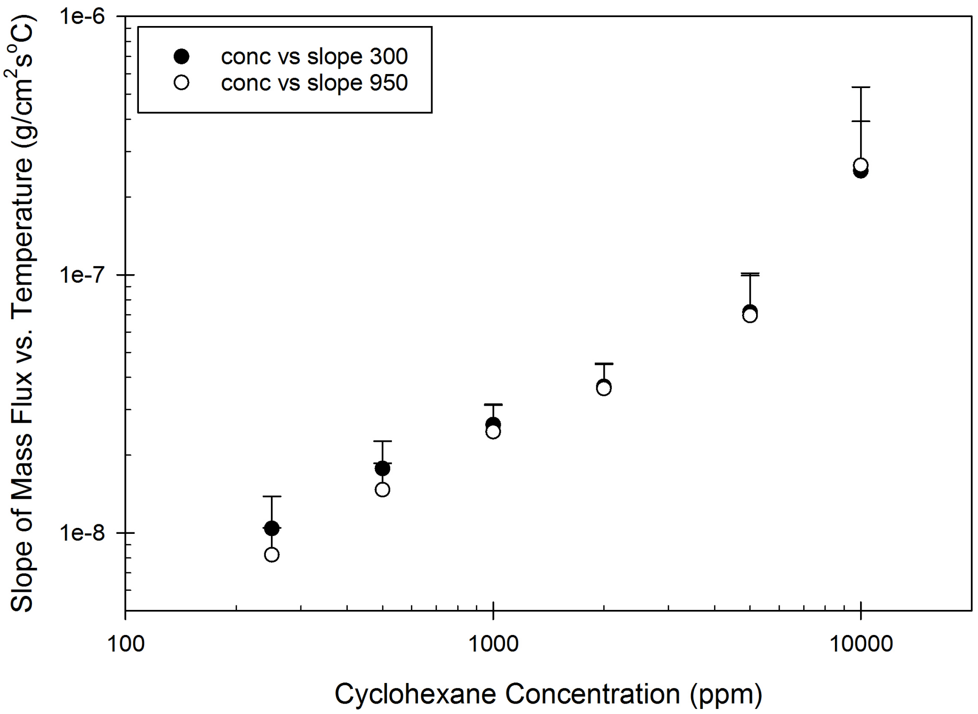

Figure 39 – Relationship Between Mass Flux and Temperature at Decreasing Concentrations of Cyclohexane for Low Grade Gangue

Smaller error bars indicate that relationship between mass flux and temperature remains strong even at low concentrations. The error bars never intersect the x-axis, so the relationship between mass flux and temperature is always statistically significant even at low cyclohexane concentrations. However, the gap between results at different pressures is always small, and a students t-test was unable to confirm a statistical difference between slopes of mass flux vs. temperature lines at 300 and 915 mbar at any concentration 10,000 ppm and lower. This indicates that mass flux is always dependent on oven temperature for low grade gangue, but there is not enough evidence to conclude that pressure also has an affect at low residual concentrations of cyclohexane.

## Unrecovered Solvents

It is important to consider that residual levels of cyclohexane may in fact be higher than what was measured in these experiments. Residual concentration was calculated using the measured levels of cyclohexane that evaporated during the experiment. The calculations did not take into account that some cyclohexane may not have evaporated from the sample during the experiment. In order to determine how much solvent may remain after an experiment, samples were left in a vacuum oven held at 70 °C and at an absolute pressure below 150 mbar. The sample was weighed immediately after the experiment, placed in the vacuum oven over night, and then weighed the next day. The resulting mass loss inside the vacuum oven is plotted against temperature and pressure for high grade gangue in Figure 40 and low grade gangue in Figure 41.

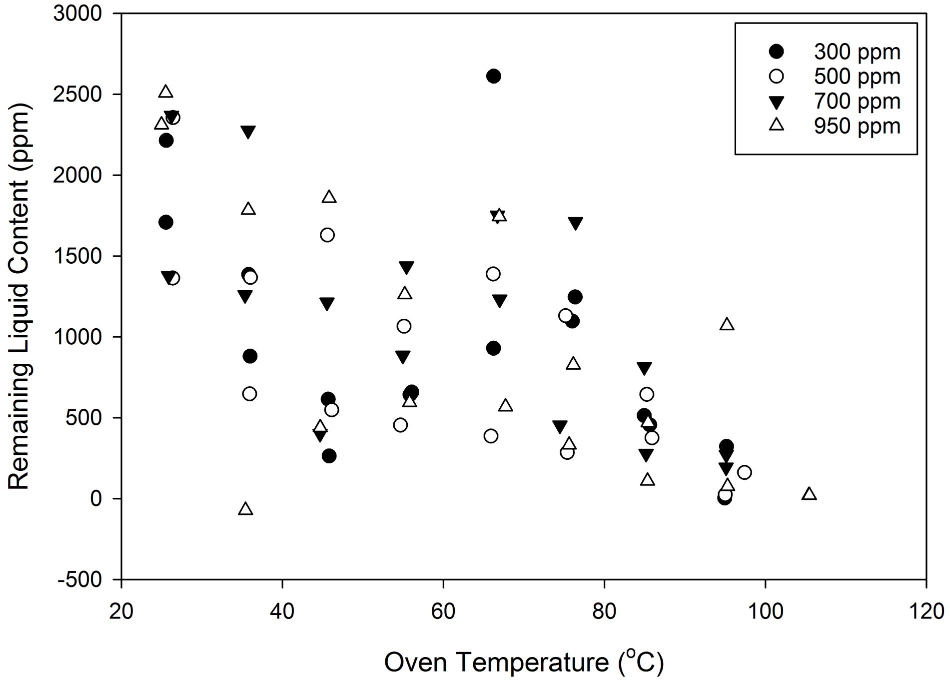

Figure 40 - Further Mass Loss After Samples Left in Vacuum Oven Over Night for High Grade Gangue

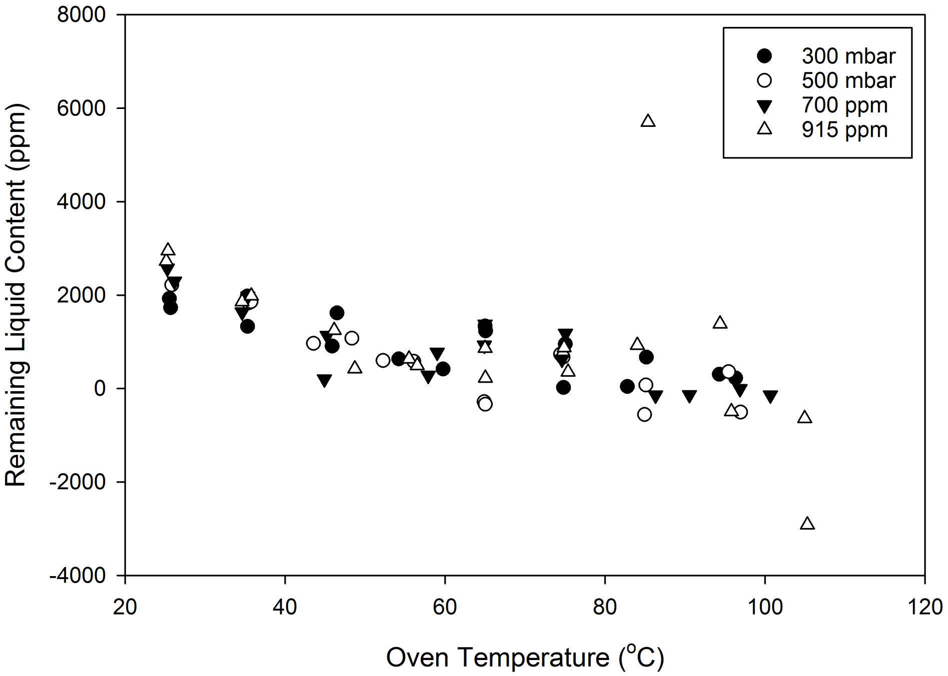

Figure 41 - Further Mass Loss After Samples Left in Vacuum Oven Over Night for Low Grade Gangue

In the worst case scenario, remaining volatile liquids constitute 0.036 g for high grade gangue and 0.068 g for low grade gangue, corresponding to concentrations of about 2700 ppm and 5600 ppm respectively. There is not a clear relationship between final mass loss and pressure, but it appears that the final mass loss decreases on average as temperature increases. It is important to keep in mind that mass lost in this stage of the experiment is not necessarily cyclohexane; it may also be water or other volatile materials. Considering that cyclohexane is much more volatile than water, it is highly likely that the majority of this further mass loss may be attributed to water rather than cyclohexane. Even if all the remaining mass was cyclohexane, the worst case scenario still gives a 98% removal of cyclohexane for high grade gangue and 95% for low grade gangue.

## Bitumen Migration Analysis

In preliminary experiments, it was observed that bitumen migrated upwards during drying. As was discussed in the literature review, there are two principle mechanisms of drying. Cyclohexane either evaporates inside the pores and diffuses out of the matrix in the vapour phase, or it is transported upwards in the liquid phase prior to evaporation on the surface. Residual bitumen is dissolved in the cyclohexane solvent, and is deposited where the cyclohexane evaporates, either inside the pores or on the surface of the sample. Both mechanisms occur simultaneously, but which mechanism dominates will affect the rate of evaporation and the model of drying.

In order to determine which mechanism of drying dominates, the extent of bitumen migration was measured. Figure 42 shows a sample of high and low grade gangue after drying. Low grade gangue had already formed into lumps prior to drying due to the high amount of water and clay binding particles together. It is possible that bitumen was transported from the inside of these lumps to the outside as drying occurred, but the lumps were too small to test and experimentally verify that hypothesis. Attempts to separate low grade gangue samples into a top and bottom layer by 50% mass failed to show quantitative results for bitumen migration, and as such only the results for high grade ore will be presented.

Figure 42 – High Grade (left) and Low Grade (right) Extraction Gangue after Drying

Over the course of the solvent removal process, high grade extraction gangue formed a thin film of bitumen on the top of the sample. After the each experiment was complete, the concentrated layer on top was carefully separated, weighed, and stored in a vial for later measurements. The layer underneath typically consisted of clean sand, and was weighed and collected separately. In the experiments conducted at lower temperatures, only two layers presented. However, in experiments conducted at higher temperatures, a third layer presented that was stuck to the base of the tin after the middle layer was extracted. When this layer formed, it was scraped off the tin and collected separately. Samples were passed through a CHNS analyzer that output what portion of the sample, by mass, was made up of carbon.

The measured carbon percentage was used to calculate remaining bitumen in each layer by subtracting the background carbon percentage attributed to carbonates in the sand, kerogens, and other forms of carbon. For high grade gangue, this value was calculated to be 0.3% based on CHNS analysis of soxlet extracted sand. The remaining carbon percentage is then divided by 0.83, as bitumen's average carbon content was measured to be 83% by mass.

$$f_{bit} = \frac{C\%_{measured} - C\%_{background}}{0.83} \tag{28}$$

The average bitumen percentage in the entire sample was calculated using a weighted average.

$$f_{bit,total} = \frac{f_{bit,top}m_{top} + f_{bit,middle}m_{middle} + f_{bit,stuck}m_{stuck}}{m_{top} + m_{middle} + m_{stuck}} \tag{29}$$

In order to analyze the response of bitumen migration to changing temperature and pressure, the sample was considered as though it had passed through a separator system with the goal of concentrating bitumen. The sample was separated into a concentration product, which was the top layer, and a tailing waste, which was the remainder of the sample. In cases where formation of a stuck layer was observed, the carbon percentage in the tailing was calculated by a weighted average of the middle and stuck layers. Figure 43 shows an idealized representation of the sample after drying is complete if all bitumen has migrated to the surface.

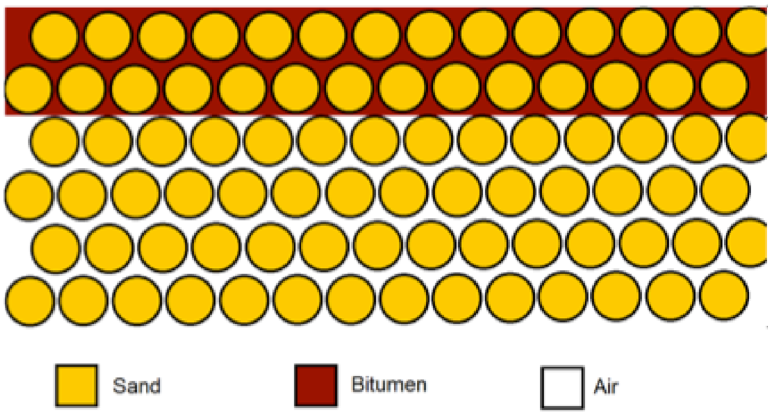

**Figure 43 - Assumed Composition of Remaining Gangue**

The enrichment ratio, which is the ratio of bitumen percentage in the top layer to the average bitumen percentage in the overall sample, was found to be the most useful parameter to represent bitumen migration.

$$Enrichment\ Ratio = \frac{f_{bit,top}}{f_{bit,total}} \tag{30}$$

The enrichment ratio shows how enriched the top layer is in comparison to the original sample by comparing bitumen percentages. An enrichment ratio greater than 1 indicates that bitumen has migrated to the top layer during drying. The enrichment ratio was plotted against temperature and pressure for high grade gangue in Figure 44 in order to quantitatively confirm if bitumen had migrated to the surface of the sample over the course of the experiments, and if changing temperature and pressure will change the extent of bitumen migration over the course of an experiment.

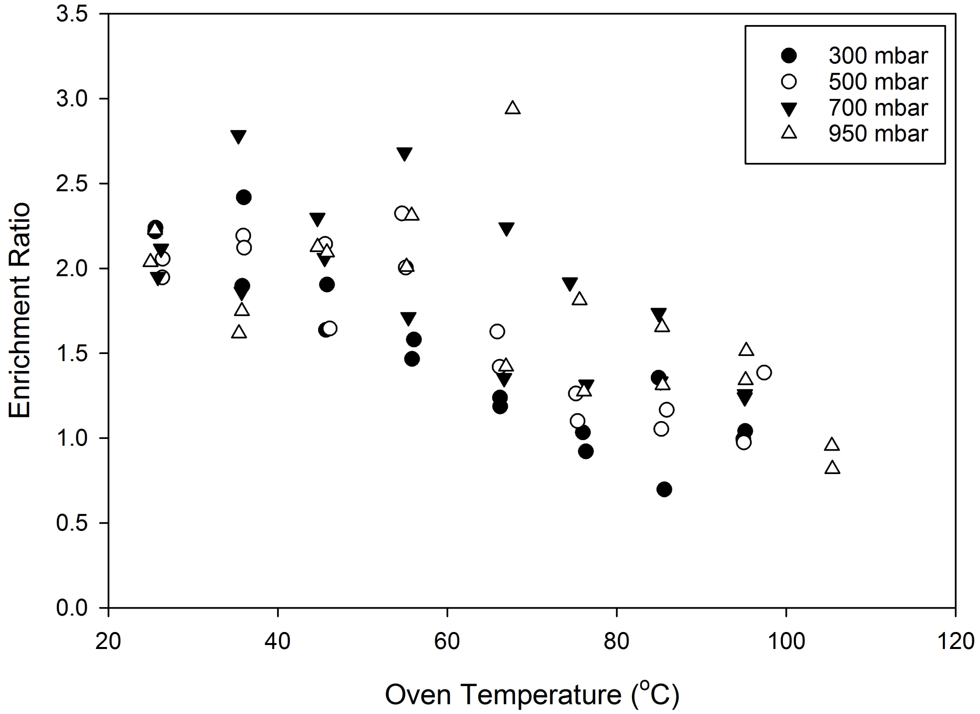

Figure 44 - Enrichment Ratio as a Function of Temperature and Pressure in High Grade Gangue

Figure 44 shows that the enrichment ratio was greater than 1 in the vast majority of cases, and in one case was almost as high as 3, proving conclusively that bitumen migrates upwards over the course of the solvent removal process in most cases. The most likely transport mechanism is that liquid films acting as a transport mechanism carry bitumen dissolved in liquid cyclohexane to the surface, and the bitumen is deposited when the cyclohexane evaporates. However, it is also clear that the enrichment ratio decreases as temperature increases. This indicates that the liquid film mechanism becomes less dominant, and that more evaporation occurs inside the pores at higher temperatures. This will be useful to consider in future work when a model of the solvent removal process is built.

The relationship between enrichment ratio and pressure is less clear, but the results at the lowest pressure of 300 mbar appear to give the lowest enrichment ratio. Unfortunately, there is too much variability within results to state conclusively that there is a relationship between bitumen migration and pressure. The variability in enrichment ratio between experiments is caused by a wide range of factors including different ratios of water, cyclohexane, residual bitumen, and fines in each sample. It was also challenging to physically separate the top layer from the rest of the sample consistently. Sometimes the top layer peeled off easily, and other times it crumbled and more sand that was not part of that top layer may have been collected. Nevertheless, results show clearly that bitumen migrates upwards during the course of drying, and the extent of bitumen migration decreases with increasing temperature.

### Batch Energy Calculations

One of the main objectives of this thesis is to find the combination of temperature and pressure that results in a minimization of total energy required to achieve cyclohexane recovery. As oven temperature and vacuum level are increased, the total power requirement to maintain the dryer in operation will increase, but the total time to achieve drying will decrease. It is reasonable to assume that there will be an optimum temperature and pressure combination where total energy requirement is minimized. As a first step to find this optimum, the net energy used in each test compared to a base case of evaporation in open air at 25 °C was calculated. Since the experiments performed were batch drying experiments, the energy calculations were performed for a batch operation. Energy requirements were broken down into 5 categories: energy to heat the sand, carrier gas, cyclohexane, water, and energy to maintain vacuum throughout the experiment.

### High Grade Gangue

Net energy input was calculated using the method in the methodology section combined with the fitted curves for subcooling and completion time, and the results are shown here. Completion time, which directly impacts the energy requirement to maintain vacuum and heat carrier gas, was calculated using the fitted curve shown in Figure 28 for all temperatures above 25 °C. At 25 °C, completion time was taken as the average completion time for the tests conducted at those pressures, except for the results at 700 mbar where the higher measured completion time was eliminated as an outlier because it skewed the results too high. Figure 45 through

Figure 48 show the calculated energy requirements compared to the base case of evaporating cyclohexane in ambient conditions at 25 °C for high grade gangue.

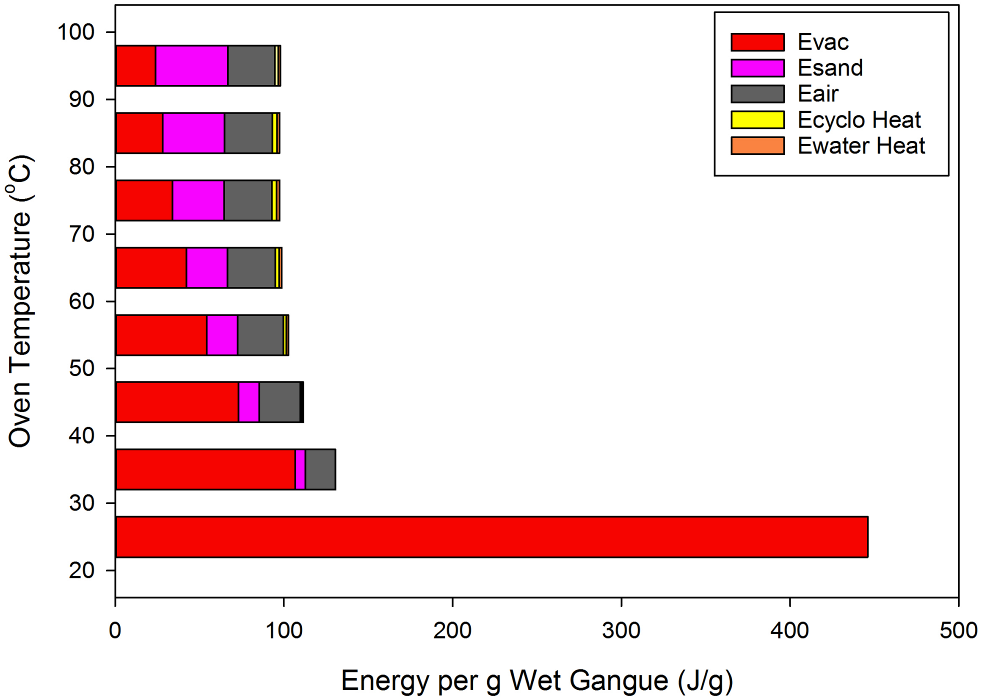

Figure 45 - Breakdown of Net Energy Input for Tests Conducted at 300 mbar on High Grade Gangue

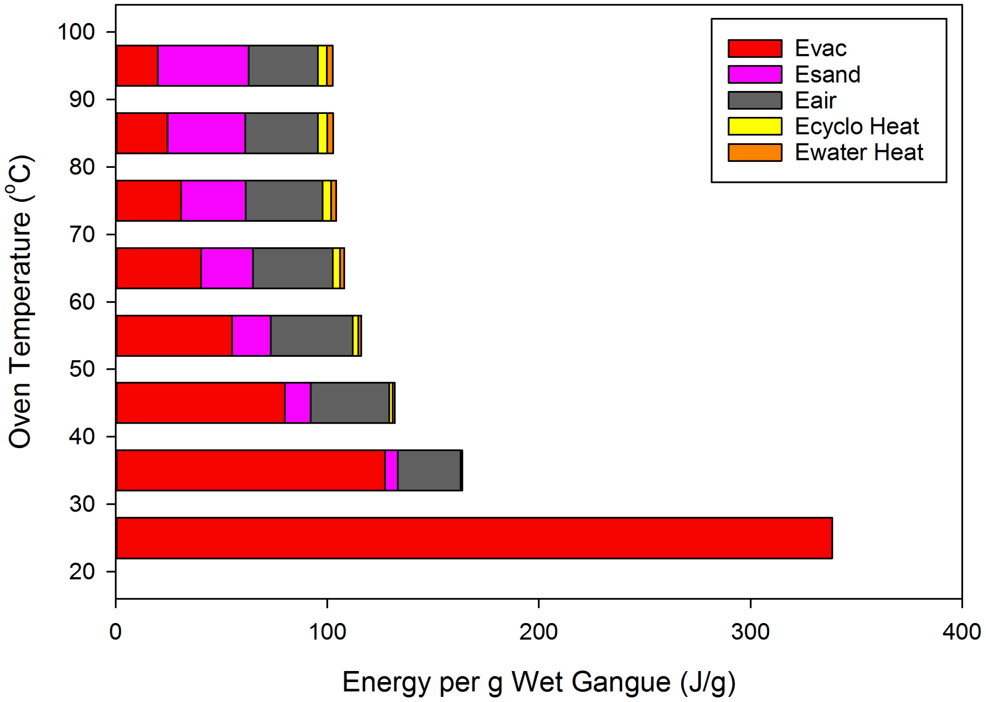

Figure 46 - Breakdown of Net Energy Input for Tests Conducted at 500 mbar on High Grade Gangue

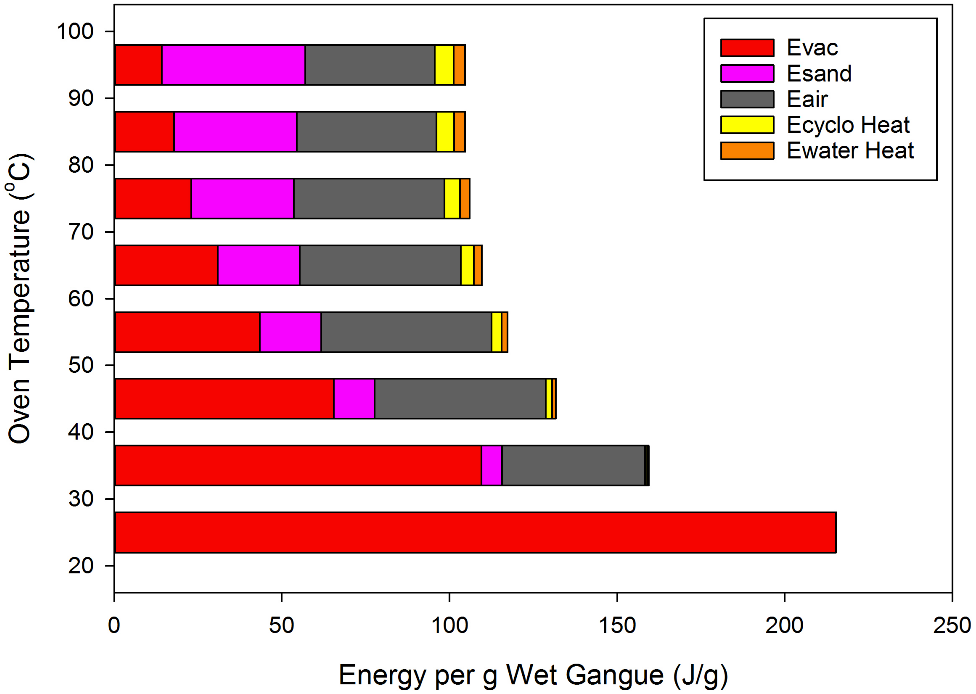

Figure 47 - Breakdown of Net Energy Input for Tests Conducted at 700 mbar on High Grade Gangue

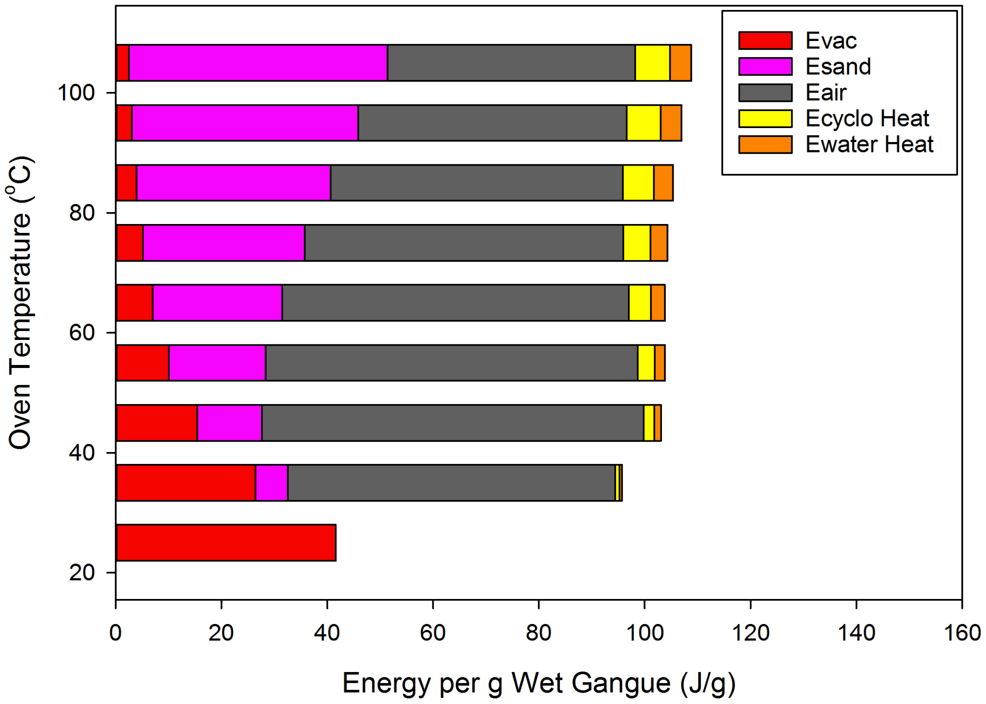

**Figure 48 - Breakdown of Net Energy Input for Tests Conducted at 950 mbar on High Grade Gangue**

The energy required to heat liquids prior to evaporation was found to be negligible, while the energy required to maintain vacuum and heat sand and carrier gas were found to be dominant. The energy requirement to maintain vacuum was found to be significant at low absolute pressures, and decreased as operating pressure increased. Energy required to maintain vacuum also decreased with increasing temperature due to the decrease in completion time. Energy required to heat the sand increased with oven temperature. Energy required to heat carrier gas was caused to increase when oven temperature was increased, but decreased with decreasing completion time. As completion time decreased with increasing temperature, there was a conflicting relationship between oven temperature and energy requirement to heat the gas. As a result of this conflict, energy requirement to heat carrier gas first increased, then reached a maximum value, and finally decreased with increasing temperature. The temperature at which this maximum value was found was different for each of the 4 pressures.

For all pressures below the atmospheric simulation pressure of 950 mbar, increasing temperature beyond 55 °C resulted in a decrease in total energy requirement due to the decrease in completion time affecting both vacuum energy and energy to heat carrier gas. This trend is not observed for the 950 mbar case, because the energy required to run the pump makes a much smaller contribution at this pressure. In order to compare cases in terms of net energy input, it is plotted as a function of temperature and pressure in Figure 49.

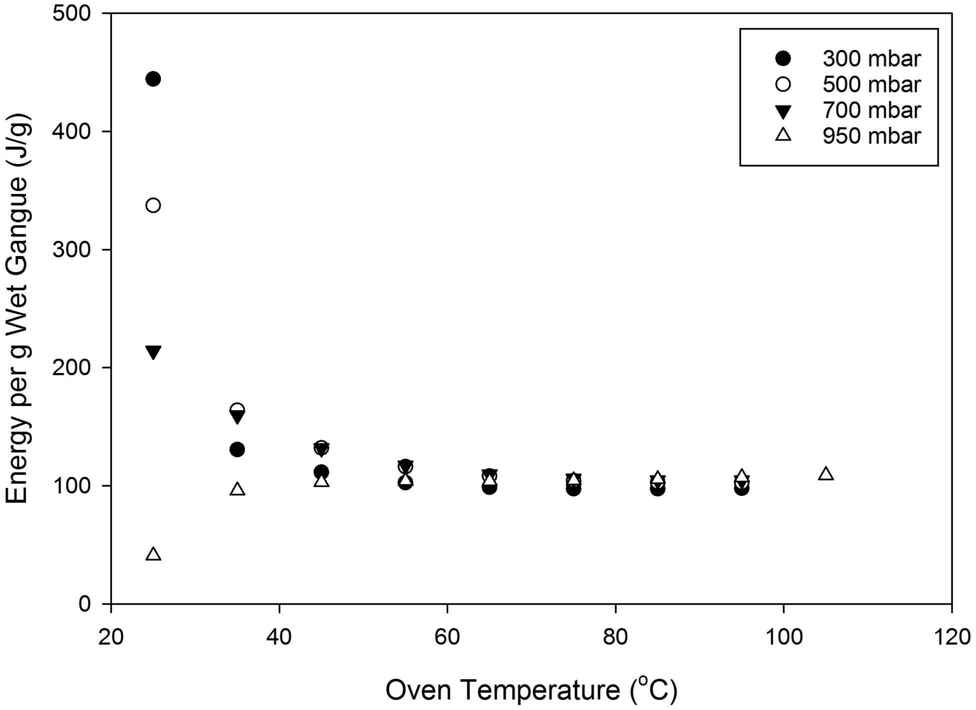

Figure 49 – Net Energy Input to High Grade Gangue as a Function of Temperature and Pressure

Figure 49 shows that the absolute minimum net energy input is found at atmospheric pressure and a temperature of 25 °C, where all heating requirements are provided by the surroundings. This is balanced with the fact that the longest completion time was found at this pressure and temperature combination. More energy input may be necessary to reduce residence times and resulting capital cost for industrial equipment. If this is the case, then it appears that increasing temperature beyond 55 °C and applying light vacuum would be beneficial as it would not significantly increase total energy requirement, but would reduce completion time and resulting size of equipment necessary to achieve drying.

## Low Grade Gangue

For comparison, the calculated energy inputs for low grade gangue are presented in Figure 50 through Figure 53.

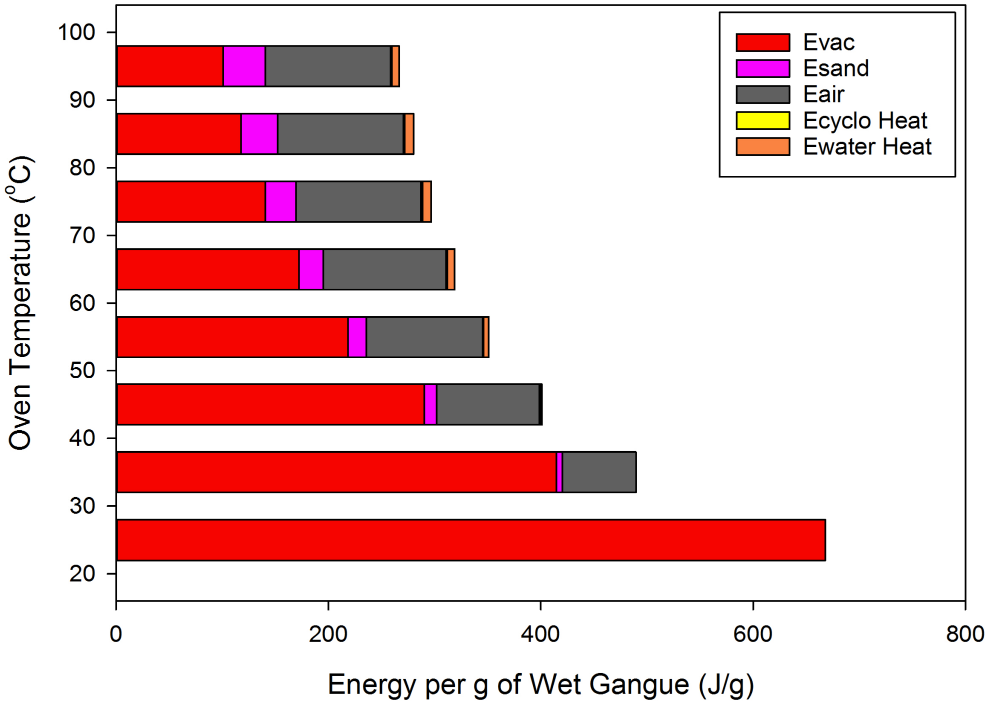

Figure 50 - Breakdown of Net Energy Input for Tests Conducted at 300 mbar on Low Grade Gangue

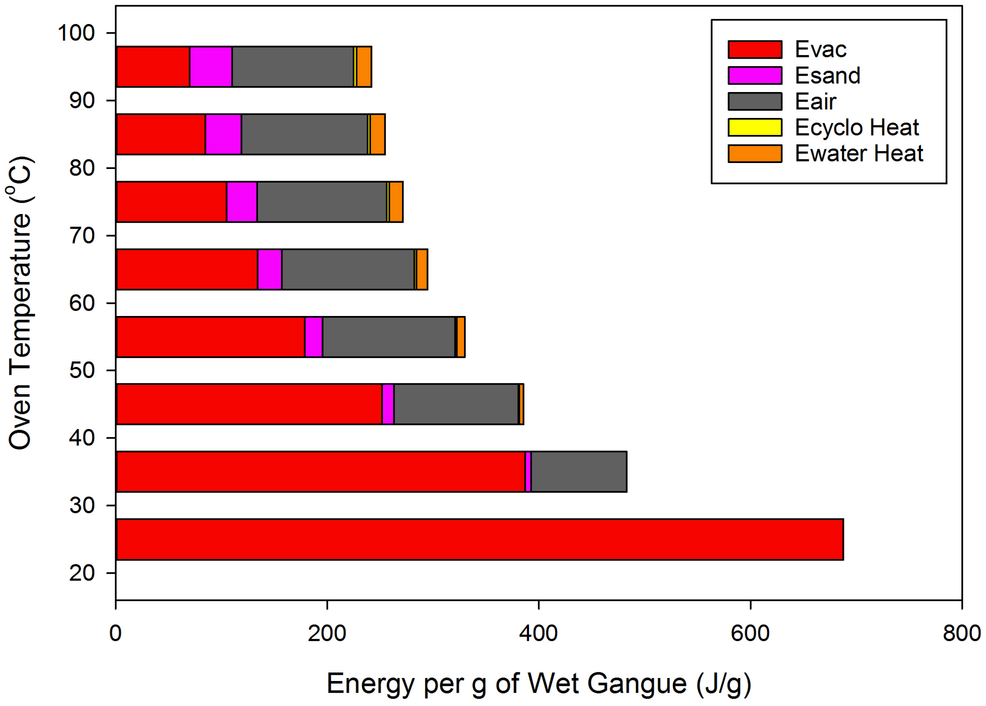

Figure 51 - Breakdown of Net Energy Input for Tests Conducted at 500 mbar on Low Grade Gangue

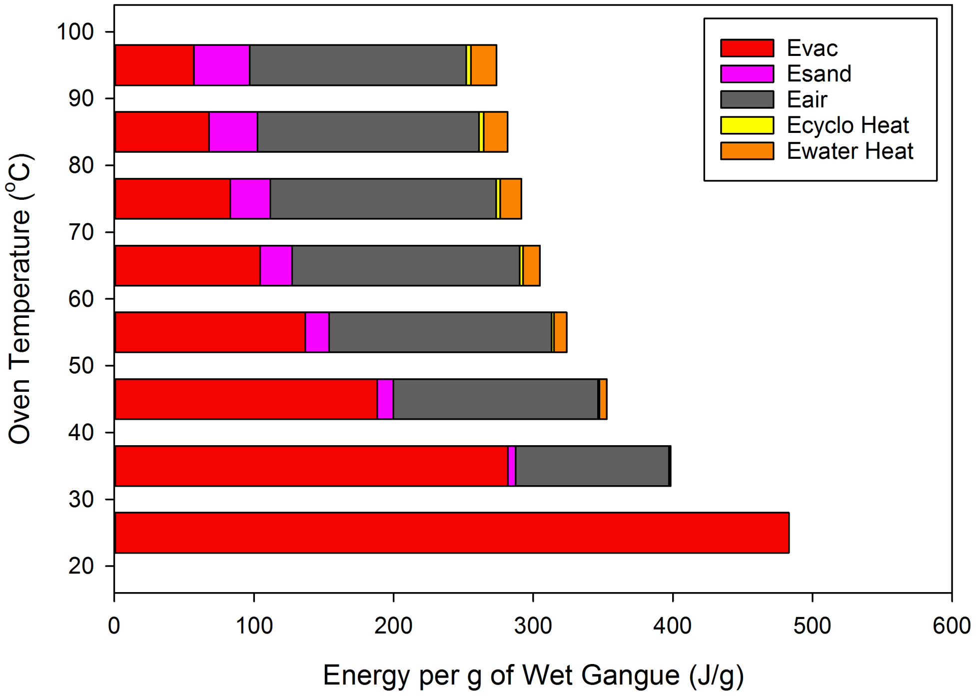

Figure 52 - Breakdown of Net Energy Input for Tests Conducted at 700 mbar on Low Grade Gangue

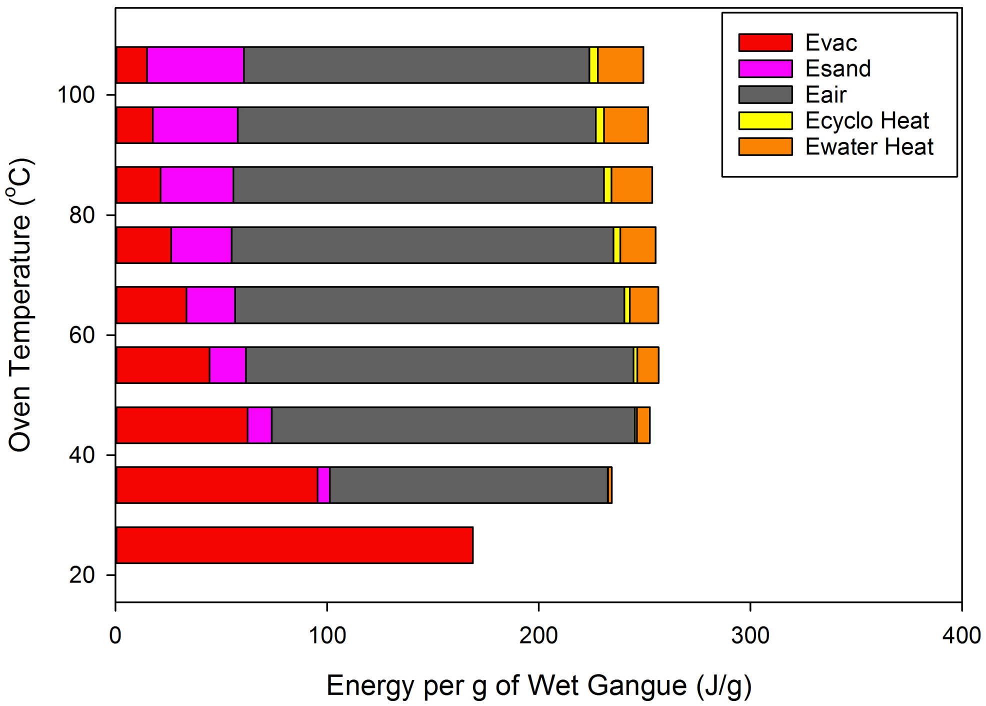

**Figure 53 - Breakdown of Net Energy Input for Tests Conducted at 915 mbar on Low Grade Gangue**

Once again, energy to heat liquids was negligible. Due to the extremely long completion time required to recover cyclohexane in low grade gangue, the energy to maintain vacuum and heat carrier gas was found to dominate. At all pressures below the atmospheric simulation condition of 915 mbar, net energy input was found to decrease with increasing temperature finding a minimum at 95 °C. The minimum overall energy requirement was again found at 25 °C and 915 mbar, the point where the maximum completion time was found. Figure 54 compares cases in terms of net energy input.

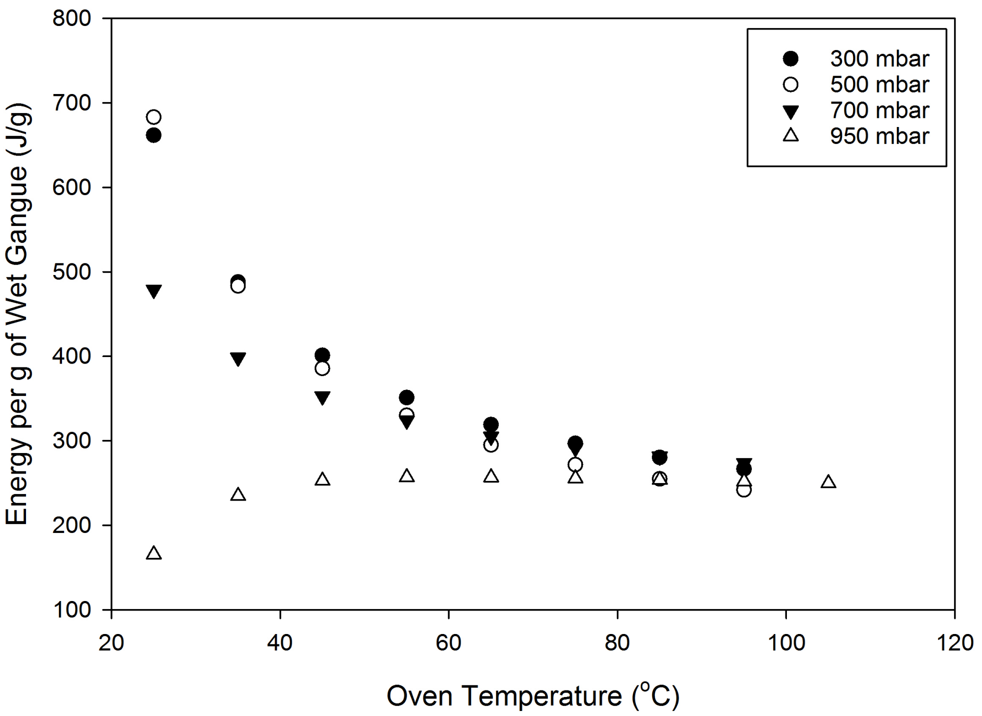

Figure 54 - Net Energy Input to Low Grade Gangue as a Function of Temperature and Pressure

If required completion time at atmospheric pressure and ambient temperature is too large, then increasing temperature beyond 65 °C and applying light vacuum would be beneficial as it would reduce the time required to remove cyclohexane from the gangue, without significantly impacting energy requirement.

Considering both grades of gangue together with this energy model, it appears that increasing temperature and applying vacuum are both beneficial as they decrease required completion time without significantly impacting the energy requirement. However, it is important to remember the limitations of this model when predicting energy inputs to a solvent recovery process on an industrial scale. These calculations were performed for a batch operation, but an industrial operation would necessarily use a continuous process. A continuous process utilizing a counter flow setup would allow the carrier gas to become more saturated with vapour than it is in these experiments, thus reducing the required carrier gas and energy costs associated with running pumps and heating carrier gas.

These calculations neglected the energy required to evaporate cyclohexane and water, which will both make significant contributions to the total energy required to fully remove cyclohexane. Their contributions were neglected partially because of uncertainty whether energy used to evaporate liquids was supplied by the surroundings or the oven. In a large scale insulated drier optimized for continuous operation, very little energy will be exchanged with the surroundings. Therefore, the energy required to evaporate liquids will need to be included explicitly in an energy balance for operation on an industrial scale. However, the energy required to evaporate cyclohexane will only weakly depend on oven temperature, and the amount of water that must be evaporated in order to fully recover cyclohexane should only vary slightly with varying oven temperatures and pressures. Thus the location of the minimum energy requirement should not be heavily affected by the inclusion of these two terms.

These calculations also do not consider that energy required to maintain vacuum would be supplied by electricity, which is more expensive than directly burning natural gas to produce heat. More natural gas would need to be burned to produce 1 J of electricity than what would be needed to produce 1 J of energy for heating. Vacuum energy also cannot be recovered, while heat can be partially recovered and re-used through heat exchangers. It is also important to consider that capital cost for vacuum equipment may be prohibitive.

A more comprehensive energy model that can predict energy requirements in a continuous process on an industrial scale is needed to draw clear conclusions about the optimum operating temperature and pressure. However, based on these results, and considering the high capital cost of vacuum equipment, it is recommended that industrial operations extract cyclohexane from gangue at atmospheric pressure. Operating at higher temperatures is also recommended to reduce completion time without significantly increasing energy requirements. Performing bitumen extraction at a temperature of 75 °C, for example, would result in a high efficiency of bitumen recovery without exceeding the boiling point of cyclohexane. Removal of cyclohexane from gangue could then be completed at the same temperature, leading to fast removal of cyclohexane. Heat exchangers could be used to preheat carrier gas and solvent to minimize energy requirements.

## Conclusions

An apparatus was successfully designed that could accurately control and measure process temperature and pressure, and separately measure the evaporation rate of both cyclohexane and water. Both high and low grade oil sand ores were processed through a solvent based extraction process with cyclohexane as the solvent.

Experiments confirmed that increasing temperature and decreasing pressure had the effect of increasing the steady state mass flux of cyclohexane evaporating from both high and low grade gangue. Vapour pressure was found to be a significant driver of cyclohexane evaporation, as steady state mass flux fit well to a curve that was directly proportional to cyclohexane vapour pressure at oven temperature. Increasing oven temperature and decreasing pressure was found to be beneficial in reducing the completion time required to reach a goal residual cyclohexane concentration of 250 ppm. However, the benefits became less significant at higher temperatures, as completion time followed a power law decay with both factors.

Mass flux at all stages of the drying process, from steady state mass flux with high cyclohexane concentrations to mass flux in the final drying stages was found to be higher for high grade gangue than it was for low grade gangue. As a result, completion time was found to be an average of 3 times longer for low grade gangue than for high grade gangue. When completion time was broken into stages for both grades of gangue, it was found that the final drying stages to recover the last 20,000 ppm of cyclohexane were short for high grade gangue, but lasted very long and in fact were dominant for low grade gangue. This, combined with the observation that more cyclohexane remained in low grade gangue at the end of the high mass flux evaporation stage, led to the significantly larger completion time.

One of the reasons that mass flux was higher in high grade gangue is related to the significantly lower water and fines contents. Prior to bitumen extraction, low grade ore contained 19.4 % ± 0.9% (n=2) by mass compared to just 11.2% ± 0.7% (n=3) for high grade ore. Low grade gangue also contained significantly more water, 12.5% ± 1.1% (n=66) on wet mass basis as compared to 2.1% ± 1.1% (n=66) for high grade gangue. Fine particles were thought to be hydrophilic in low grade gangue, as they formed clumps held together by water. As a result of hydrophilic clumps forming on the evaporating surface, the surface was less saturated with cyclohexane in low grade gangue and steady state cyclohexane mass flux was lower in low grade gangue.

Mass flux was also lower during the final stages of drying in low grade gangue as a result of the increased fines and water content. Fine particles create smaller pores, that suppress vapour pressure due to the kelvin effect, and slow vapour diffusion by creating a more tortuous path for vapour to exit the sample. This effect is more significant at low residual concentrations when all the cyclohexane that was held in the larger pores has evaporated and only the cyclohexane left in the small pores remains. Residual liquid water, which is also more prominent in low grade gangue, may also slow the final cyclohexane removal stages by physically blocking or slowing evaporation of cyclohexane molecules that must diffuse through the liquid water to evaporate.

Another reason for increased mass flux in high grade gangue, as confirmed by bitumen migration measurements, is that liquid films were more dominant in high grade gangue. Liquid films accelerate the evaporation process by transporting cyclohexane to the surface of the gangue in the liquid phase, so it may evaporate there instead of inside the pores where it would have to diffuse out of the matrix in the gas phase. This will increase evaporation rates to near steady state drying rates and prolong the high mass flux evaporation stage by maintaining a near saturated drying surface. However, evidence was presented showing that the dominance of liquid films decreased as temperature increased. This may help explain why the benefits of increasing temperature diminished at higher temperatures.

Energy analysis was performed for these lab scale batch experiments. Analysis indicated that minimum energy input to achieve cyclohexane removal on a lab scale was achieved at a temperature of 25 °C and atmospheric pressure. However, the longest completion time was also found at this temperature and pressure combination, and it is likely that higher temperatures would be necessary on an industrial scale to reduce capital costs associated with equipment size. Net energy input also stabilized at higher temperatures due to reduced energy requirement to run the pumps and heat carrier gas balanced with increased heating costs for sand and liquids. Therefore, it would be beneficial to run at higher temperatures as the completion time would be reduced without dramatically increasing the energy requirement.

## Recommendations

Overall, the experiments were successful and new insight was gained into the mechanism of recovering solvent from extraction gangue. The mechanism is complex and building a comprehensive model of the process will be difficult. This research has helped understand the effect of temperature and pressure on the process, but there is still a significant amount of work to be done.

More work is needed to understand the effect of residual water on the final stages of solvent recovery. As evaporation of water is very energy intensive, it is important to understand if it is necessary to evaporate all the water in the gangue in order to fully recover cyclohexane, and how the amount of water that must be evaporated changes with changing operating temperature and pressure. Due to condensation issues, and high levels of variability in this data set, we were unable to draw clear conclusions on this issue.

A comprehensive model will need to be developed that encompasses all stages of cyclohexane removal. This will be a very challenging task, as the process is very complex and affected by many variables. Beyond the effect of temperature and pressure on the drying process, the model will need to incorporate the effect of liquid films, which changes with changing operating temperature. The effect of residual bitumen on the solvent removal process must also be studied and incorporated, as well as the effect of residual liquid water and fine particles in the final stages of solvent removal. While the energy model developed in this thesis is valuable to give basic insights into the optimum range of operating parameters, a more comprehensive energy model that can predict energy requirements for a continuous process on an industrial scale will also be necessary in order to determine this optimum range.

# References

[1] Government of Alberta. (September, 2014). *Talk about Oil Sands*.

[2] Government of Alberta. (January, 2014). *Alberta's Clean Energy Story*.

[3] J. Masliyah, J. Czarnecki and Z. Xu, *Handbook on Theory and Practice of Bitumen Recovery from Athabasca Oil Sands*. Canada: Kingsley Knowledge Publishing, 2011.

[4] IHS Energy. Comparing GHG intensity of the oil sands and the average US crude oil. IHS Energy. 2014.

[5] Suncor Energy. *The Oil Sands Story (1960s, 1970s & 1980s)*.

[6] K. L. Kasperski and R. J. Mikula. Waste streams of mined oil sands: Characteristics and remediation. *Elements 7(6),* pp. 387-392. 2011.

[7] Canadian Oil Sands Innovation Alliance. (September, 2014). *Tailings Centrifuge*.

[8] D. W. Schindler. Unravelling the complexity of pollution by the oil sands industry. *Proc. Natl. Acad. Sci. U. S. A. 111(9),* pp. 3209-3210. 2014.

[9] R. A. Frank, J. W. Roy, G. Bickerton, S. J. Rowland, J. V. Headley, A. G. Scarlett, C. E. West, K. M. Peru, J. L. Parrott, F. M. Conly and L. M. Hewitt. Profiling oil sands mixtures from industrial developments and natural groundwaters for source identification. *Environmental Science and Technology 48(5),* pp. 2660-2670. 2014.

[10] A. Parajulee and F. Wania. Evaluating officially reported polycyclic aromatic hydrocarbon emissions in the athabasca oil sands region with a multimedia fate model. *Proc. Natl. Acad. Sci. U. S. A. 111(9),* pp. 3344-3349. 2014.

[11] P. Gosselin, S. Hrudey, A. Naeth, A. Plourde, R. Therrien and G. Van Der Kraak, "Envionmental and health impacts of canada's oil sands industry," The Royal Society of Canada Expert Panel, Ottawa, Ontario, 2010.

[12] J. Masliyah, Z. Zhou, Z. Xu, J. Czarnecki and H. Hamza. Understanding water-based bitumen extraction from athabasca oil sands. *Can. J. Chem. Eng. 82(4),* pp. 628-654. 2004.

[13] P. Painter, P. Williams and A. Lupinsky. Recovery of bitumen from utah tar sands using ionic liquids. *Energy and Fuels 24(9),* pp. 5081-5088. 2010.

[14] K. Yu, Z. Wang, Y. Jin, Z. Sun, Y. Liu, J. Yang and Y. Cai. Single- and multi-stage counter-current solvent extractions of bitumen from xinjiang oil sand. *Energy and Fuels 27(11),* pp. 6491-6500. 2013.

[15] T. Wang, C. Zhang, R. Zhao, C. Zhu, C. Yang and C. Liu. Solvent extraction of bitumen from oil sands. *Energy and Fuels 28(4),* pp. 2297-2304. 2014.

[16] D. Y. Han, Z. B. Cao and X. Q. Xu. Study on solvent extraction of mongolia outcrop oil sands. *Energy Sources, Part A: Recovery, Utilization and Environmental Effects 35(14),* pp. 1368-1374. 2013.

[17] A. Holland, D. Wechsler, A. Patel, B. M. Molloy, A. R. Boyd and P. G. Jessop. Separation of bitumen from oil sands using a switchable hydrophilicity solvent. *Canadian Journal of Chemistry 90(10),* pp. 805-810. 2012.

[18] H. Yang, Y. Wang, M. Ding, B. Hu and S. Ren. Water-assisted solvent extraction of bitumen from oil sands. *Industrial and Engineering Chemistry Research 51(7),* pp. 3032-3038. 2012.

[19] A. Hooshiar, P. Uhlik, Q. Liu, T. H. Etsell and D. G. Ivey. Clay minerals in nonaqueous extraction of bitumen from alberta oil sands: Part 1. nonaqueous extraction procedure. *Fuel Process Technol 94(1),* pp. 80-85. 2012.

[20] P. Painter, P. Williams and E. Mannebach. Recovery of bitumen from oil or tar sands using ionic liquids. *Energy and Fuels 24(2),* pp. 1094-1098. 2010.

[21] X. Li, W. Sun, G. Wu, L. He, H. Li and H. Sui. Ionic liquid enhanced solvent extraction for bitumen recovery from oil sands. *Energy and Fuels 25(11),* pp. 5224-5231. 2011.

[22] H. Nikakhtari, S. Wolf, P. Choi, Q. Liu and M. R. Gray. Migration of fine solids into product bitumen from solvent extraction of alberta oilsands. *Energy and Fuels 28(5),* pp. 2925-2932. 2014.

[23] J. Wu and T. Dabros. Process for solvent extraction of bitumen from oil sand. *Energy and Fuels 26(2),* pp. 1002-1008. 2012.

[24] H. Nikakhtari, L. Vagi, P. Choi, Q. Liu and M. R. Gray. Solvent screening for non-aqueous extraction of alberta oil sands. *Can. J. Chem. Eng.* 2012.

[25] D. E. Cormack, J. M. Kenchington, C. R. Phillips and P. J. LeBalnc. PARAMETERS AND MECHANISMS IN THE SOLVENT EXTRACTION OF MINED ATHABASCA OIL SAND. *Can. J. Chem. Eng. 55(5),* pp. 572-580. 1977.

[26] X. Li, L. He, G. Wu, W. Sun, H. Li and H. Sui. Operational parameters, evaluation methods, and fundamental mechanisms: Aspects of nonaqueous extraction of bitumen from oil sands. *Energy and Fuels 26(6),* pp. 3553-3563. 2012.

[27] H. Leung and C. R. Phillips. Solvent extraction of mined athabasca oil sands. *Industrial and Engineering Chemistry Fundamentals 24(3),* pp. 373-379. 1985.

[28] E. W. Funk. BEHAVIOR OF TAR SAND BITUMEN WITH PARAFFINIC SOLVENTS AND ITS APPLICATION TO SEPARATIONS FOR ATHABASCA TAR SANDS. *Can. J. Chem. Eng. 57(3),* pp. 333-341. 1979.

[29] C. M. Gable, E. A. Duncan and E. R. Freitas, "Selective Solvent Extraction Plus Filtration of Tar Sands," 3475318, October 28, 1969.

[30] M. Farcasiu and D. Whitehurst, "Double Solvent Extraction of Organic Constituents from Tar Sands," 4046668, September 6, 1977.

[31] E. W. Funk, W. G. May and J. C. Pirkle, "Solvent Extraction Process for Tar Sands," 4347118, August 31, 1982.

[32] E. M. Haschke, G. A. Gimber and K. O. Groves, "Process for Recovery of Solvent from Tar Sands Bitumen," 4532024, July 30, 1985.

[33] W. J. Rosenbloom, "Method and Apparatus for the Solvent Extraction of Oil from Bitumen Containing Tar Sand," 5534136, July 9, 1996.

[34] J. M. Kenchington and C. R. Phillips. OPERATING COST PARAMETERS IN SOLVENT EXTRACTION OF BITUMEN FROM OIL SAND MINERAL DEPOSITS. *Energy Sources 5(4),* pp. 317-338. 1981.

[35] A. G. Yiotis, A. G. Boudouvis, A. K. Stubos, I. N. Tsimpanogiannis and Y. C. Yortsos. Effect of liquid films on the drying of porous media. *AICHE J. 50(11),* pp. 2721-2737. 2004.

[36] M. Prat. On the influence of pore shape, contact angle and film flows on drying of capillary porous media. *Int. J. Heat Mass Transfer 50(7-8),* pp. 1455-1468. 2007.

[37] N. Shokri and D. Or. Drying patterns of porous media containing wettability contrasts. *J. Colloid Interface Sci. 391(0),* pp. 135-141. 2013. . DOI: 10.1016/j.jcis.2012.08.074.

[38] N. Sghaier and M. Prat. Effect of efflorescence formation on drying kinetics of porous media. *Transp. Porous Media 80(3),* pp. 441-454. 2009.

[39] N. Shokri and D. Or. What determines drying rates at the onset of diffusion controlled stage-2 evaporation from porous media? *Water Resour. Res. 47(9),* 2011.

[40] C. L. Yaws. *Yaws' Transport Properties of Chemicals and Hydrocarbons (Electronic Edition)*.2010Available: http://app.knovel.com/hotlink/toc/id:kpYTPCHEE8/yaws-transport-properties.

[41] C. L. Yaws, *Yaws' Critical Property Data for Chemical Engineers and Chemists*. Knovel, 2014.

[42] Omega. (June, 2013). *Introduction to Thermocouples*.

[43] Parker Hannifin Corporation, *Parker O-Ring Handbook*. 2007.

[44] University of Waterloo, Microelectronics Heat Transfer Laboratory. (). *Fluid Properties Calculator*.

# Appendix A – Design Calculations

In order to perform experiments, I needed to design an apparatus for testing. This appendix shows the calculations that were performed in an effort to design an apparatus that will give accurate results. Two designs were constructed. The first featured a large vacuum oven with a battery operated scale inside. The sample was placed on the scale, and drying was conducted under vacuum. Mass loss curves were generated individually for water and cyclohexane using the data from the mass spectrometer, and a total mass loss curve was generated using the scale.

The mass loss curves generated by the mass spec were found to be within reasonable agreement with those generated by the scale, but there were some transient problems. One of the assumptions for the generation of the mass loss curve from the mass spec signal was that the air in the oven was well mixed. Due to the large residence time of the carrier gas in the mass spec, the assumption of a well mixed oven was not reasonable and the transient response of the mass spec was too slow as a result. To correct this, a much smaller vessel was designed for drying experiments. The scale could not fit in this new vessel, but we could not find an electronic scale that would operate above a temperature of 40 °C, so the scale would have to be removed for 75% of the experiments anyway. The new vessel performed very well, and the majority of the work featured in this thesis was conducted using this vessel.

## Appendix A1 – Vacuum Oven

### Description of Design

The original design is shown schematically in Figure 55, and is pictured in Figure 56. The rotameter on the far left of the design was connected to a nitrogen line and used to maintain a constant flow rate of 1 Standard Litre per Minute (SLPM). Valve 1 on the schematic was placed between the outlet of the rotameter and the inlet of the vacuum oven to ensure that the rotameter did not operate under vacuum, which could compromise its accuracy. The sample was placed on a battery powered scale inside the oven on the apparatus shown in Figure 57. Two type T thermocouples were placed in the sample at heights of 2 and 4 mm to measure the temperature inside the sample, and another one was placed just above the sample to measure the oven temperature during drying. A camera was set up to take a picture of the scale's reading every 8 seconds. The pictures were later converted to a data set giving the mass of the sample with respect to time. The black tape was placed on the oven to reduce glare and improve image quality.

The piping on the outlet of the vacuum oven was separated into two parts using a tee junction, and then reconnected before the pump using another tee junction. Each section had its own valve. The section controlled by valve 2 was a straight pipe for venting, while the other contained a vacuum regulator, which was preset to the desired pressure before the experiment was started. At the start of the experiment, valve 2 was opened until the desired set point pressure was achieved, and then promptly closed. The rotameter was then opened to achieve a steady flow rate of 1 SLPM, and the valve on the vacuum regulator was opened creating an uninterrupted path between the inlet of the rotameter and the outlet of the pump. The outlet of the pump was connected to a Dynamic Sampling Mass Spectrometer (DSMS), which sampled the outlet gas. The gas that was not sampled by the mass spec was vented to a fume hood. The vacuum pump's pressure transducer was connected to the top of the vacuum oven to monitor the pressure during the experiment.

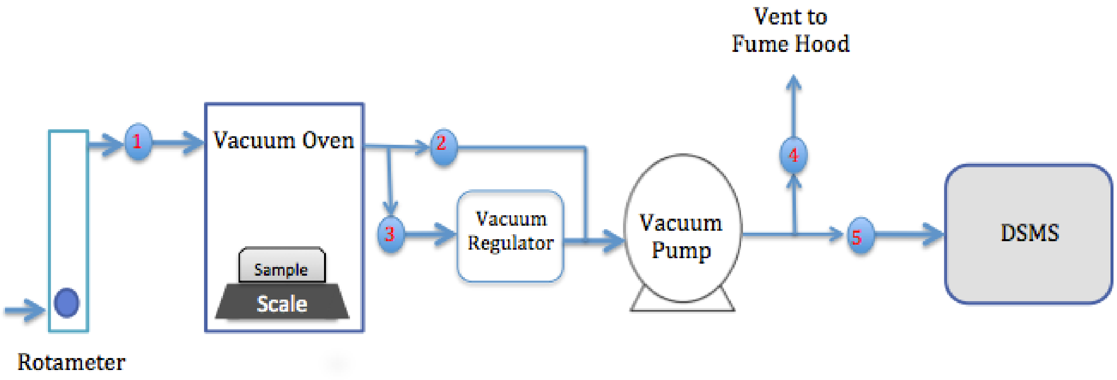

Figure 55 - Schematic for Original Experimental Apparatus

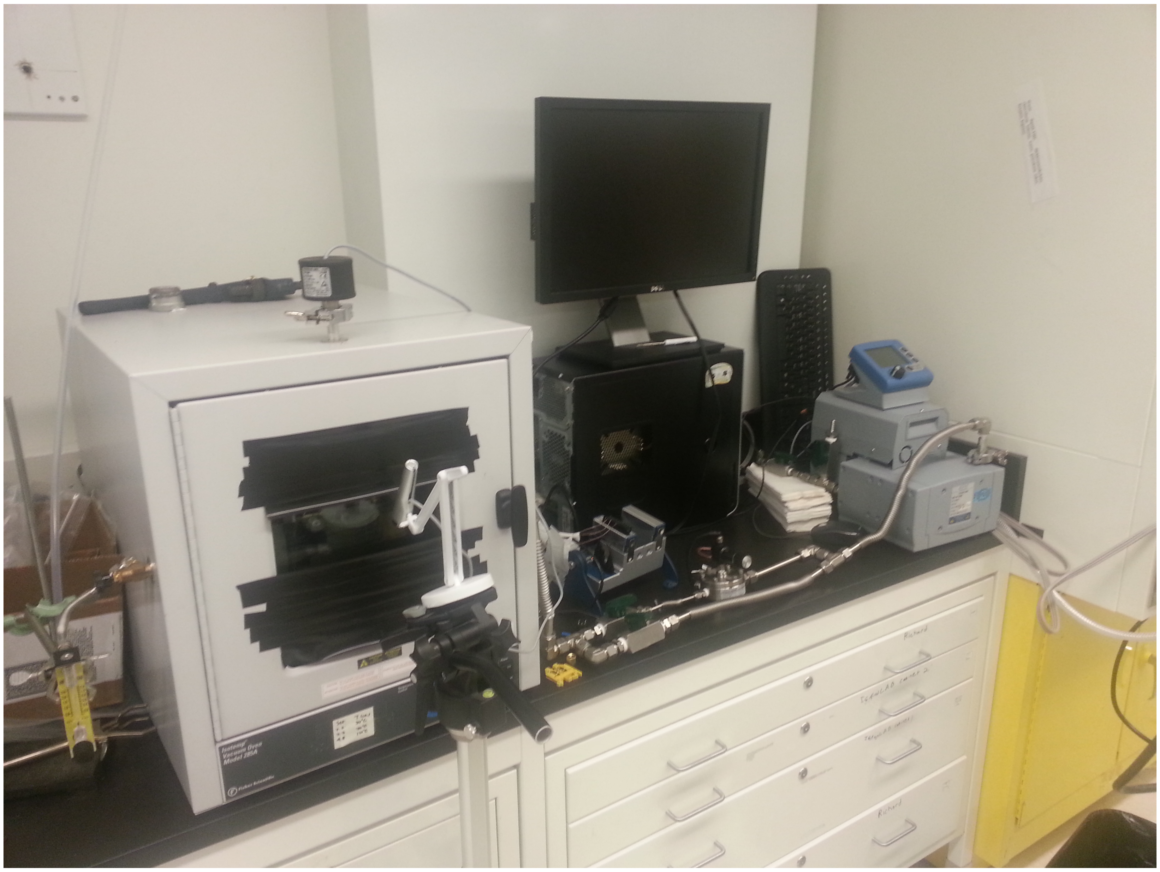

Figure 56 - Original Experimental Apparatus

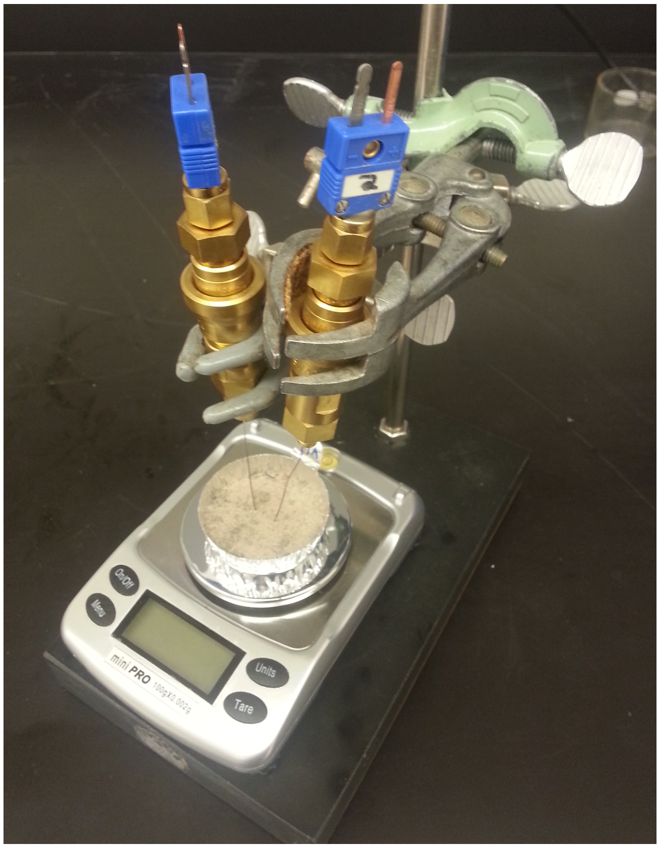

Figure 57 - Apparatus to Embed Thermocouples in Sample

### Time to Achieve Set Pressure

Experiments were to be run at steady pressure through the course of the experiment. A pump was selected that could achieve the desired pressure within a small time frame so that significant mass was not lost at the start of the experiment before the chamber pressure reached the desired set point. The inner dimensions of the vacuum oven were quite large (12" X 12" X 19"), so a large pump needed to be chosen to reach the desired set point fast enough. 11 aluminum blocks measuring 11" X 11" by 1" were placed inside the oven to reduce the internal volume of the oven, thus reducing its residence time and the time it takes to achieve set pressure. A pump was selected to achieve the set pressure within a very small time frame.

The manufacturer provided pump curves that give the flow rate of the pump against absolute pressure for the pressure range that the pump operates under. Figure below shows the pump curve for the pump that was chosen, the Vacuubrand MD 4 NT Vario.

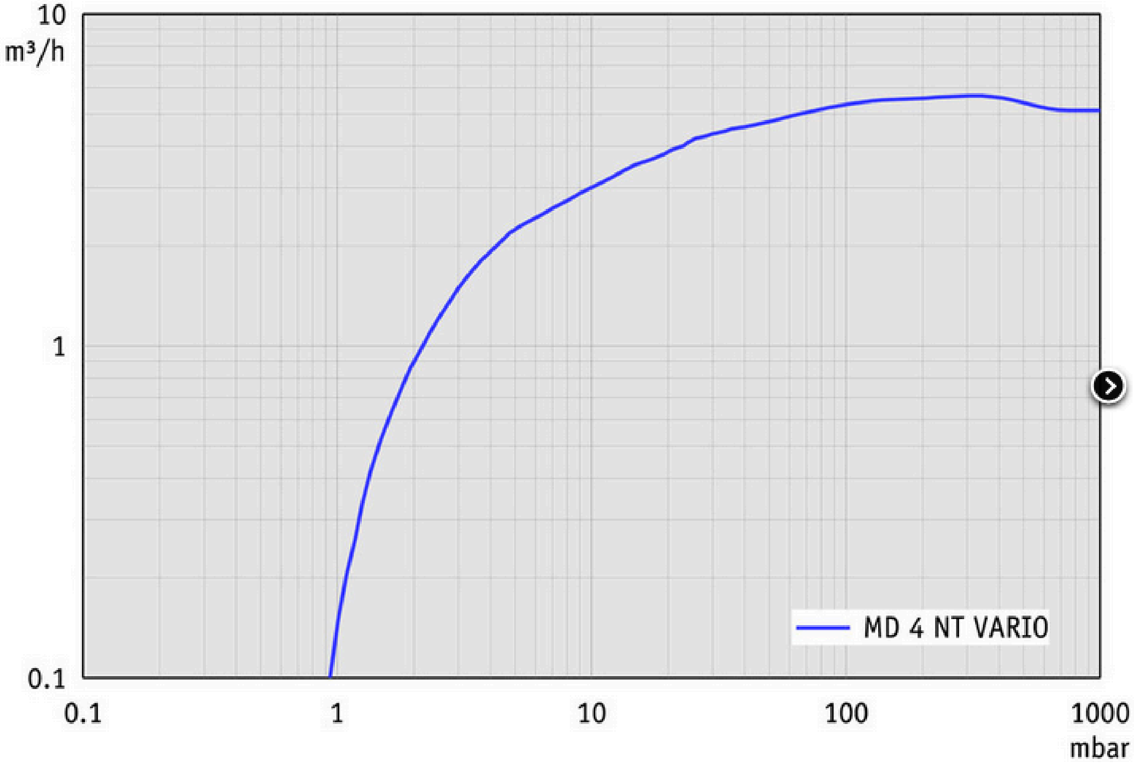

Figure 58 - Pump Curve for Vacuubrand MD 4 NT Vario

A graph digitizer (GraphClick) was used to convert the given curve into a numerical data set that could be used to perform pump down calculations in Matlab. A Matlab script was then used to calculate the time it would take each pump to get the pressure in the vacuum oven down to 11.3 kPa, the vapor pressure of cyclohexane. The solution made use of a discretized time domain with a time step of 0.01 seconds.

All pump down calculations were performed assuming that the oven was initially filled with air at 20°C and 101.325 kPa. At the start of the calculation, the total mass of air in the oven was calculated to be 0.0277 kg using the total free space of the oven, which was 23 L after the aluminum blocks were inserted. Within each time step, the pressure in the oven was calculated using the mass of remaining air in the oven.

$$P_i = \frac{m_i RT}{V_{oven}}$$

Flow rate was then interpolated at the calculated pressure from the previously obtained pump curve data set. Flow rate was then used to calculate the mass of air in the oven for the next time step:

$$m_{i+1} = m_i - \frac{m_i}{V_{oven}} Q_i \Delta t$$

The process was repeated until the pressure fell below the desired set point, and pump down time was taken as the total time that it took to reach this pressure. The Matlab script used to perform this calculation can be found in Appendix C1. Figure 59 below shows how oven pressure was predicted with time for the selected pump.

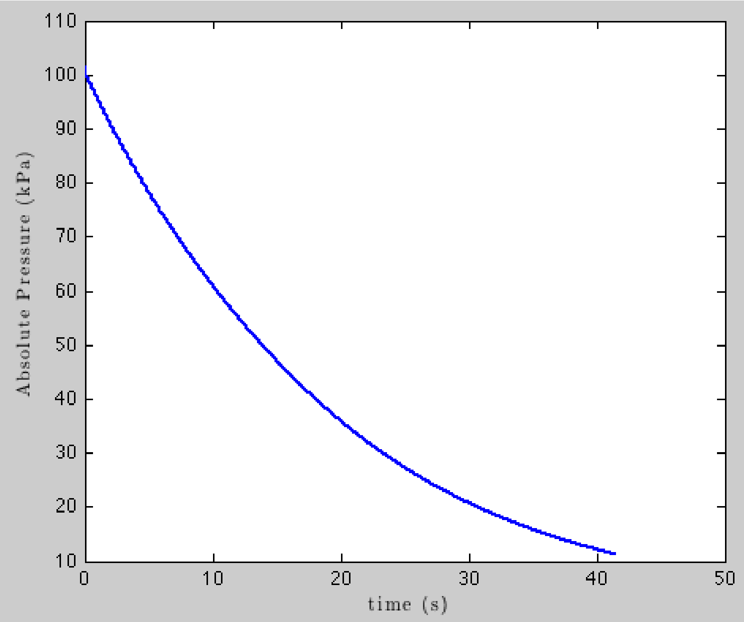

Figure 59 - Predicted Pump Down Curve for MD 4 NT Vario

Table 9 below shows the calculated pump down times for each of the pumps that were tested.

Table 9 - Pump Down Times for Potential Pumps

| Unit | Pump Down Time to 11.3 kPa (s) | Pump Down Time to 300 mbar (s) |
|---|---|---|
| MZ 2C NT Vario | 68.47 | 36.45 |
| MD 12C NT Vario | 15.3 | 8.04 |
| MD 4 NT Vario | 41.43 | 23.35 |
| MV 10C NT Vario | 16.67 | 8.9 |
| ME 16 NT | 15.03 | 6.61 |
| MV 2 NT Vario | 57.59 | 31.39 |

The first column shows pump down time to reach 11.3 kPa, and the second shows time to reach 300 mbar, which was the lowest pressure that would be tested in this thesis. Total drying time in previous experiments in an environmental chamber had averaged about 20 minutes. The MD 4 NT Vario pump was selected as 23.35 seconds to reach the desired set pressure of 300 mbar was considered reasonable. Note that the Vario pumps have an option for variable speed, which could be used to control the set pressure. This option was selected in case the vacuum regulator did not work.

## Carrier Gas Flow Rate Selection

In order for evaporation to occur consistently throughout the experiment, a flow rate needed to be selected such that the partial of cyclohexane in the exhaust stream of the vacuum pump never exceeded its vapour pressure of 11.3 kPa. In order to calculate the expected partial pressure of cyclohexane in the exhaust stream, data was needed on the expected evaporation rate of cyclohexane. Preliminary tests were run in an environmental chamber at 25 °C with a large fan that accelerated evaporation. 15 g wet samples with an average liquid content of 2 g were dried in approximately 20 minutes. Other tests performed in a fume hood required a drying time of 40 minutes, and those performed in closed chambers with a carrier gas at a low flow rate required significantly longer to achieve drying. For a conservative calculation, the drying time was taken to be 20 minutes for 2 g of solvent.

The goal is to calculate the flow rate that must be exceeded so that partial pressure of cyclohexane in the exhaust stream does not exceed its vapour pressure. In order to calculate the minimum required flow rate, the ideal gas law was modified for use with a moving fluid. Flow rate was substituted for volume, and evaporation rate was substituted for number of moles of gas.

$$PQ = \dot{n}RT$$

The final modification to find flow rate is to convert molar rate of evaporation in the above equation to mass rate of evaporation.

$$Q_{min} = \frac{\dot{m}RT}{P_{vap}M_{cyclo}}$$

Substituting in the known values and using a temperature of 25 °C gives a minimum required flow rate of 260.5 ml/min. It should be noted that this calculation is an approximation, as the total pressure of gas at the exit will be atmospheric pressure plus the vapor pressure of cyclohexane, and this has not been accounted for. However, this unaccounted for effect will actually increase the total volume flow rate at the outlet of the vacuum oven, which will decrease the required flow rate of nitrogen carrier gas. The calculation is thus conservative. To account for increasing mass flux at higher temperatures and lower pressures, a flow rate of 1000 ml/min was chosen to allow for an increase in evaporation rate of about 4 times.

## Choice of Thermocouples

Type T thermocouples were ordered from Omega. Type T thermocouples were chosen as they had an operating range from -250 to 350 °C and the highest stated accuracy of 1°C within our operating range[42]. Grounded probes were chosen to improve response time over an ungrounded probe, but give protection against contamination over an exposed junction. Probes with a diameter of 0.01'' were chosen as those were the smallest probes available for a type T thermocouple. Smaller probes give a faster response time and reduce the probability of the probe getting stuck in the sample. The probes were sheathed in stainless steel to prevent contamination. The part number for the probes was TMQSS-010-G-6.

## Sealing Thermocouples into the Oven

In order to obtain a data set for temperature with respect to time, thermocouple probes needed to be inside the oven, but they needed to transfer data to a computer outside the oven. Fortunately, unlike a data transfer cable that would have multiple elements that need to be sealed around, each thermocouple probe contains only 2 wires that must be sealed in. The vacuum oven used in this apparatus featured a 1'' NPT port at the back to attach a larger vacuum pump if necessary. This port was re-purposed, as an adapter was built to fasten onto it. Figure 60 below shows a computer generated section view of the adapter. The two ⅛'' NPT ports on top were used to attach Conax sealing glands (MHC1-020-A4-T). Each sealing gland had space for 4 wires, or 2 thermocouples, and both were used to seal in a total of 4 thermocouple probes. The 1'' NPT hole on the bottom was used to screw the adapter onto the port at the back of the vacuum oven, and slots were cut in the sides of the adapter to help fit a pipe wrench around it. The engineering drawing for the adapter can be found in Appendix D1.

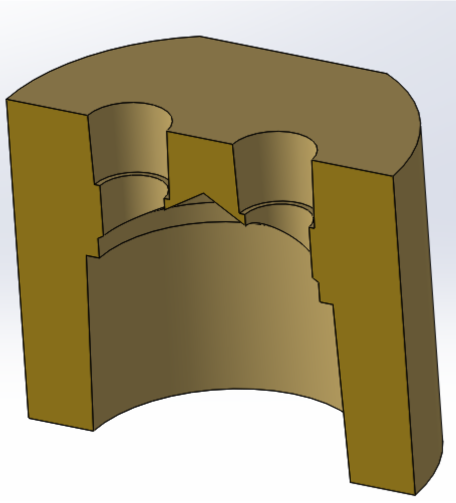

Figure 60 - Adapter to Seal Thermocouples into Vacuum Oven

## Residence Time

The vacuum oven apparatus worked well as a proof of concept type of experiment, but eventually needed to be modified for more accurate results. Even when spacers were put in, the oven was too large and it affected the transient results. A differential equation was derived in the main body of the report to account for this, but the derivation of that equation assumed that the oven was well mixed. The size of the vacuum oven, combined with the relatively slow flow rate of 1 SLPM made this assumption invalid. In an attempt to illustrate this problem, the residence time of the vacuum oven, which is the average time that one molecule of carrier gas would spend in the oven, is calculated below.

The oven measured 12" X 12" X 19", and had eleven 11" X 11" X 1" aluminum blocks placed inside to reduce the dead space in the oven. The total remaining dead space in the oven was equal to 23 L. The volume taken up by the sample, thermocouple apparatus, and scale were not accounted for in this calculation, but are considered negligible as the purpose of this calculation is for illustration purposes. The residence time at atmospheric pressure is the total dead space volume divided by the flow rate of gas.

$$t_{res} = \frac{V_{oven}}{Q}$$

Using the above equation with a flow rate of 1 SLPM, the residence time at STP is calculated to be 23 minutes, which is too large. It should be noted, however, that the 1 standard litre per minute flow rate is measured at STP, or conditions of 0 °C and 100 kPa. The volume flow rate under slight vacuum will actually be larger because the molecules will spread out at higher temperature and lower pressure. The volume flow rate can be corrected by assuming that the carrier gas behaves as an ideal gas both at STP and under process conditions.

$$Q_{actual} = \frac{P_{STP} T_{actual}}{P_{actual} T_{STP}} Q_{STP}$$

This correction will reduce the residence time. Under the most favorable conditions tested in the vacuum oven, 300 mbar and 40 °C, the flow rate corrects to 3.83 litres per minute, which reduces the residence time to approximately 6 minutes. Unfortunately, 6 minutes is still too large a residence time for good transient results. Furthermore, the method needs to work for all combinations of temperature and pressure tested, so even if 6 minutes was a small enough residence time, there are still tests at atmospheric pressure that would have a much larger residence time.

Another problem with a large residence time is that the vacuum oven lets in atmospheric air when it is opened to put the sample in, even if it was initially filled with nitrogen. The air that is let into the system contains water vapour from the air, which takes at least 1 residence time to fully leave the system. Thus, it is difficult to tell from the mass spec signal what water is evaporating from the sample, and what water is left over from the initial influx of atmospheric air when the sample was put in.

In order to solve both these problems, the vacuum oven was replaced with a smaller brass vessel. This brass vessel, along with the calculations done during its design process, will be examined in Appendix A2.

## Appendix A2 – Brass Vessel

After some time experimenting with the vacuum oven, it was discovered that the residence time of the oven was simply too large to get good transient results. The temperature control on the vacuum oven was also not quite as accurate as initially believed. In order to correct these errors, a much smaller brass vessel was designed to sit on top of a hot plate with a PID control algorithm to maintain constant temperature within 1 °C. The design calculations performed on the brass vessel are outlined in this appendix. The Engineering drawings for the vessel can be found in Appendix D2.

The overall apparatus is mostly unchanged, except that the vacuum oven is replaced with a smaller brass vessel sitting on a hot plate, the rotameter is replaced with an electronic mass flow controller (Omega FMA3807 for high grade gangue, later replaced by Omega FMA-7407 for low grade gangue), and the gas is preheated on the hotplate before it reaches the vessel. Figure 61 below depicts the new apparatus schematically.

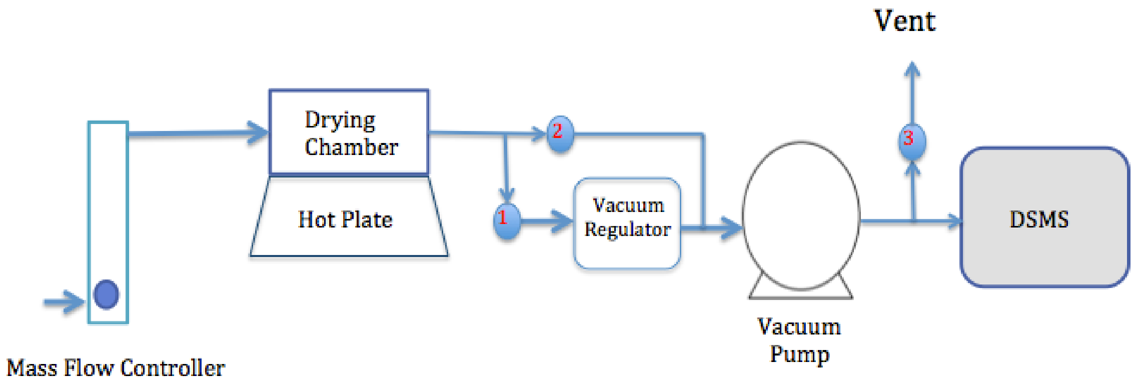

Figure 61 - Schematic for New Apparatus

Figure 62 shows a computer generated sectional view of the brass vessel. The vessel has two parts, a lid and a base. The sample sits in the recess in the middle of the base. Nitrogen carrier gas flows through an electronic mass flow controller connected to a NPT ¼'' port on the left of the left side of the vessel, picks up evaporated solvent from the sample, and carries the solvent to the outlet on the right side of the base. 3 type T thermocouples are threaded through the NPT ⅛'' port in the middle of the lid using a sealing gland (Conax MHC1-020-A4-T). Two of the thermocouples were embedded inside the sample, one at a height of 2mm, the other at a height of 4 mm from the bottom of the sample to measure temperature inside the sample as evaporation occurred. The last thermocouple probe tip rested near the top of the lid to measure air temperature inside the vessel as evaporation occurred. When the experiment was done, all 3 thermocouples shared the same reading.

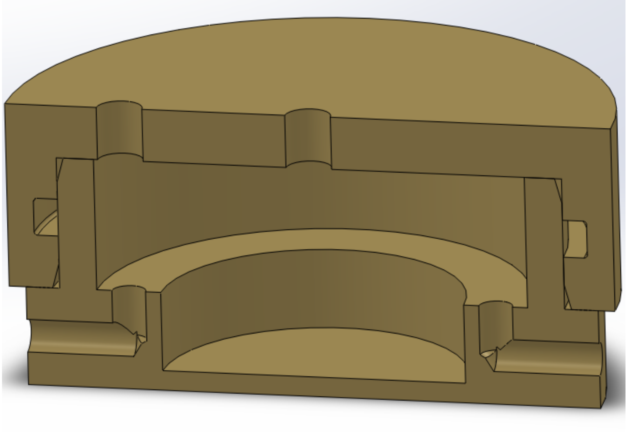

Figure 62 - Computer Generated Sectional View of Brass Drying Vessel

The other NPT ⅛'' port on the lid was attached to a pressure transducer (Omega PX309-015A5V) that measured absolute pressure inside the vessel. 1 foot of ⅛'' OD stainless steel tubing was connected between the pressure transducer and the vessel to protect the transducer from overheating. The vessel was sealed with an O-ring that was placed in the grove in the lid shown in Figure 62. High Vacuum Grease was used to lubricate the O-ring to improve sealing and ease of lifting an lowering the lid.

An additional pressure transducer (Omega PX309-050A5V) was connected between the vacuum oven and the DSMS to measure the pressure at the point where the mass spec was sampling, and another type T thermocouple was placed at the same point for a temperature correction.

Prior to the start of the experiment, nitrogen carrier gas was pumped through the system for at least an hour to ensure that the baseline signals for cyclohexane and water were low and stable. At the start of the experiment, the vessel was opened by closing valves 1 and 2, cutting off the carrier gas' exit. The carrier gas still flowing in through the mass flow controller caused a build up of pressure, which lifted the lid of the vessel. The lid was removed, the sample placed in the recess, and the lid carefully positioned above the vessel. Valve 2 was opened at first, causing a vacuum that lowered the lid and closed the vessel, then valve 2 was closed and valve 1 was opened so that pressure level could be controlled using the vacuum regulator.

### Residence Time

Part of the need for a new vessel arose because the residence time of the vacuum oven was far too large. The vacuum oven was 23 L in size, giving a residence time of 23 minutes for a carrier gas flow rate of 1 LPM at atmospheric pressure. The new vessel has an internal volume of 197 ml, giving a residence time of 11.8 seconds under the same conditions. The new vessel is considered to be a significant improvement over the old one.

### O-Ring Design Calculations

The vessel was sealed with a piston style O-ring seal. This was done so that the thermocouple probes in the lid could slide to the same position within the sample every time the vessel was closed. The design of the seal was a balance between minimizing friction so that the vessel could be easily opened and closed, and minimizing the leak rate into the vessel. All O-ring calculations were performed according to methods outlined in the Parker O-Ring Handbook[43].

The leak rate for an O-Ring lubricated with high vacuum grease with a squeeze of less than 30% can be approximated according to the equation below[43]:

$$L = 0.5\,F\,D\,P\,(1 - S)^2$$

Where:

L = Leak Rate of Seal (ml/s)
F = Permeability Rate of Gas through Elastomer (ml cm/(cm$^2$ s bar))
D = Inside Diameter of O-ring (inches)
P = Pressure Differential Across Seal (psi)
S = Fractional squeeze on O-ring

The frictional force on a rod groove O-ring sealing under a pressure differential of 15 lbs with a shore A hardness of 70 can be approximated by the following formula[43]:

$$F_r = 6.67\,S\,L_r + 10A_r$$

Where:
$F_r$ = Frictional force on O-ring (lbs)
S = Fractional Squeeze on O-ring
$L_r$ = Circumference of O-ring rubbing area (in)
$A_r$ = O-ring rubbing area (in$^2$)

Polyurethane O-rings were chosen because they were readily available, have an extremely low gas permeability, and had a low shore A hardness of 70. The O-ring groove was placed in the lid, so that when the vessel closes the O-ring is pushed to the top of the groove where it's position will be re-enforced by direction of air pressure trying to get into the vessel. The size of the O-ring was constrained by the size of the inside of the vessel. The diameter of the vessel base where the O-ring sealed was 3.75''. An ASTM-343 O-ring size was chosen as this had the largest cross section for all standard sized O-rings in that size range. It was thought that a larger cross section would provide a better seal in the event that the sealing surfaces were accidentally scratched or deformed. With this information known, the O-ring groove could be designed. **Error! Reference source not found.** below gives alculated values for frictional force caused by the O-ring as well as expected leak rate. Values are given for the designed size of the O-ring groove in the second row, as well as the minimum and maximum sizes of the groove that are possible with the tolerances used.

Table 10 –Calculated Values for O-Ring Design

| Piston OD (in) | O-ring ID (in) | Groove OD (in) | O-ring stretch (%) | O-ring Squeeze (%) | Friction (lb) | Leak Rate (ml/min) |
|---|---|---|---|---|---|---|
| 3.752 | 3.725 | 4.104 | 0.7 | 15.5 | 36.9 | 4.08E-06 |
| 3.75 | 3.725 | 4.109 | 0.7 | 13.8 | 35.6 | 4.24E-06 |
| 3.748 | 3.725 | 4.114 | 0.6 | 12.1 | 34.3 | 4.40E-06 |

It is recommended that O-ring stretch does not exceed 5%[43], and this condition was well met. Leak rate was found to be minimal, especially in comparison to the carrier gas flow rate of 1000 ml/min. Frictional force was found to be 35.6 lb, which is actually quite large. Indeed, if the experimentalist had to open or close the vessel himself, he would have a great deal of difficulty. However, the vessel will be closed by applying a vacuum using the pump, and by applying additional pressure using the carrier gas from the nitrogen line. The main base has an inside diameter of 3.2 inches. Pressing against this cross sectional area, a pressure differential of only 4.4 psi, or 305 mbar, would be needed to overcome this frictional force. Both the pump and Nitrogen line are easily capable of achieving this pressure to lift or lower the lid.

### Preheating the Carrier gas

The new vessel was much smaller, and had a much smaller residence time as a result. However, the vessel also contained much less thermal mass, and there were concerns that the carrier gas would not have enough time in the vessel to heat to the operating temperature of the experiment, which could be as high as 105 °C. In order to avoid this potential problem, the gas was preheated by heating the ⅛” OD stainless steel tubing used to carry the carrier gas from the mass flow controller to the vessel. The tubing was wrapped around the vessel maintaining constant contact with the hot plate used to heat the vessel. In this way, the hot plate heated both the carrier gas and the vessel itself.

A thermal resistance model with the assumption of constant wall temperature was used to calculate the rate of heat transfer from the hotplate to the carrier gas. This model was discretized into differential lengths of 0.1 mm. The rate of heat transfer was calculated for each element, then the change in temperature within that element was calculated and used to find the inlet temperature of the next element. The process was repeated until the carrier gas temperature was within 0.1°C of the hot plate temperature, which was set to 105 °C for the calculation. Thermal resistance, in °C/W, is the sum of conductive thermal resistance of the tube wall and the convective thermal resistance of the nitrogen itself.

The equations solved will be derived below, and all property values used in this calculation will be summarized in a table at the end of this section. The thermal resistance of the tube wall is easily calculated by the formula below, and is the same for every element with the same differential length dL.

$$R_{wall} = \frac{\ln \frac{d_o}{d_i}}{2\pi k_{metal} dL}$$

$k_{metal}$ in the above formula is the thermal conductivity of the stainless steel, $d_o$ is the outer diameter of the tube, and $d_i$ is the inner diameter. The convective thermal resistance of the nitrogen itself can be more complicated to calculate. It is introduced in the equation below.

$$R_{air} = \frac{1}{\pi d_i h_{air} dL}$$

The complication is in finding the convective heat transfer coefficient of the nitrogen. First we find if the Reynolds number is greater or less than 2300 using the following formula:

$$Re = \frac{4Q}{\pi d_i \nu}$$

The Reynolds number was calculated to be 862, which is much less than 2300, so flow is expected to be laminar. Because pipe flow is laminar, and we are already assuming constant wall temperature, the Nusselt number of the nitrogen stream can be considered as a constant 3.657. The convective heat transfer coefficient of the nitrogen can then be calculated by:

$$h_{air} = 3.657 \frac{k_{air}}{d_i}$$

The thermal conductivity of nitrogen varies with temperature. In order to achieve a higher accuracy, the thermal conductivity of nitrogen was calculated within each element using the a polynomial fit based on temperature in k [40].

$$k_{air} = A + B\,T^2 + C\,T^3 + D\,T^4$$

With both thermal resistances calculated, the rate of heat transfer into the element can be calculated.

$$q_i = \frac{T_{wall} - T_i}{R_{wall} + R_{air}}$$

The temperature change in the element can be calculated by using the specific heat capacity of nitrogen, which was calculated at the mid-range temperature of 65 °C.

$$T_{i+1} = T_i + \frac{q_i}{\dot{m}_{air} Cp_{air}}$$

Table 11 - Values Used to Calculate Length of Required Tubing to Preheat Carrier Gas

| Property | Value | Source |
|---|---|---|
| Outside Diameter of Stainless Steel Tubing, $d_o$ (in) | 0.125 | |
| Inside Diameter of Stainless Steel Tubing, $d_i$ (in) | 0.0625 | |
| Thermal Conductivity of Stainless Steel, $k_{metal}$ (W/(m k)) | 16 | |
| Flow Rate of Nitrogen Carrier Gas, Q (ml/min) | 1000 | |
| Kinematic Viscosity of Nitrogen Carrier Gas, ν ($m^2/s$) | $1.55 \times 10^{-5}$ | [44] |
| Polynomial Coefficient for Thermal Conductivity of Nitrogen, A | $-2.2678 \times 10^{-4}$ | [40] |
| Polynomial Coefficient for Thermal Conductivity of Nitrogen, B | $1.0275 \times 10^{-4}$ | [40] |
| Polynomial Coefficient for Thermal Conductivity of Nitrogen, C | $-6.0151 \times 10^{-8}$ | [40] |
| Polynomial Coefficient for Thermal Conductivity of Nitrogen, D | $2.233 \times 10^{-11}$ | [40] |
| Wall Temperature used for Calculation, $T_{wall}$ (°C) | 105 | |
| Conductive Thermal Resistance of Tube Wall, $R_{wall}$ (k/W) | 68.9 | |
| Specific Heat Capacity of Nitrogen, $Cp_{air}$ (J/(kg k)) | 1042 | [44] |

The method described above was implemented using a MATLAB script, which can be found in Appendix C2. Using the code, the required length of ⅛" OD tubing was found to be 0.366 m to heat carrier gas from 25 °C to 105°C. 1 m of tubing was used to add an extra factor of safety. Figure 63 below shows the calculated air temperature as distance from the mass flow controller increases.

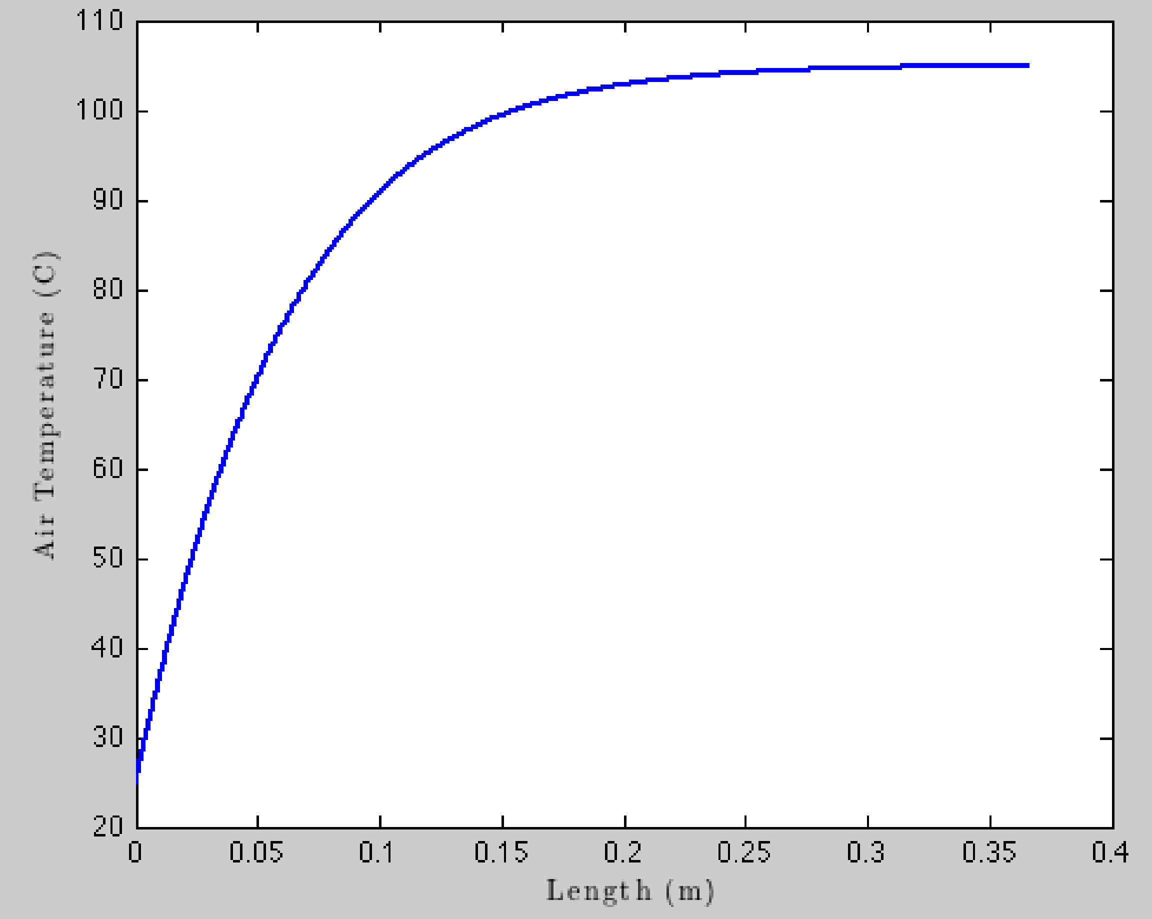

Figure 63 - Calculated Air Temperature vs. Tube Length for Preheated Carrier Gas

# Appendix B – Calibration and Validation of DSMS

## Appendix B1 – Calibration of DSMS

In order to calculate the evaporation rate of each solvent at any given time, the DSMS must be calibrated for each solvent to find the concentration of solvent vapour at the point of detection. In order to calibrate, solvent of known concentration was introduced in the DSMS and the response analyzed. This was accomplished by feeding a gas of known concentration to the DSMS using an Intelligent Gas Analyzer (Hiden Analytical), and measuring its response. Figure 64 below shows a schematic diagram of the calibration setup including the Intelligent Gas Analyzer.

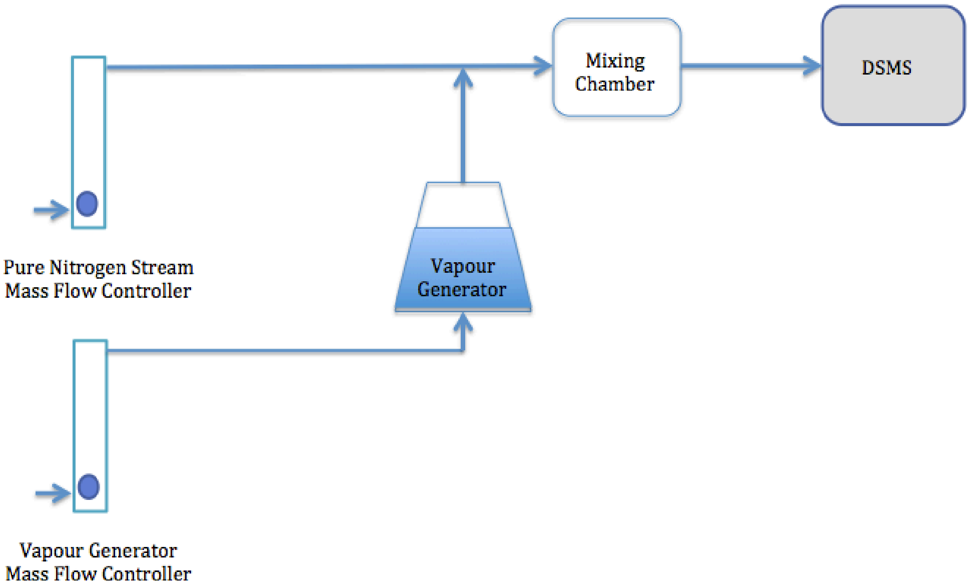

Figure 64: Calibration Setup Schematic

There were two nitrogen streams. One stream maintained a flow of pure nitrogen, and the other was passed through a vapour generator that worked by maintaining a pool of solvent, either water or cyclohexane, in a liquid state at a constant temperature of 30 °C. The nitrogen that had passed through the vapour generator was then saturated with solvent at its vapour pressure at 30 °C, 136.6 mbar for cyclohexane and 42.5 mbar for water. Both streams were mixed after the vapour generator to give a known partial pressure of solvent vapour. The total volume flow rate of nitrogen was kept constant at 100 ml/min, but the proportion of nitrogen passing through each stream was varied to give different data points.

The DSMS detects the partial pressure of solvent after the 2 streams have mixed. In order to calculate the partial pressure of solvent at the point of detection, the molar flow rate of solvent passing through the vapour generator was calculated using the molar flow rate of the carrier gas through the vapour generator.

$$\dot{n}_{solvent} = \frac{P_{vap}\dot{n}_{N2,generator}}{P_{tot} - P_{vap}}$$

$P_{tot}$ in the above equation is the total pressure in the chamber, and $P_{vap}$ is the vapour pressure of the solvent. Molar flow rate is used instead of volume flow rate because the solvent vapour will have the effect of increasing total volume flow rate. To calculate the total volume flow rate at the point of detection, the ideal gas law is used with the total sum of molar flow rate.

$$Q_{tot} = \frac{\left(\dot{n}_{solvent} + \dot{n}_{N2,generator} + \dot{n}_{N2,pure\ stream}\right)RT}{P_{tot}}$$

Finally, partial pressure of the solvent at the point of detection is found using the ideal gas law again.

$$P_{solvent} = \frac{\dot{n}_{solvent}RT}{Q_{tot}}$$

The calibration was found to fit a linear trend for both cyclohexane and water. Figure 65 shows the linear calibration for cyclohexane, and Figure 66 shows the calibration for water.

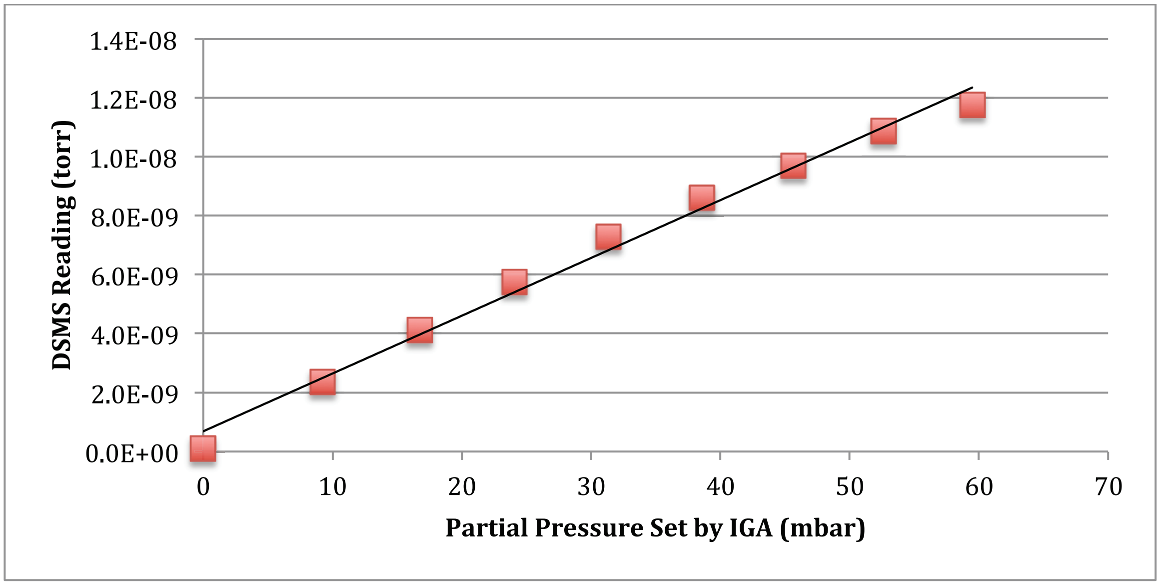

Figure 65 - DSMS Calibration Data for Cyclohexane

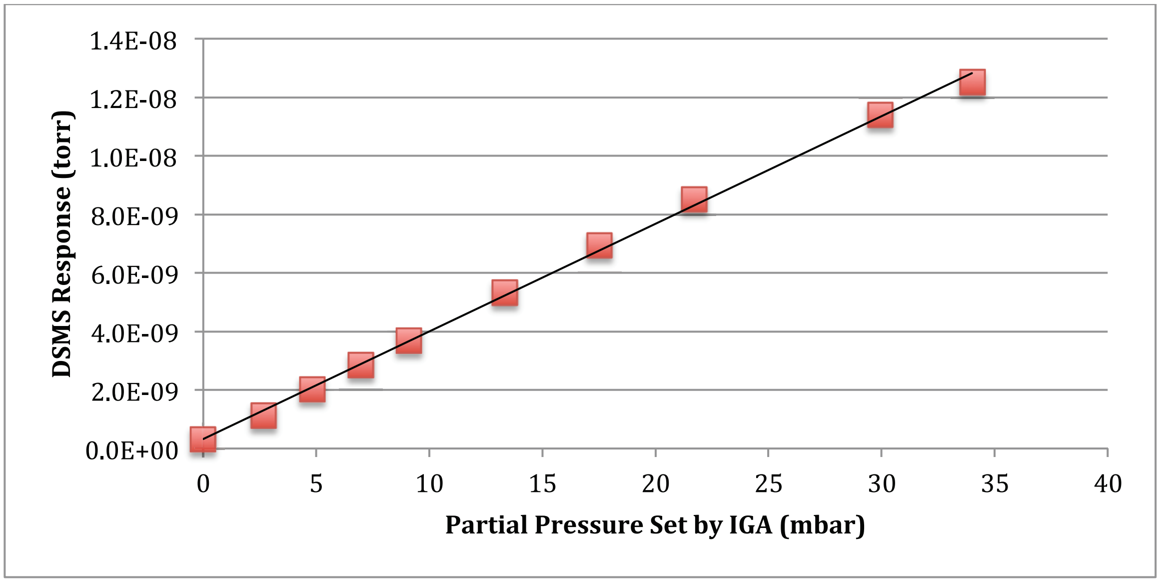

Figure 66 - DSMS Calibration Data for Water

Table 12 below summarizes the linear fit for both cyclohexane and water.

Table 12 - Linear Calibration Data for Cyclohexane and Water

| Vapour | Slope, $a_{gas}$ (torr/mbar) | Intercept, $b_{gas}$ (torr) | $R^2$ |
|---|---|---|---|
| Water | 3.68E-10 | 3.20E-10 | 0.999 |
| Cyclohexane | 1.96E-10 | 6.81E-10 | 0.990 |

In preliminary experiments, the cyclohexane reading stabilized between $10^{-13}$ and $10^{-14}$ at the end, but the water baseline stabilized much higher. There was also a leak rate of atmospheric air into the system associated with the vacuum regulator. This caused the water baseline to be different for differing test pressures. Using the linear equation with both the slope and intercept would give negative partial pressure for cyclohexane at the end of the experiments, and would not accurately represent water. To compensate for this, only the slope was used in the calibration. The cyclohexane signal was processed as it was, and the average water signal over the last 10 minutes of each experiment was subtracted from the water signal at every data point.

The final step in the calibration was to convert partial pressure of the gas, which was found using the linear calibration above, to concentration at the exit in g/ml. To do this, the ideal gas law was used to find the concentration in mol/ml, and the result was multiplied by the molar mass of the solvent to give concentration in g/ml. The resulting equation to convert DSMS reading, $S_{solvent}$ to concentration is given below.

$$C_e = \frac{S_{solvent}}{a_{solvent} T_e R} M_{solvent}$$

## Appendix B2 - Validating the Calibration

Before performing experiments on extraction gangue, where the true ratio of cyclohexane to water was unknown, validation tests were run to ensure that the procedure could produce valid results that measure the true ratio of water to cyclohexane. Preliminary tests estimated that the initial liquid content in extraction gangue was 11% cyclohexane by mass, and 3% water. In a 15 g sample, this means 1.65 g of wet gangue is cyclohexane, 0.45 g is water. Validation runs were performed by injecting these masses of cyclohexane and water into 12.9 g of soxlet extracted gangue, running the constructed sample through the process described in the methodology section of this thesis, and comparing the measured amounts of cyclohexane and water to the actual amounts injected. A total of 8 validation runs were performed at an oven temperature of 72 °C. 1.65 g of cyclohexane was injected in each of the validation runs along with either 0.45 g of water or no water. Figure 67 shows the results of the total mass of each solvent, cyclohexane and water, both measured and injected.

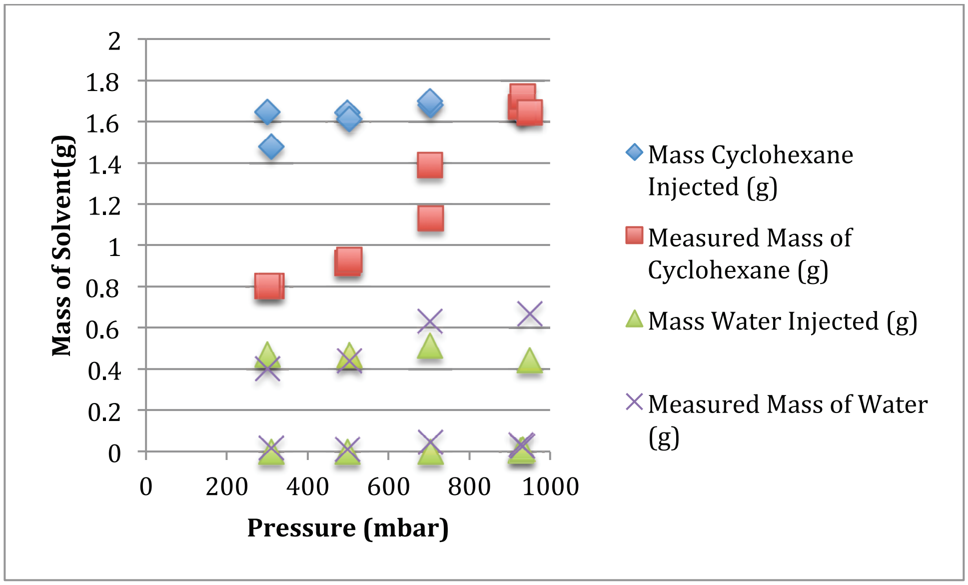

Figure 67 - Results from Validation Runs

There appears to be a relationship whereby decreasing absolute pressure results in a decreased measurement. These errors presented despite attempts to compensate for all potential errors including leak rate. It was assumed that these errors were systemic and a result of unknown factors. In an attempt to compensate for these errors, the results were renormalized by multiplying by total mass of both solvents injected and dividing by total measured mass. This forced parity between injected and measured total mass injected.

$$m_{renorm,solvent} = \frac{m_{injected,cyclo} + m_{injected,water}}{m_{measured,cyclo} + m_{measured,water}} m_{measured,solvent}$$

Figure 68 shows the renormalized validation results. The renormalization clearly removes the trend in the data, but does not remove all error. There is still some systemic error in the results whereby the mass of water measured is now slightly too high, and the mass of cyclohexane measured is slightly too low. This trend is less existent in the cases where no water was injected, but that is only because the renormalization forces exact parity on the results. It is possible that this effect is a result of the calibration curves obtained from the IGA for water and cyclohexane being slightly off. However, the renormalization effectively removed the trend between measured total mass and pressure. Thus, the renormalization will be used from now on for all results. The renormalization will be applied to the generated curves of mass flux and mass loss vs. time. Any results reported for recovered mass of cyclohexane or water, as well as mass flux and time to 250 ppm recovery will be affected by this renormalization.

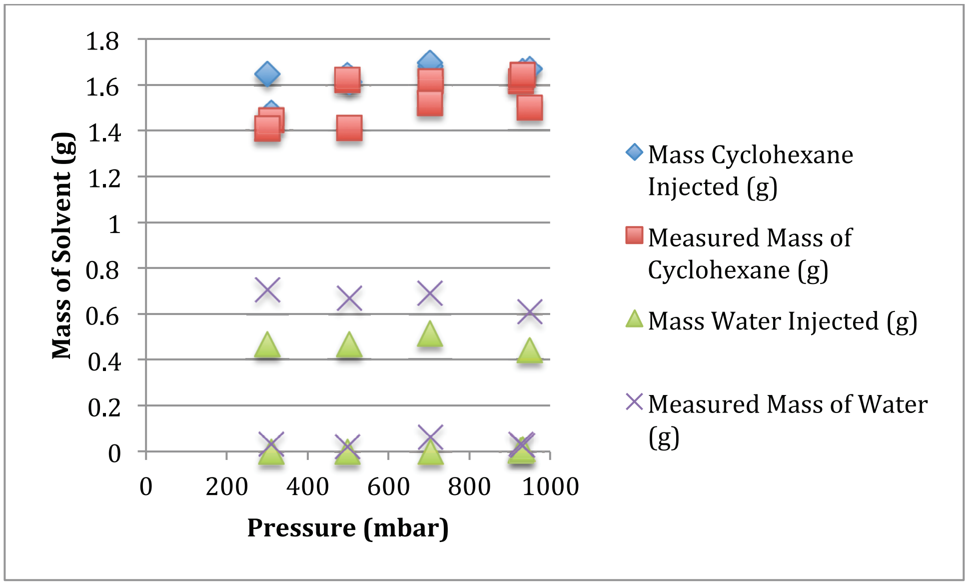

Figure 68 - Renormalized Results from Validation Runs

## Appendix C – MATLAB Scripts

MATLAB was used heavily to perform calculations in this thesis. This appendix shows the MATLAB scripts that were written and utilized to process the data and perform calculations in this thesis.

### Appendix C1 – Pump Down Calculation

The following script was used to calculate the total time that it takes a pump to take the original vacuum oven from an atmospheric pressure of 101.325 kPa to a desired set point of 11.3 kPa, the vapor pressure of cyclohexane. The equations used to perform these calculations are described in Appendix A1.

```
function tfinal = vactime(FlowVsPres)
%Function to calculate the total time needed to pump the
vacuum oven down
%from 101.325 kPa to a desired set point of 11.3 kPa.

% load FlowVsPres.txt
Qcurve=FlowVsPres(:,2); %m3/hr
Pcurve=FlowVsPres(:,1); %mbar

Qcurve=Qcurve./3600; %m3/s
Pcurve=Pcurve.*100; %Pa
Qsize=length(Qcurve);
Qmax=Qcurve(Qsize);

T=20+271.15; %T in K
R = 287; %J/kg*k
% Rmol=8.314; %J/mol*k
% Mnitrogen = 14.007*2/1000; %kg/mol
% R=Rmol/Mnitrogen; %J/kg*k
rho_initial = 1.204; %kg/m3
```

```
deltat=0.01; %second
Vtot = 12*12*19-11^3; %in^3
Vtot = Vtot*0.0254^3; %m^3
P_initial=101325; %Pa

m_initial=Vtot*rho_initial;

mi=m_initial;
P(1)=P_initial;
Pfinal=11300; %Pa
%Pfinal = 30000; %Pa
i=1;
t(1)=0;

Pmax=max(Pcurve); %Pa

while P(i) >= Pfinal
    if P(i) >= Pmax
        Q(i)=Qmax;
    else
    Q(i) = interp1(Pcurve,Qcurve,P(i));
    end
    rhoi=mi/Vtot;
    Vloss=Q(i)*deltat;
    mloss=rhoi*Vloss;
    mi=mi-mloss;

    i=i+1;
    P(i)=mi*R*T/Vtot;
    t(i)=t(i-1)+deltat;
end
```

```
Q(i)=Q(i-1);
Q=Q.*(1000000000/60);
tfinal=t(i);
%Pfinal=P(i);
P=P./1000;

plot(t,P,'LineWidth',2)
xlabel('time (s)','interpreter','latex')
ylabel('Absolute Pressure (kPa)','interpreter','latex')

figure
semilogy(t,Q)
xlabel('time (s)')
ylabel('Flow Rate (ml/min)')

end
```

## Appendix C2 – Calculating Length of Tubing Necessary to Preheat Carrier Gas

In order to maintain constant temperature in the brass vessel throughout the experiment, the inlet carrier gas needed to be preheated to the oven temperature. The code below was used to calculate how much ⅛" OD stainless steel tubing held at the oven temperature would be required to preheat the carrier gas.

```
function Ltube = vacintemp3
%Function to calculate the length of tube required to reach
a certain
%equilibrium temperature
%make equilibrium temperature on the outside within 1% of
the equilibrium
%temperature inside
%Specific for Nitrogen
```

```
Tin=25; %C
Twall=105; %C

%Calculate Thermal Resistance of Tube Wall
%ksteel=43; %W/m k
%kcopper=385; %W/m k
kstainless = 16; %W/m k
kmetal=kstainless;
d1=0.0625; %in
r1=d1*0.0254/2; %m
d2=0.125;%in
r2=d2*0.0254/2; %m
dL=0.0001; %m = differential length
Rmetal=log(r2/r1)/(2*pi*kmetal*dL);

%Calculate Mass Flow Rate of Carrier Gas
rhoair=1.1421; %kg/m3
Qair = 1000; %ml/min
Qair= Qair/(60*10^6); %m3/s
mdotair=Qair*rhoair; %kg/s

%Check Reynolds Number to Ensure Laminar Flow
vair= Qair/(pi*r1^2); %m/s
viscosityair = 1.55E-5; %m2/s
Reair=vair*2*r1/viscosityair;

Cpair=1000; %J/kg*k

%Step through and calculate how long of a tube we need
i=1;
L(1)=dL;
```

```
k(1)=conductivity(Tin);
Tdiff = 10000;
while Tdiff>0.1
    k(i+1)=conductivity(Tin(i));
    hair=3.657*k(i+1)/(2*r1);
    Rair=1/(hair*2*pi*r1*dL);
    Rtot=Rmetal+Rair;
    qi=(Tin(i)-Twall)/Rtot;
    Tin(i+1)=Tin(i)-qi/(mdotair*Cpair);
    L(i+1)=L(i)+dL;
    i=i+1;
    Tdiff = abs(Tin(i)-Twall);
end

Ltube = max(L);

%Plot Resulting Temperature vs. Length
plot(L,Tin,'b-','LineWidth',1.5)
xlabel('Length (m)','interpreter','latex')
ylabel('Air Temperature (C)','interpreter','latex')

end

function k = conductivity(T)
%Thermal Conductivity of Nitrogen

T=T+273.15;

AN=-2.26779433664028E-04;
BN=1.02746291864698E-04;
CN=-6.01514195584557E-08;
DN=2.23319071274301E-11;
```

```
kN = AN + BN*T + CN*T^2 + DN*T^3;

k = kN;
end
```

## Appendix C3 – Main Script used to Process Thesis Results

This is the main function that was used to process data for this thesis. Results were obtained using 2 computers, one for the DSMS, and the other for all other sensors. The data sets were originally on 2 different time scales with the DSMS using non-uniform time steps. In order to run calculations, the results from both computers needed to be interpolated onto the same uniform time scale. Time steps were chosen to be 0.025 s to minimize the error associated with the calculation, and data sets were interpolated and compiled into one data set using the function inter_compile found in this appendix. After interpolation, the function spec2results was used to convert the raw data to mass loss and mass flux curves using the equations found in the methodology section of this thesis and processed further to give useful data. The results obtained using this script can be found in the Results and Discussion section of this thesis.

```
function results = vacdry_process_fullrenorm
%This code will process the data using an iterative
correction that
%compensates for the leak rate by renormalizing everything

%Load in data from the scales for either high or low grade
gangue
% load MP_Data_Low.csv
% M_P_data = MP_Data_Low;
load M_P_data.csv
M_P_data = M_P_data;

end

function results = spec2results(Date,MPdata,dname,oldnew)
%Converts sensor readings to results
```

```
R = 8.314; %J/mol*k
Mcyclo = 84.16; %g/mol
Mwater = 18.02; %g/mol

%make use of data
interptime=Date(:,1);
cyclo_interpd = Date(:,2);
water_interpd = Date(:,3);
O2_interpd = Date(:,4);
temp_interpd = Date(:,5);
Te = Date(:,6);
Poven = Date(:,7);
Patm = Date(:,8);
T0 = Date(:,9);
T1 = Date(:,10);

Morig = MPdata(1); %Original wet mass of gangue
dm_actual = MPdata(2); %Actual change in mass measured by
scale
%Mass loss in vacuum oven after experiment
if oldnew == 1 %Low Grade Ore
    Mvac = MPdata(3);
else %High Grade Ore
    Mvac = MPdata(9);
end

%Time Step
dt = interptime(2) - interptime(1); %s

%Find new total flow rate using molar flow rate of each
component.
%Start with just the leak plus carrier, noting that the
mass flow
%controller was changed between data sets, and the
calibration temperature
%changed with it.
PSTP = 1000; %mbar
if oldnew == 0
    TSTP = 273.15+21.1; %k
    QSTP = 1020; %ml/min
else
    TSTP = 273.15; %k
    QSTP = 1000; %ml/min
end
ndotcarrier = QSTP*PSTP/(R*TSTP); %different units than SI
Patm_spec = 1.1E-7; %torr
PO = Patm*0.21.*O2_interpd/Patm_spec;
```

```
ndotleak2 = ndotcarrier*mean(PO)./(0.21*Patm - mean(PO));

%remove background concentration of water
index_range = length(interptime);
L10min_index = index_range - 10*60/dt;
Watav_L10min =
mean(water_interpd(L10min_index:index_range));
water_interpd = water_interpd - Watav_L10min;

Acyclo = 1.96211E-10; %torr/mbar
Awater = 3.67829E-10; %torr/mbar
%Convert to Pa
Acyclo = Acyclo/100; %torr/Pa
Awater = Awater/100; %torr/Pa

%Set Constants
Voven=197; %ml
Poven = Poven*100; %Pa
Pe = Patm; %mbar
Pe = Pe*100; %Pa

%initialize error and number of iterations
noit=0;
CFerror = 1;
%Calculate maximum mass loss during experiment, and
renormalize and
%recalculate in loops until result agrees with measured
value by the scale.
%It was done this way so that the renormalization could
also apply to the
%leak rate
while CFerror > 0.001 && noit < 6

    %calculate partial pressures at outlet
    Pcyclo = cyclo_interpd/(Acyclo*100); %cyclohexane
pressure at outlet in mbar
    Pwater = water_interpd/(Awater*100); %water pressure at
outlet in mbar

    %calculate molar flow rates at outlet
    ndotcyclo = Pcyclo.*(ndotleak2 + ndotcarrier)./(Patm-
Pcyclo-Pwater);
    ndotwater = Pwater.*(ndotleak2 + ndotcarrier)./(Patm-
Pcyclo-Pwater);

    %Molar flow rates with and without solvents
    ndot_wsolvent2 = (ndotleak2 + ndotcarrier + ndotcyclo +
ndotwater);
```

```
    Qe_wsolvent2 = ndot_wsolvent2*R.*Te./Patm;

    %Estimate Average leak rate
    Qe_nosolvent2 = (ndotleak2 + ndotcarrier)*R.*Te./Patm;
    Leak =
mean(Qe_nosolvent2)*mean(ndotleak2)/(mean(ndotleak2)+ndotca
rrier);

    %Find factor for differential equation that compensates
for leak rate
    f = (ndotcyclo + ndotwater + ndotcarrier)./(ndotcyclo +
ndotwater + ndotleak2 + ndotcarrier);

    %Calculate Flow Rate
    Flow = Qe_wsolvent2/60; %ml/s

    %Convert to g/ml concentration
    Cyclo = cyclo_interpd./(Acyclo*R*Te); %mol/m3
    Cyclo = Cyclo/1000000; %mol/ml
    Cyclo = Cyclo*Mcyclo; %g/ml
    Water = water_interpd./(Awater*R*Te);
    Water = Water/1000000; %mol/ml
    Water = Water*Mwater; %g/ml

    %Calculate time derivative
    dcyclodt = diff(Cyclo)/dt;
    dcyclodt(index_range) = 0;
    dwaterdt = diff(Water)/dt;
    dwaterdt(index_range) = 0;

    %Calculate integration coefficient for differential
term
    Tau = f.*(Voven.*Poven.*Te)./(temp_interpd.*Pe);

    %Apply differential equation
    dmcyclodt= (Flow.*Cyclo + Tau.*dcyclodt);
    dmwaterdt= (Flow.*Water + Tau.*dwaterdt);

    %Integrate to give total mass
    mcyclo_original = cumtrapz(interptime,dmcyclodt);
    mwater_original = cumtrapz(interptime,dmwaterdt);
    mtot_original = mwater_original + mcyclo_original;

    %now calculate the derivatives %(dm/dt)
    mtotderiv = dmcyclodt + dmwaterdt;
    mcycloderiv = dmcyclodt;
    mwaterderiv = dmwaterdt;
```

```
    %Correction factor
    delta_m_spec = max(mtot_original);
    CorrectionFactor = (dm_actual/delta_m_spec);

    %Calculate %Error
    if noit == 0
        Ediff = (delta_m_spec - dm_actual)/dm_actual*100;
    end

    cyclo_interpd = cyclo_interpd*CorrectionFactor;
    water_interpd = water_interpd*CorrectionFactor;
    PO = PO*CorrectionFactor;
    ndotleak2 = ndotcarrier*mean(PO)./(0.21*Patm -
mean(PO));

    %Calculate correction factor imbalance
    CFerror = abs(1-CorrectionFactor);
    noit=noit+1;
    if noit >4
        if CFerror>0.005
            fprintf('Warning: CFerror %s did not converge
%.3f\n',dname,CFerror)
        end
    end
end

%Filter mderiv data so that we don't get non-physical
negative values
mcycloderiv=smooth(mcycloderiv,2001);
mwaterderiv=smooth(mwaterderiv,2001);
mtotderiv = mcycloderiv + mwaterderiv;

tlength = length(mcyclo_original);
index_range = tlength;

%generate interptime
dt=0.025;
interptime = transpose(linspace(0,dt*tlength-dt,tlength));

%Find average Temperature and Pressure during experiment
Tav = mean(temp_interpd)-273.15;
Pav = mean(Poven);

%Find oven Temperature using last 10 minutes of experiment
so as not to get
%interference from the drying solvent lowering the
temperature
last10index = index_range - 10*60/dt;
```

```
Tamb_av = mean(temp_interpd(last10index:index_range));

%Find time to finish stage 1 drying
%First find the time that the maxium occurs
changetotmax_index = find(mtotderiv ==
max(mtotderiv),1,'first');
changecyclomax_index = find(mcycloderiv ==
max(mcycloderiv),1,'first');
changewatermax_index = find(mwaterderiv ==
max(mwaterderiv),1,'first');
%Now find where the deriv is 18% of this first after the
maximum
mderiv2tot = mtotderiv(changetotmax_index:index_range);
mderiv2cyclo =
mcycloderiv(changecyclomax_index:index_range);
mderiv2water =
mwaterderiv(changewatermax_index:index_range);
tchangetot_index =
find(mderiv2tot<0.18*max(mtotderiv),1,'first')+changetotmax
_index;
tchangecyclo_index =
find(mderiv2cyclo<0.18*max(mcycloderiv),1,'first')+changecy
clomax_index;
tchangewater_index =
find(mderiv2water<0.18*max(mwaterderiv),1,'first')+changewa
termax_index;
tchangetot = interptime(tchangetot_index);
tchangecyclo = interptime(tchangecyclo_index);
tchangewater = interptime(tchangewater_index);
mchangetot = mtot_original(tchangetot_index);
mchangecyclo = mcyclo_original(tchangecyclo_index);
mchangewater = mwater_original(tchangewater_index);
%For an easier to explain comparison, check out what it is
for 50%
tchangecyclo50_index =
find(mderiv2cyclo<0.5*max(mcycloderiv),1,'first')+changecyc
lomax_index;
tchangecyclo50 = interptime(tchangecyclo50_index);
mchangecyclo50 = mcyclo_original(tchangecyclo50_index);


%Plot and save Original mass evaporated curves with and
without legend
mfig = figure;
plot(interptime,mcyclo_original,'r-
',interptime,mwater_original,'b-',...
    interptime,mtot_original,'g-',0,dm_actual,'bs')
xlabel('time (s)','interpreter','latex')
```

```
ylabel('total evaporated mass (g)','interpreter','latex')
print(mfig,'-dpng',strcat(dname,' Mass Data'))
legend('Cyclohexane Mass','Water Mass','Total Mass','Actual
Total Mass Loss','Location','SouthEast')
print(mfig,'-dpng',strcat(dname,' Mass Data with Legend'))

% Renormalize the mass data
delta_m_spec = max(mtot_original);
mtot_renormal = mtot_original*(dm_actual/delta_m_spec);
mcyclo_renormal = mcyclo_original*(dm_actual/delta_m_spec);
mwater_renormal = mwater_original*(dm_actual/delta_m_spec);

%Plot and save renormalized curves with and without legend
mfig = figure;
plot(interptime,mcyclo_renormal,'r-
',interptime,mwater_renormal,'b-',...
    interptime,mtot_renormal,'g-')
xlabel('time (s)','interpreter','latex')
ylabel('total evaporated mass (g)','interpreter','latex')
print(mfig,'-dpng',strcat(dname,' Renormal Mass Data'))
legend('Cyclohexane Mass','Water Mass','Total
Mass','Location','SouthEast')
print(mfig,'-dpng',strcat(dname,' Renormal Mass Data with
Legend'))

%Calculate mass flux as a function of time for both
components and total
Dtin = 5.8; %cm
Atin = pi*Dtin^2/4; %cm^2
Mflux_tot = mtotderiv/Atin; %g/(cm^2 s)
Mflux_cyclo = mcycloderiv/Atin;
Mflux_water = mwaterderiv/Atin;

%Figure out time bounds for maximum mass flux excluding
first 50 seconds
MfluxMax_tot = max(Mflux_tot(50/dt:tlength));
MfluxMax_cyclo = max(Mflux_cyclo(50/dt:tlength));
MfluxMax_water = max(Mflux_water(50/dt:tlength));
%Use within 10% of maximum as the criteria, find indices
maxfluxstart_tot = find(Mflux_tot(50/dt:tlength) >=
0.9*MfluxMax_tot,1,'first')+50/dt-1;
maxflux_tot = find(Mflux_tot(50/dt:tlength) ==
MfluxMax_tot,1,'first')+50/dt-1;
maxfluxend_tot = find(Mflux_tot(maxflux_tot:tlength) <=
0.9*MfluxMax_tot,1,'first') + maxflux_tot;
maxfluxstart_cyclo = find(Mflux_cyclo(50/dt:tlength) >=
0.9*MfluxMax_cyclo,1,'first')+50/dt-1;
maxflux_cyclo = find(Mflux_cyclo(50/dt:tlength) ==
```

```
MfluxMax_cyclo,1,'first')+50/dt-1;
maxfluxend_cyclo = find(Mflux_cyclo(maxflux_cyclo:tlength)
<= 0.9*MfluxMax_cyclo,1,'first') + maxflux_cyclo;
maxfluxstart_water = find(Mflux_water(50/dt:tlength) >=
0.9*MfluxMax_water,1,'first')+50/dt-1;
maxflux_water = find(Mflux_water(50/dt:tlength) ==
MfluxMax_water,1,'first')+50/dt-1;
maxfluxend_water = find(Mflux_water(maxflux_water:tlength)
<= 0.9*MfluxMax_water,1,'first') + maxflux_water;

%Find the average maximum mass flux for top 90%
Mflux_AvMax_tot =
mean(Mflux_tot(maxfluxstart_tot:maxfluxend_tot));
Mflux_AvMax_water =
mean(Mflux_water(maxfluxstart_water:maxfluxend_water));
Mflux_AvMax_cyclo =
mean(Mflux_cyclo(maxfluxstart_cyclo:maxfluxend_cyclo));

%Find actual maximum mass flux
Mflux_max_tot = max(Mflux_tot);
Mflux_max_cyclo = max(Mflux_cyclo);
Mflux_max_water = max(Mflux_water);

%Renormalize both data
Mflux_avmaxrenorm_tot =
Mflux_AvMax_tot*(dm_actual/delta_m_spec);
Mflux_avmaxrenorm_cyclo =
Mflux_AvMax_cyclo*(dm_actual/delta_m_spec);
Mflux_avmaxrenorm_water =
Mflux_AvMax_water*(dm_actual/delta_m_spec);
Mflux_maxrenorm_tot =
Mflux_max_tot*(dm_actual/delta_m_spec);
Mflux_maxrenorm_cyclo =
Mflux_max_cyclo*(dm_actual/delta_m_spec);
Mflux_maxrenorm_water =
Mflux_max_water*(dm_actual/delta_m_spec);

%Find where the mass flux is within 2% of it's minimum
value and only plot
%the part of the curve that happens before that.
plotend = find(Mflux_tot(maxflux_tot:tlength) <=
0.02*MfluxMax_tot,1,'first') + maxflux_tot;
fluxplottime = interptime(1:plotend);
Mfluxplot_tot = Mflux_tot(1:plotend);
Mfluxplot_cyclo = Mflux_cyclo(1:plotend);
Mfluxplot_water = Mflux_water(1:plotend);

%Find average temperature for both probes in the region
```

```
within 10% maxflux
Tbottom_maxflux =
mean(T0(maxfluxstart_cyclo:maxfluxend_cyclo));
Ttop_maxflux =
mean(T1(maxfluxstart_cyclo:maxfluxend_cyclo));

%Find temp at maximum cyclo mass flux
Tbottom_maxflux2 = T0(maxflux_cyclo);
Ttop_maxflux2 = T1(maxflux_cyclo);

%Calculate degree of subcooling
Subcool1 = Tamb_av - Ttop_maxflux;
Subcool2 = Tamb_av - Ttop_maxflux2;

%Create vectors for dry mass fractions
mcycloevap = max(mcyclo_renormal);
mwaterevap = max(mwater_renormal);
mtotdry = Morig - dm_actual - Mvac;
%Create curve for fcyclo
fcyclo = (mcycloevap - mcyclo_renormal)/mtotdry;
fwater = (mwaterevap - mwater_renormal)/mtotdry;
%Note: above takes Mvac into account for denominator but
not numerator

%Calculate the critical mass fractions at maximum flux
fcrit_cyclomax = fcyclo(maxflux_cyclo);
fcrit_watermax = fwater(maxflux_water);

%plot generated curves
mfig = figure;
plot(fcyclo,Mflux_cyclo,'r-',fwater,Mflux_water,'b-')
xlabel('Dry Weight Fraction','interpreter','latex')
ylabel('Mass Flux (kg/(m^2 s))','interpreter','latex')
legend('Cyclohexane','Water','location','southeast')
print(mfig,'-dpng',strcat(dname,' Mflux dryfrac'))

%Plot log linear mass flux curve
mfig = figure;
semilogy(interptime,Mflux_cyclo,'r-
',interptime,abs(Mflux_water),'b-')
xlabel('time (s)')
ylabel('Mass Flux')
legend('Cyclohexane','Water')
print(mfig,'-dpng',strcat(dname,' Mflux semilog'))

% %%plot the mass flux vs. time on a linear scale
mfig = figure;
plot(fluxplottime,Mfluxplot_tot,'g-
```

```
',fluxplottime,Mfluxplot_cyclo,'r-',...
    fluxplottime,Mfluxplot_water,'b-')
xlabel('time (s)','interpreter','latex')
ylabel('Mass Flux (g/(cm2 s))','interpreter','latex')
print(mfig,'-dpng',strcat(dname,' Mass Flux Data'))
legend('Total','Cyclo','Water')
print(mfig,'-dpng',strcat(dname,' Mass Flux Data Legend'))

% %also plot temperature within this region showing
location of maximum
% mass flux
mfig = figure;
plot(fluxplottime,T0(1:plotend),'r-
',fluxplottime,T1(1:plotend),'b-',...

fluxplottime(maxflux_cyclo),T0(maxflux_cyclo),'ro',fluxplot
time(maxflux_cyclo),T1(maxflux_cyclo),'bo')
xlabel('time (s)','interpreter','latex')
ylabel('Temperature (C))','interpreter','latex')
print(mfig,'-dpng',strcat(dname,' Temperature Evolution'))
legend('Bottom Temperature','Top Temperature','Location of
Maximum Flux','Location','SouthEast')
print(mfig,'-dpng',strcat(dname,' Temperature Evolution
Legend'))

close all

%Find time to 80%, 90%, 95%, 99%, 99.5% maximum recovery of
cyclohexane
mcyclomax = max(mcyclo_original);
t_80 = find(mcyclo_original >=0.8*mcyclomax,1,'first');
t_90 = find(mcyclo_original >=0.9*mcyclomax,1,'first');
t_95 = find(mcyclo_original >=0.95*mcyclomax,1,'first');
t_99 = find(mcyclo_original >=0.99*mcyclomax,1,'first');
t_99p5 = find(mcyclo_original >=0.995*mcyclomax,1,'first');
%Note: above are just the indices

%Find time to reach low concentrations
t250ppm = find(fcyclo <= 250e-6,1,'first');
t500ppm = find(fcyclo <= 500e-6,1,'first');
t1000ppm = find(fcyclo <= 1000e-6,1,'first');
%t1500ppm = find(fcyclo <= 1500e-6,1,'first');
t2000ppm = find(fcyclo <= 2000e-6,1,'first');
t5000ppm = find(fcyclo <= 5000e-6,1,'first');
t10000ppm = find(fcyclo <= 10000e-6,1,'first');
t20000ppm = find(fcyclo <= 20000e-6,1,'first');
%Note: above are just indices
```

```
%Find temperature at 99.5% recovery and 250 ppm
Tbot250ppm = T0(t250ppm)-273.15;
Ttop250ppm = T1(t250ppm)-273.15;

%Find outlet cyclohexane vapour pressure using renormal
mass flux
Mflux_cyclo_renormal =
Mflux_cyclo*(dm_actual/delta_m_spec);
Mflux_water_renormal =
Mflux_water*(dm_actual/delta_m_spec);
Q=1000 + Leak; %Flow in ml/min
Pcyclo_exit =
Mflux_cyclo_renormal*Atin*8.314*298/(Q*84.16)*60E3; %kPa

%Find where found partial pressure of cyclohexane exceeds
vapour pressure
if max(Pcyclo_exit) >= 12.29;
    cyclovapindex1 = find(Pcyclo_exit >=12.29,1,'first');
    cyclovapindex2 = find(Pcyclo_exit >=12.29,1,'last');
    %find time that it is over the limit
    tover_cyclo = interptime(cyclovapindex2)-
interptime(cyclovapindex1);
    %find mass loss in that time
    mover_cyclo = mcyclo_renormal(cyclovapindex2)-
mcyclo_renormal(cyclovapindex1);
else
    tover_cyclo = 0;
    mover_cyclo = 0;
end

%Calculate Energy Breakdown to achieve 250 ppm recovery in
batch process
%First calculate energy dependent on time
Troom=21+273.15;
%Make sure you consider how the flow rate changes with
pressure
Evac = 1000/60*10^-6*(100000-
mean(Poven))*interptime(t250ppm)/0.9; %J
Esand = 0.703*(Morig-dm_actual)*(Tamb_av-Troom); %J
Eair = 1000/60*10^-6*1.04*1.165*(Tamb_av-
Troom)*interptime(t250ppm); %J
Ecyclo_evap = max(mcyclo_renormal)*32000/84.16;
Ewater_evap = max(mwater_renormal)*2260;

%Now calculate energy to heat sand and cyclohexane
Ecyclo_heat = (cyclorenormip1 -
mcyclo_renormal(1:t250ppm)).*(1.211*(T1(1:t250ppm)-Troom));
Ewater_heat = (waterrenormip1 -
```

```
mwater_renormal(1:t250ppm)).*(4.1813*(T1(1:t250ppm)-
Troom));
Etotal = Evac + Esand + Eair + Ecyclo_evap + Ewater_evap +
Ecyclo_heat + Ewater_heat;

%Calculate new way to find average water mass flux
T1a = T1(maxflux_cyclo:tlength)-273.15;
TdoneA = find(T1a >=
0.95*max(T1a),1,'first')+maxflux_cyclo;
TdoneB = find(T1a >= max(T1a) - 0.25*(max(T1)-
Ttop_maxflux2),1,'first')+maxflux_cyclo;
t_TdoneA = interptime(TdoneA);
t_TdoneB = interptime(TdoneB);
MwateravfluxA = mwaterevap/(t_TdoneA*Atin);
MwateravfluxB = mwaterevap/(t_TdoneB*Atin);
%Calculate water removed at t250ppm using this method
mwatendA = MwateravfluxA*interptime(t250ppm)*Atin;
mwatendB = MwateravfluxB*interptime(t250ppm)*Atin;

%Calculate Evaporative Energy Loss at Point of Maximum
Cyclo Mass Flux
WaterFlux_cyclomax = Mflux_water_renormal(maxflux_cyclo);
Eloss_Cyclo = Mflux_maxrenorm_cyclo*32000/84.16*Atin; %W
Eloss_Water = WaterFlux_cyclomax*2260*Atin; %W

results = zeros(1,43);
%Average Oven Pressure during Experiment
results(1) = Pav;
%Oven Temperature during last 10 minutes of experiment
results(2) = Tamb_av-273.15;
%Time to end of stage 1 drying
results(3) = tchangetot;
results(4) = tchangecyclo;
results(5) = tchangewater;
%Total Mass Loss before renormalization
results(6) = max(mtot_original);
results(7) = max(mcyclo_original);
results(8) = max(mwater_original);
%Renormalized mass of cyclohexane and water
results(9) = mcycloevap;
results(10) = mwaterevap;
%Stage 1 mass change results (using the individual stage 1
times)
results(11) = mchangetot;
results(12) = mchangecyclo;
results(13) = mchangewater;
%Temperature for both probes at point of maximum mass flux
results(14) = Tbottom_maxflux2 - 273.15;
```

```
results(15) = Ttop_maxflux2 - 273.15;
%Average temperature for both probes within 90% of maximum
mass flux
results(16) = Tbottom_maxflux - 273.15;
results(17) = Ttop_maxflux - 273.15;
%Maximum mass flux not renormalized (within 10%)
results(18) = Mflux_AvMax_tot;
results(19) = Mflux_AvMax_cyclo;
results(20) = Mflux_AvMax_water;
%Maximum mass flux renormalized (within 10%)
results(21) = Mflux_avmaxrenorm_tot;
results(22) = Mflux_avmaxrenorm_cyclo;
results(23) = Mflux_avmaxrenorm_water;
%Maximum mass flux not renormalized
results(24) = Mflux_max_tot;
results(25) = Mflux_max_cyclo;
results(26) = Mflux_max_water;
%Maximum mass flux renormalized
results(27) = Mflux_maxrenorm_tot;
results(28) = Mflux_maxrenorm_cyclo;
results(29) = Mflux_maxrenorm_water;
%Time to 80,90,95,99,99.5% recovery of cyclohexane
results(30) = interptime(t_80);
results(31) = interptime(t_90);
results(32) = interptime(t_95);
results(33) = interptime(t_99);
results(34) = interptime(t_99p5);
%Mass of water recovered at these points
results(35) = mwater_renormal(t_80);
results(36) = mwater_renormal(t_90);
results(37) = mwater_renormal(t_95);
results(38) = mwater_renormal(t_99);
results(39) = mwater_renormal(t_99p5);
%Total time for the experiment to run
results(40) = max(interptime);
%Time at maximum mass flux of cyclohexane
results(41) = interptime(maxflux_cyclo);
%dry mass fraction of solvents remaining at point of max
mass flux
results(42) = fcrit_cyclomax;
results(43) = fcrit_watermax;
%time to 250ppm residual cyclohexane
results(44) = interptime(t250ppm);
%Average Temperature throughout entire run
results(45) = Tav;
%Probe Temperatures at 250 ppm
results(46) = Tbot250ppm;
results(47) = Ttop250ppm;
```

```
%Cyclohexane mass flux with limited cyclohexane remaining
results(48) = Mflux_cyclo_renormal(t250ppm);
results(49) = Mflux_cyclo_renormal(t500ppm);
results(50) = Mflux_cyclo_renormal(t1000ppm);
results(51) = Mflux_cyclo_renormal(t2000ppm);
results(52) = Mflux_cyclo_renormal(t5000ppm);
results(53) = Mflux_cyclo_renormal(t10000ppm);
%Time spent over vapour pressure of cyclohexane
results(54) = tover_cyclo;
%mass evaporated during that time
results(55) = mover_cyclo;
%Leak rate
results(56) = Leak;
%Degree of subcooling
results(57) = Subcool1; %using avmax
results(58) = Subcool2; %Using max
results(59) = Ediff; %Error based on difference between
calculated and actual
results(60) = Evac;
results(61) = Esand;
results(62) = Eair;
results(63) = Ecyclo_heat;
results(64) = Ewater_heat;
results(65) = Ecyclo_evap;
results(66) = Ewater_evap;
results(67) = Etotal;
%Time to achieve small residual recovery levels
results(68) = interptime(t20000ppm);
results(69) = interptime(t10000ppm);
results(70) = interptime(t5000ppm);
results(71) = interptime(t2000ppm);
results(72) = interptime(t1000ppm);
results(73) = tchangecyclo50;
results(74) = mchangecyclo50;
results(75) = mwater_renormal(t250ppm);
results(76) = mwatendA;
results(77) = mwatendB;
results(78) = t_TdoneA;
results(79) = t_TdoneB;
results(80) = Eloss_Cyclo;
results(81) = Eloss_Water;
%Evaporative Energy Loss At Point of Maximum Cyclo Mass
Flux
end

function Data = inter_compile(Date_spec,Date_temp,dt)
%Interpolate the data onto a uniform time scale with a very
small time
```

```
%scale so that calculations can be carried out later.

%Load in ambient temperature Data
temptime=Date_temp(:,1);
temp_0=Date_temp(:,2)+273.15; %Convert to Kelvin
temp_1=Date_temp(:,3)+273.15;
temp_2=Date_temp(:,4)+273.15;
temp_3=Date_temp(:,5)+273.15;
pres=Date_temp(:,6); %Pressure in mbar
Pout=Date_temp(:,7); %Outlet Pressure in mbar

%Load in mass spec data
spectime=Date_spec(:,1);
cyclospec=Date_spec(:,4);
waterspec=Date_spec(:,2);
oxyspec=Date_spec(:,3);
vaclvl=Date_spec(:,5);

%Before we do anything, we need to figure out how to zero
the new time
%scale.  A correction will need to be added to the mass
spec time to
%account for the amount of time that it takes for the
solvent to go from
%the top of the sample to the mass spec itself.

%Our inlet flow rate is 1 SPLM (1000 ml/min at 1 bar and 0
C
Qbefore = 1000; %ml/min
Qinside = Qbefore*1000*mean(temp_3)/(273.15*mean(pres));
%It basically spends all it's time at room temperature so
we use temp_3
%because heat transfer is so fast
%length of tubing under vacuum and after pump
lquarter_vac = 65.5+30; %cm, extra 30 cm is for the pump
lhalf_vac = 74; %cm
Qatm = Qbefore*1000*mean(temp_3)/(273.15*mean(Pout));
lquarter_atm = 17.5; %cm
lhalf_atm = 8; %cm
Dquarter = 0.2*2.54; %cm
Dhalf = 0.48*2.54; %cm
tdelay = lquarter_vac*pi*Dquarter^2*60/(4*Qinside) + ...
    lhalf_vac*pi*Dhalf^2*60/(4*Qinside) + ...
    lquarter_atm*pi*Dquarter^2*60/(4*Qatm) + ...
    lhalf_atm*pi*Dhalf^2*60/(4*Qatm);

%subtract tdelay from spectime to get original time
spectime = spectime-tdelay;
```

```
%Now need to write code to figure out where the starting
point of timing
%should be.  Start with the first point where spec signal
is > 10^-12
tguess_index = find(cyclospec(10:length(cyclospec)) > 1E-
12,1,'first')+9;
tguess = spectime(tguess_index);
%make 40 second interval around this guess time, and start
the time at the
%first point where the pressure was less than 50% greater
than the
%difference between mean pressure throughout experiment and

Pmean = mean(pres);
Poutmean = mean(Pout);
Pstart = Pmean + (Poutmean-Pmean)/2;

templowindex = find(temptime >= tguess-10,1,'first');
temphighindex = find(temptime >= tguess+60,1,'first');
tempstartindex = find(pres(templowindex:temphighindex) <=
Pstart,1,'first') + templowindex-1;
tempstart = temptime(tempstartindex);
delta_t = dt; %second

%Set interptime to start at zero
timezero = tempstart;
spectime=spectime-timezero;
temptime=temptime-timezero;

%Build new uniform time scale starting from first mass
point and ending at
%the highest time that we have
if max(temptime) > max(spectime)
    tmax = floor(max(spectime)); %maximum time
else
    tmax = floor(max(temptime));
end
tmax_index = floor(tmax/delta_t); %maximum time index
index_range = tmax_index;
interptime = transpose(linspace(0,dt*index_range-
dt,index_range));

%Renormalize mass spec data using last 10 minutes of vaclvl
from mass spec
vacstartindex = find(spectime >= max(spectime) -
10*60,1,'first');
vacav = mean(vaclvl(vacstartindex:length(spectime)));
```

```
cyclospec = cyclospec*(10^-6)/vacav;
waterspec = waterspec*(10^-6)/vacav;
oxyspec = oxyspec*(10^-6)/vacav;

%Interpolate spec data onto new uniform time scale
cyclo_interpd = interp1(spectime,cyclospec,interptime);
water_interpd = interp1(spectime,waterspec,interptime);
oxy_interpd = interp1(spectime,oxyspec,interptime);

%Interpolate Temp Data onto new uniform time scale
tin_interpd = interp1(temptime,temp_2,interptime);  %Oven
Air Temperature
tout_interpd = interp1(temptime,temp_3,interptime); %Outlet
Temperature
P_interpd = interp1(temptime,pres,interptime); %Oven
Pressure
Pout_interpd = interp1(temptime,Pout,interptime); %Outlet
Pressure
T0_interpd = interp1(temptime,temp_0,interptime); %Bottom
Temperature
T1_interpd = interp1(temptime,temp_1,interptime); %Top
Temperature

Data(:,1) = interptime; %Uniform time scale
Data(:,2) = cyclo_interpd; %Mass Spec reading for
Cyclohexane
Data(:,3) = water_interpd; %Mass Spec reading for Water
Data(:,4) = oxy_interpd; %Mass Spec reading for Oxygen
Data(:,5) = tin_interpd; %Oven Air Temperature
Data(:,6) = tout_interpd; %Outlet Temperature
Data(:,7) = P_interpd; %Oven Pressure
Data(:,8) = Pout_interpd; %Outlet Pressure
Data(:,9) = T0_interpd; %Bottom Probe Temperature
Data(:,10) = T1_interpd; %Top Probe Temperature

end
```

# Appendix D – Engineering Drawings

This appendix shows the engineering drawings that were made and sent to the CME machine shop in order to build new parts of the apparatus.

## Appendix D1 – Thermocouple Sealing Adapter

This part was built to adapt to an existing 1'' NPT port on the back of the first vacuum oven and feed in two Conax sealing glands through ⅛'' NPT holes. The part is described in more detail in Appendix A1.

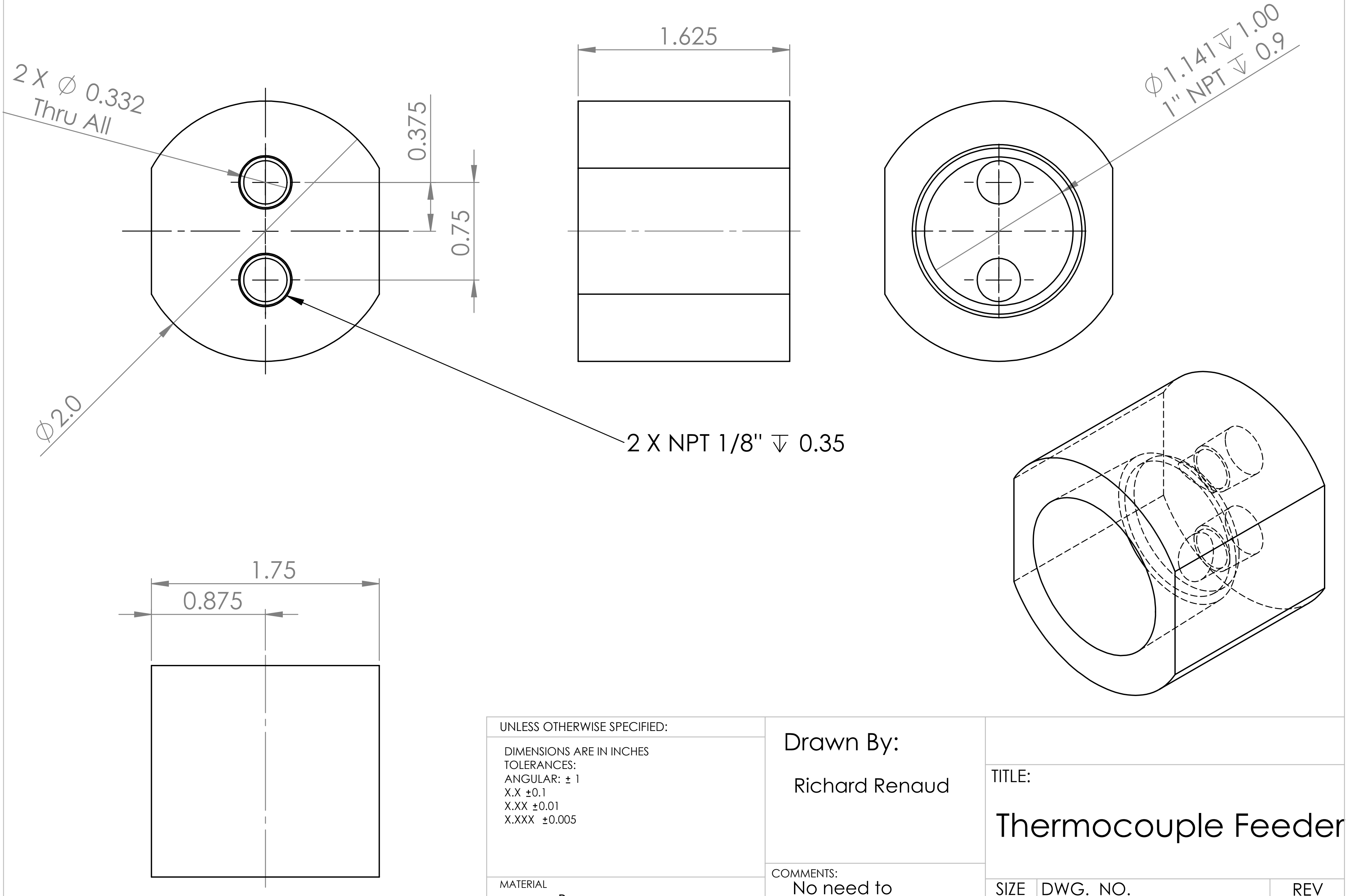

UNLESS OTHERWISE SPECIFIED:

DIMENSIONS ARE IN INCHES
TOLERANCES:
ANGULAR: ± 1
X.X ±0.1
X.XX ±0.01
X.XXX ±0.005

MATERIAL
Brass

Surface Finish
In micro inches where stated

Drawn By:
Richard Renaud

COMMENTS:
No need to machine outside diameter
Break all edges approx 0.005 R

TITLE:
# Thermocouple Feeder

SIZE
**A**
DWG. NO.
REV
SCALE: 1:1
SHEET 1 OF 1

## Appendix D2 – Brass Drying Vessel

When it was discovered that the original large vacuum oven was too large to deliver good transient response, a smaller brass vessel was designed. The vessel was designed to seal with a piston style O-ring so that thermocouple probes in the lid would slide to the same positions inside the sample every time to give strong repeatability for temperature data between experiments. The vessel and the calculations done to design it are described in detail in appendix A2. The vessel consists of two parts, a base and a lid. The engineering drawings for both are shown below.

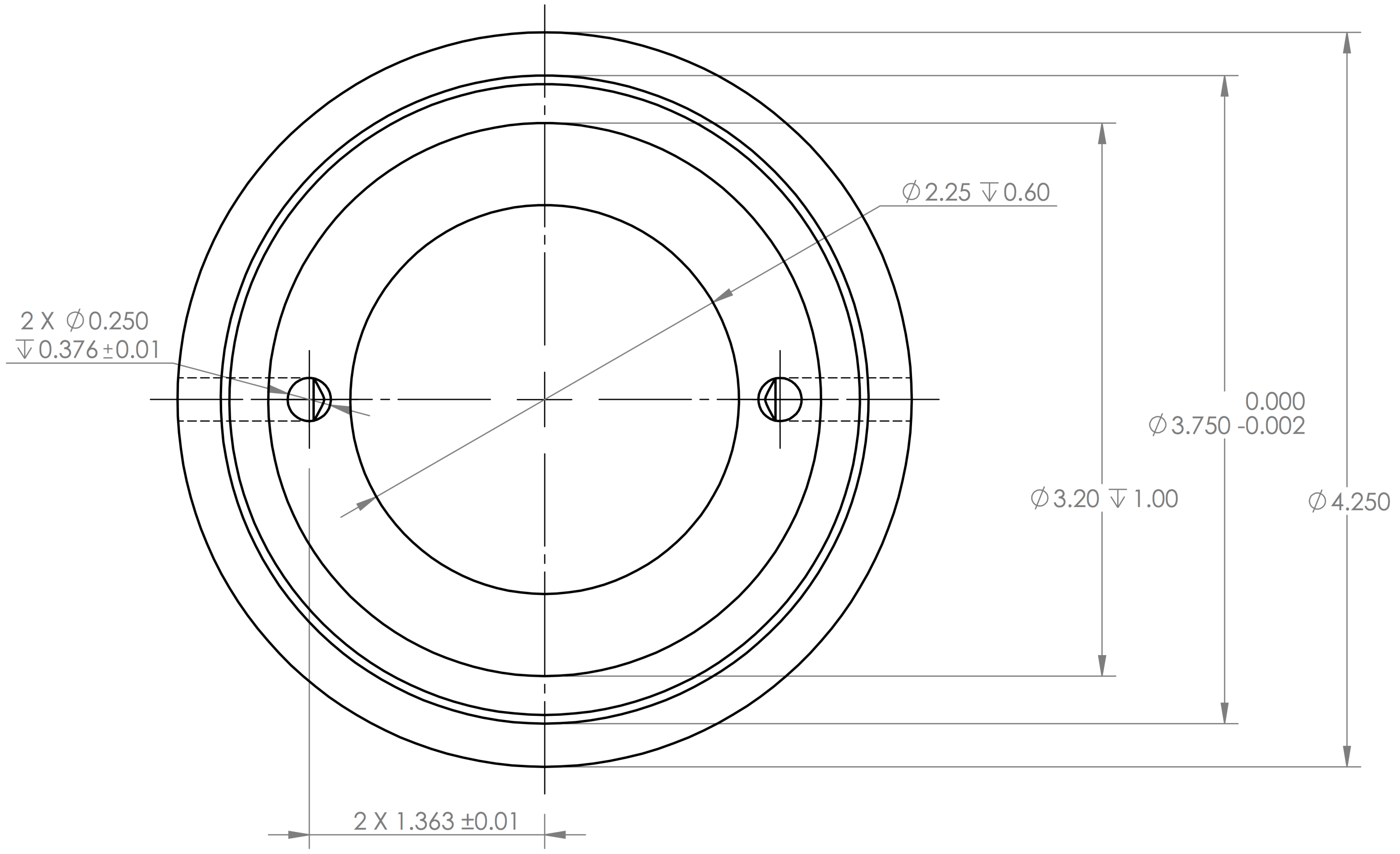

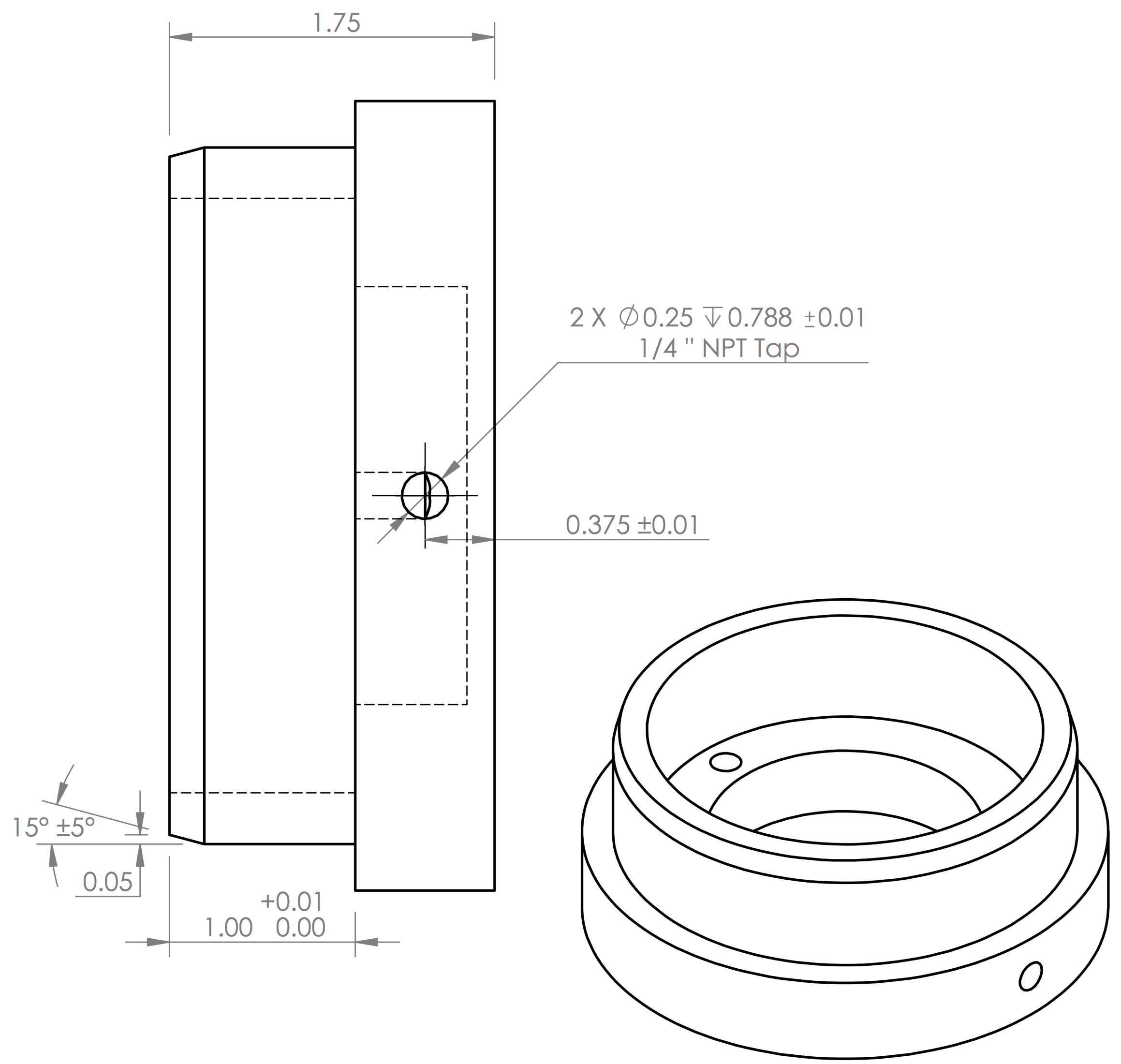

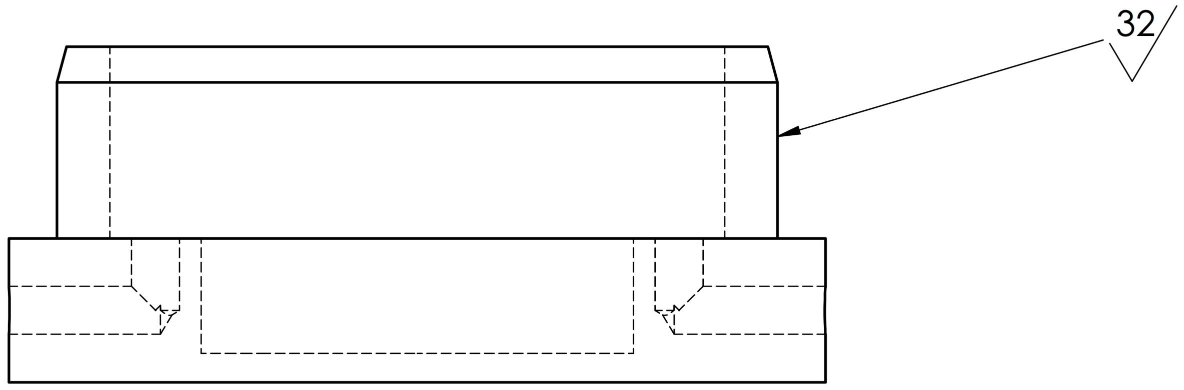

Comments:

Break all corners
approx 0.005 rad

UNLESS OTHERWISE SPECIFIED:

DIMENSIONS ARE IN Inches
TOLERANCES:
X = ± 0.5
X.X = ± 0.1
X.XX = ± 0.01
X.XX = ± 0.005

SURFACE FINISH
in micro inches where stated

MATERIAL: Stainless Steel

DRAWN BY:
**Richard Renaud**

Sunday, September 22, 2013 10:13:59 PM
Friday, September 06, 2013 11:25:02 PM

UNIVERSITY OF ALBERTA

TITLE:
Main Container

SIZE **B**

Part supplier/manufacturer

REV

SCALE: 1:1

Mass:

SHEET 1 OF 1

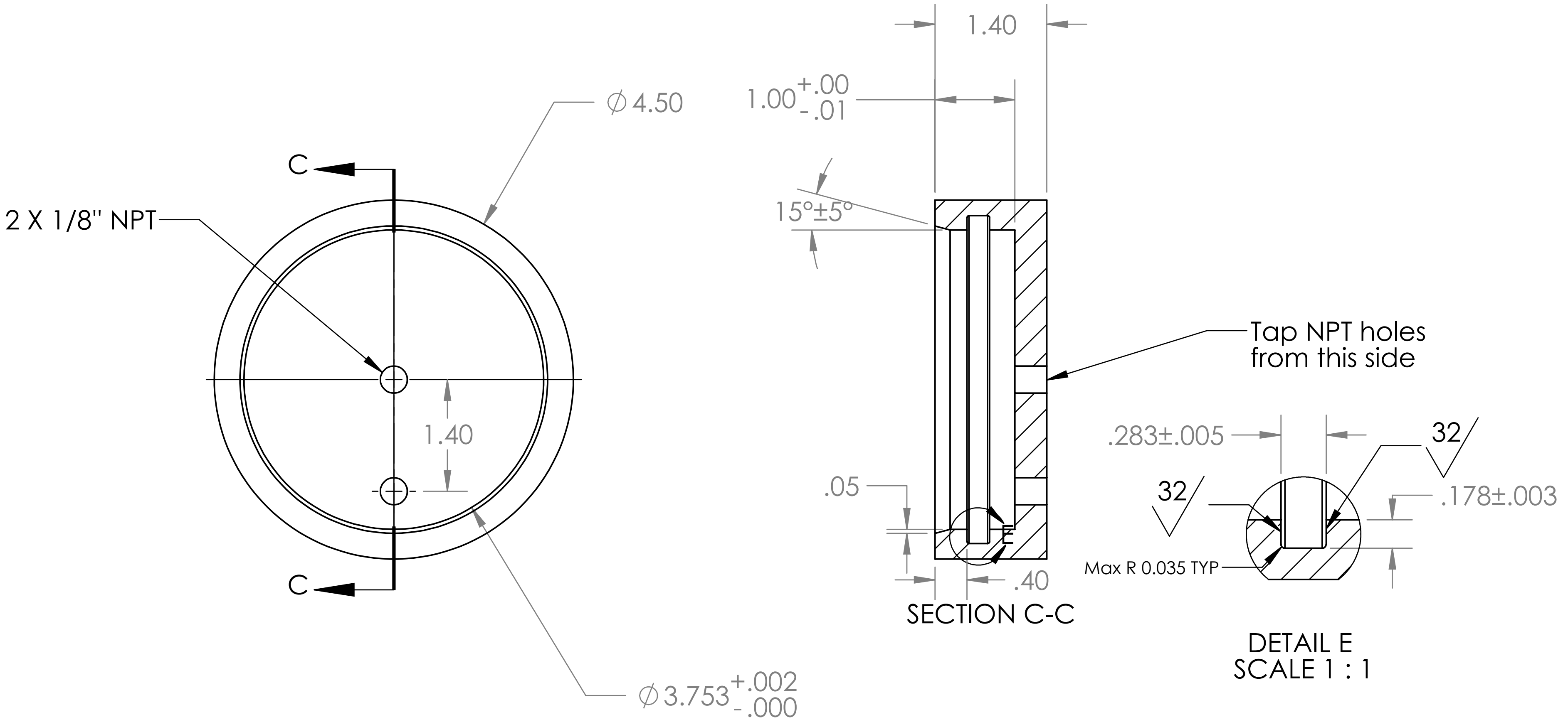

UNLESS OTHERWISE SPECIFIED:

DIMENSIONS ARE IN INCHES
TOLERANCES:
ANGULAR: ± 1
X.X ±0.1
X.XX ±0.01
X.XXX ±0.005

MATERIAL
Stainless Steel

Surface Finish
In micro inches where stated

Drawn By:
Richard Renaud

COMMENTS:
No need to machine outside diameter
Break all edges approx 0.005 R

TITLE:
Lid

SIZE
A
DWG. NO.
REV
SCALE: 1:2
SHEET 1 OF 1